THE UNIVERSITY OF MICHIGAN

INDUSTRY PROGRAM OF THE COLLEGE OF ENGINEERING

THE BEHAVIOR OF SLUGGING GAS-FLUIDIZED SOLIDS

Robert H. Kadlec

A dissertation submitted in partial fulfillment
of the requirements for the degree of
Doctor of Philosophy in The
University of Michigan
Department of Chemical and Metallurgical Engineering
1961

September, 1961

IP-532

Doctoral Committee:

Professor G. Brymer Williams, Chairman
Doctor Gordon Atkinson
Assistant Professor Dale Rudd
Associate Professor M. R. Tek
Professor J. Louis York

ACKNOWLEDGMENTS

I gratefully acknowledge the assistance of Professors G. B. Williams, J. L. York, D. R. Rudd, G. Atkinson and M. R. Tek in all phases of this work. Thanks are also due to the University of Michigan Industry Program and my wife Kathleen for great assistance in the preparation of the manuscript. I wish also to thank the National Science Foundation for three year's support.

TABLE OF CONTENTS

TABLE OF CONTENTS
(continued)

LIST OF FIGURES

LIST OF FIGURES
(continued)

LIST OF FIGURES

LIST OF FIGURES
(continued)

LIST OF FIGURES
(continued)

LIST OF TABLES

NOMENCLATURE

A	constant; bed cross sectional area
A_p	projected area of a particle
C, C'	constants
C_d	drag coefficient
c	particle speed
D	constant, diameter
d_p	collision particle diameter
E	constant
e	base for natural logarithm
F	force
f	friction factor
g	acceleration of gravity
g_c	gravitational constant
H	height
I	integral
K	constant
L	static bed length
m	mass
N_p	particle number density
n	counting index
P	distribution function, pressure
R	reading
Re	Reynolds number

t	time
u	velocity
v	velocity, volt
v_r	relative velocity
$\bar{w}$	nonrandom component of particle velocity; solids downflow rate
w_a	solids downflow rate
$\bar{x}$	cartesian coordinate; coordinate of the top of a slug
$\bar{y}$	cartesian coordinate; length of a slug
$\bar{z}$	cartesian coordinate; coordinate of the bottom of a slug
Z_c	collision frequency
α, β	constants, variables: defined as required
γ	dimensionless nonrandom particle speed
δ	Dirac delta function
ε	porosity, dimensionless particle speed
θ	polar coordinate, measure of solids downflow rate
ρ	density
σ	standard deviation
τ	period
ϕ	polar coordinate
ψ	function symbol

Superscripts

$\dot{}$	first time derivative
$\ddot{}$	second time derivative
$'$	derivative, prime
$''$	second derivative, double prime
$\bar{}$	average

Subscripts

B	bottom
b	bubble
C	collision
C.G.	center of gravity
D	drag
g	gas
fb	fixed bed
gmf	gas, minimum fluidization
M	middle
O	initial condition
P	pressure, particle, projected
S	solid, slip
T	top
t	tube
ts	true, solid
x	X direction

Subscripts

xs	excess
y	Y direction
z	Z direction

INTRODUCTION

A wealth of information has been obtained in the field of fluidization in recent years. The most studied area has been that of gas fluidized solids, principally because of applications in the petroleum industry. Necessity has demanded that the majority of studies be correlative in nature. It is the goal of this work to select a specific type of gas solid fluidization, slugging, and develop an understanding of the basic concepts which determine the behaviour of such a system.

A slugging fluid bed is a system in which slugs of high solids density alternate with regions of low solids density. This study is concerned with linear systems, that is, systems in which there are practically no variations in the directions perpendicular to direction of gas flow. All systems will be batch systems, i.e., beds which have a constant solids inventory. The variables to be studied are bed diameter, bed height, gas and gas velocity. The effect of solids variables is not studied because solids characterizations is a tough problem in itself and would unnecessarily complicate the problem of interest.

When one attempts to develop a technique for prediction, or mathematical model, there are always several alternative routes to investigate. It is fortunate if the first attempt succeeds, but discarded approaches can be quite valuable because of the information gained in the attempt. In this work three approaches were tried; the third was successful. This report will begin with a discussion of the two abandoned approaches because each contains information of value.

The remainder of the discussion will be devoted to the construction, verification and use of a technique for predicting the behaviour of certain fluidized systems.

PRELIMINARY WORK

Part A. Microscopic Approach.

One possible approach to the behaviour of fluid systems, which was not pursued in this investigation, is to consider a single particle and its immediate surroundings. If one could predict the motion of one particle from a knowledge of the properties of fluid surrounding it and of the macroscopic properties of porosity or solids concentration and bed geometry in its vicinity, a firm basis for a microscopic scale model would be established. At least one such attempt has been made. Bowman attempted to describe fluidization by considering events occurring on the microscopic scale and applying statistical methods. Details of this work are apparently not available.(2)

The principles of statistical mechanics are unfortunately not applicable to the motion of a collection of particles which move at ordinary velocities. The number of particles involved is not great enough nor is there any resemblance of a fluidized system to an equilibrium system. Further, the Ergodic hypothesis is not satisfied, that is, the point in phase space representing the system does not pass through all possible states in a short period of time.

A logical procedure would seem to be to write a force balance on an individual particle. The forces to be considered are gravity, buoyancy, impact due to collision, viscous drag, and wall friction in the case of a moving plug section. Such a balance will yield a second order differential equation. Boundary conditions can most likely be written at the bed support, the upper bed surface, and the walls of the bed. This equation, coupled with a continuity equation for the gas, some sort of material balance equation for the solid, and the pressure drop equations for the

gas should permit solution for solids velocity and concentration; gas velocity and density. These are four variables; four equations have been listed. The force balance on an individual particle will be considered first.

One of the most important questions to be answered before any microscopic approach can succeed is the problem of the drag on a particle under conditions varying from isolation to dense packing. The two extreme cases have been treated in detail. The existing correlations for drag on isolated particles are lacking in only two respects: shape is a variable which still cannot be accurately treated; and drag under accelerative conditions still has not been thoroughly investigated. The question of shape is of concern in all cases where one deals with particles of irregular shape; unfortunately, this is most often the case with fluidized solids.

The question of drag on particles in a fixed bed has probably been answered more satisfactorily from an engineering viewpoint. The problem of the effect of shape still exists, but the problem of the effect of acceleration no longer exists. One can, therefore, eliminate a major objection to the use of drag correlations by restricting the materials used to spherical particles.

The weakest area of drag theory is the region of hindered settling. This term is here intended to encompass the entire range of porosity from zero for isolated particles to some value less than one for the packed bed. These are conditions under which an individual particle is partially restricted in its motion by the influence of neighboring particles. However, sufficient information is available to be able to treat this topic quantitatively.

The following would be feasible correlations to use for determining drag forces, or pressure drops which may be converted to average drag force per particle:

1. Isolated sphere: $(\varepsilon = 0.0)$

(1) $$F_D = \frac{1}{2} C_D \rho_f A_p v_r^2 = \frac{\pi}{8} C_D \rho_f D_p^2 v_r^2$$

Plot of C_D versus Re.

2. Hindered settling: $(\varepsilon = 0.0 \text{ to } \varepsilon_{fb})$

(2) $$F_D = \frac{\pi}{8} C_D \rho_f D_p^2 v_r^2$$

Plot of $(Re/C_D)^{1/3}$ versus $(C_D Re^2)^{1/3}$

(A comprehensive plot of this nature appears on page 235 of Zenz and Othmer[12])

3. Fixed bed: $(\varepsilon = \varepsilon_{fb})$

(3) $$\frac{\Delta P}{L} = 2 f \rho_f v_r^2 / g D_p$$

Plot of f versus Re at ε parameters

(A comprehensive plot of this nature appears on page 181 of Zenz and Othmer[12])

These account for the drag force on a particle under all conceivable conditions. A relative velocity, v_R, between particle and fluid, must be used in computing F_D, Re and $\Delta P/L$. One force upon a particle required for writing a force balance is thus determined.

One might next inquire about the impact force upon a particle when it collides with a neighbor. If one further assumes hard particles, or in other words perfectly elastic collisions, the force from one such collision might be represented by a Dirac delta function as follows:

(4) $$F_{impact} = (\overrightarrow{\Delta m v}) \, \delta[\psi(t, x, y, z)]$$

where $(\overrightarrow{\Delta m v})$ represents the momentum exchanged between the colliding particles.

A moment's consideration shows that the form of Ψ should be as follows:

$$(5) \quad \Psi = t_o + 1 / \overline{\overline{\overline{Z}}}_c (t,x,y,z)$$

where $\overline{\overline{\overline{Z}}}_c (t,x,y,z)$ = collision frequency.

This indicates that one must obtain the collision frequency in order to determine the impact force upon a particle.

It is apparent that collision frequency will not depend explicitly on time and position. It will be some explicit function of particle motion and particle concentration or in other words an implicit function of time and position. One can imagine the velocity of a particle to consist of a random component, with equal mean cartesian components, and a non-random component due to drag, bouyant, and gravitational forces. The random component would arise from two sources, turbulent vortices of the fluidizing medium and collisions. A simplified version of this problem, namely the case where only random components exist, is the problem treated by the kinetic theory of gases. This theory produces the collision frequency for this simplified case[4]:

$$(6) \quad \overline{\overline{\overline{Z}}}_c(t,x,y,z) = N_p(t,x,y,z)\, \pi D_p^2 \left(\bar{v}_1^2 + \bar{v}_2^2\right)^{\frac{1}{2}}$$

where N_p (t,x,y,z) number of particles per unit volume
v_1 = average velocity of colliding particle number 1
v_2 = average velocity of colliding particle number 2

If $v_1 = v_2 = \bar{v}$ or for the case of similar particles:

$$(7) \quad \overline{\overline{\overline{Z}}}_c(t,x,y,z) = N_p(t,x,y,z) \sqrt{2}\, \pi\, D_p^2\, \bar{v}$$

However, a particle in a fluid bed definitely possesses a non-random component of velocity. This causes great complication of the mechanics of obtaining an average collision frequency. One must begin

with an assumed statistical distribution of individual particle velocities. A convenient and reasonable assumption is that the two horizontal components of particle velocity are normally distributed about a zero mean and that the vertical component is normally distributed about a non-zero mean which is a function of time and position. These distribution functions are:

$$(8) \quad P(V_x) = \frac{1}{\sigma_x \sqrt{2\pi}} e^{-\frac{V_x^2}{2\sigma_x^2}}$$

$$(9) \quad P(V_y) = \frac{1}{\sigma_y \sqrt{2\pi}} e^{-\frac{V_y^2}{2\sigma_y^2}}$$

$$(10) \quad P(V_z) = \frac{1}{\sigma_z \sqrt{2\pi}} e^{-\frac{(V_z - w(x,y,z))^2}{2\sigma_z^2}}$$

where w(x,y,z) is the non-random vertical velocity component. If one further assumes that

$$\sigma_x = \sigma_y = \sigma_z = \sigma$$

one may obtain the distribution of particle speeds:

$$(11) \quad P(c) = \frac{2c}{w\sigma\sqrt{2\pi}} e^{-\frac{(c^2+w^2)}{2\sigma^2}} \sinh\left(\frac{cw}{\sigma^2}\right)$$

Details of the development of Equation (11) are included in Appendix A. Geometrical considerations show that the number of collisions between a particle moving with speed c with stationary particles of concentration N_p per unit volume is:

$$(12) \quad \mathcal{Z}_c = N_p(t,x,y,z)\,\pi\, D_p^2\, c$$

Details of the development of Equation (12) are included in Appendix A. If one is dealing with a set of particlesnormally distributed about a mean diameter $\overline{D_p}$ with a standard deviation σ_1, an immediate average over

particle diameters yields:

$$(13)\quad \bar{\bar{Z}}_c = N_p(t,x,y,z)\,\pi c\left[\bar{D}_p^2 + \sigma_1^2/4\right]$$

Details of the development of Equation (13) are included in Appendix A. Thus, if one defined d_p by

$$(14)\quad d_p^2 = \left[\bar{D}_p^2 + \sigma_1^2/4\right]$$

then

$$(15)\quad \bar{\bar{Z}}_c = N_p(t,x,y,z)\,c\pi d_p^2$$

Equation (15) holds for a particle moving at a fixed speed c through stationary particles. What is desired is an expression for collision frequency of particle whose speed is distributed according to Equation (11) with particles whose speeds are distributed according to Equation (11). Averaging $\bar{Z}_c$ over the speeds of the particles, one obtains:

$$(16)\quad \bar{\bar{Z}}_c = \frac{\sqrt{2\pi}\,N_p\,\sigma\,d_p^2}{6\varepsilon\gamma}\left\{\left[2(\varepsilon+\gamma)^3+3(\varepsilon+\gamma)\right]\left[\frac{\sqrt{\pi}}{2}\,\mathrm{erf}(\varepsilon+\gamma)\right]\right.$$
$$-\left[2(\varepsilon-\gamma)^3+3(\varepsilon-\gamma)\right]\left[\frac{\sqrt{\pi}}{2}\,\mathrm{erf}(\varepsilon-\gamma)\right]$$
$$\left.+\,e^{-(\varepsilon+\gamma)^2}\left[(\varepsilon+\gamma)^2+1\right]-e^{-(\varepsilon-\gamma)^2}\left[(\varepsilon-\gamma)^2+1\right]\right\}$$

where $\varepsilon = \dfrac{c}{\sqrt{2}\,\sigma}$ (dimensionless)

and $\gamma = \dfrac{w}{\sqrt{2}\,\sigma}$ (dimensionless)

Details of the development of Equation (16) are included in Appendix A.

Equation (16) holds for a particle moving at fixed speed c through particles whose speeds are distributed according to Equation (11). Averaging $\overline{\overline{Z}}_c$ over the speeds of the particle under consideration, one obtains:

$$(17)\quad \overline{\overline{Z}}_c = 4\sqrt{\pi}\, N_p \sigma d_p^2 \left\{ \frac{1}{6}\left[\frac{e^{-2\gamma^2} - 1}{\gamma^2} \right] + \frac{\sqrt{2}}{6}\left(4\gamma + \frac{3}{\gamma}\right)\frac{\sqrt{\pi}}{2}\,\mathrm{erf}(\sqrt{2}\,\gamma) + \frac{2}{6}e^{-2\gamma^2} \right\}$$

where again $\gamma = \dfrac{w}{\sqrt{2}\,\sigma}$

Details of the development of Equation (17) are included in Appendix A. The average collision frequency is thus seen to be a function of the non-random velocity component, the particle concentration, and the standard deviation of the distribution of random particle velocity components.

At this point it becomes apparent that the terms involved in setting up just a force balance on a single particle are complex and nonlinear to such an extent that there can be no hope of an analytical solution. Numerical solutions would at best be very difficult.

The microscopic approach was abandoned for these reasons.

Part B. Macroscopic Approach

In the foregoing discussion it was not necessary to limit in any way the type of fluidization under consideration. Appropriate equations and boundary conditions would conceivably handle all imaginable cases. The macroscopic approach does, however, necessitate the formulation of certain assumptions concerning the geometry and operation of the fluidized system to be described. The remainder of this work will be concerned with systems that:

1. Consist of only two phases, gas and solid.
2. Are batch systems, that is, systems with a constant solids inventory.
3. Operate in the slugging regime of fluidization.
4. Are vertical in orientation.

A slugging fluid bed is one in which regions of low solids concentration completely fill the bed cross section and alternate with regions of high solids concentration which also completely fill the bed cross section. A slug is a region of solids concentration in the range from the solids concentration of a bed at incipient fluidization to the fixed bed solids concentration. A void space is a region of lower solids concentration. A bubbling bed is a fluid bed in which void spaces exist but do not fill the entire bed cross section.

Let us now consider a system consisting of one slug. Figure 1 will be of assistance in visualizing the variables to be discussed. There is some superficial gas velocity in the system, v_g. The length

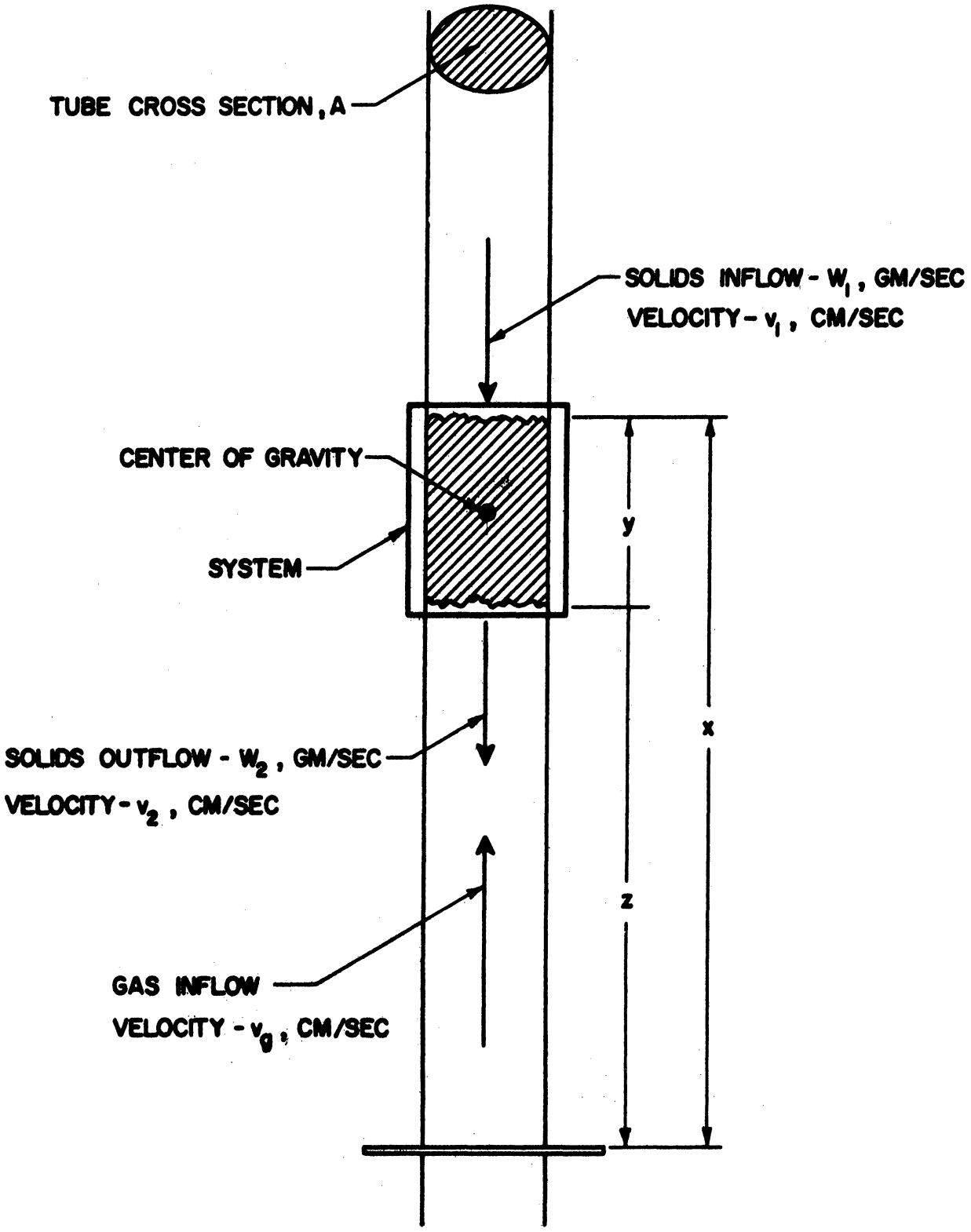

Figure 1. Physical Description of Terms Used in Discussing Slugging Fluidization.

of the slug is y. The elevation of the upper surface is x with respect to some arbitrary reference level. The elevation of the lower surface is z, so by definition:

$$(18) \quad X = Y + Z$$

The solids density in the slug is assumed to be constant and given by ρ_s. Consequently the mass of the slug is:

$$(19) \quad m = \rho_s A y$$

If there is a mass flow into the top of the slug of w_1 and a mass flow from the bottom of w_2, the mass balance for the system is:

$$(20) \quad \frac{dm}{dt} = w_1 - w_2 = \rho_s A \dot{y}$$

The momentum balance for the system will be considered next. Its form is:

$$(21) \quad \frac{d(mv)_{SYS}}{dt} = \sum \text{external forces} + \frac{mV_{IN}}{\text{time}} - \frac{mV_{OUT}}{\text{time}}$$

For purposes of a momentum balance, the velocity of the system is the velocity of its center of mass:

$$(22) \quad V_{c.g.} = \frac{d\left(x - \frac{1}{2}y\right)}{dt} = \dot{x} - \frac{1}{2}\dot{y}$$

The gravitational force on the system is:

$$(23) \quad F_g = \rho_s A y g$$

The frictional force exerted by the wall should be negligible if the slug is at incipient fluidization, for at that point drag renders the

particles weightless and hence they can exert no normal force on the wall. The momentum carried in by solids inflow is:

$$(24)\quad \text{Rate of momentum in} = W_1 V_1$$

The momentum transported out of the system by solids outflow presents a small problem. When a solid particle leaves the lower surface of the slug, it leaves at the slip velocity of the slug. The slip velocity of the slug is the velocity of a particle within the slug relative to the bed wall. From the moment the particles leave, they begin accelerating until they reach terminal velocity or encounter another slug. The slip velocity of the slug may be defined in two ways:

$$(25)\quad V_S = \dot{X} - \frac{W_1}{\rho_S A} = \dot{Z} - \frac{W_2}{\rho_S A}$$

Therefore the momentum transported out with the effluent solids is:

$$(26)\quad \text{Rate of momentum out} = W_2\left(\dot{Z} - \frac{W_2}{\rho_S A}\right) = W_2\left(\dot{X} - \frac{W_1}{\rho_S A}\right)$$

Buoyancy will of course contribute a term to the momentum balance.

$$(27)\quad F_b = A y (1-\varepsilon)\rho_g$$

This term is small and may be neglected in comparison to gravitational forces.

The most important external force is the pressure differential across the slug. This pressure drop is the sole agent tending to cause the slug to slip in the upward direction. The question is that of predicting the pressure drop through the slug for varying gas velocities.

If the slug is assumed to be at the state of incipient fluidization, this pressure drop is a known constant quantity. This is true because the pressure drop at incipient fluidization is a characteristic and well defined value. For batch beds, one may write:

$$(28)\quad -\left(\frac{\Delta P}{L}\right)_{INCIP.\ FL.} = \rho_{bed}\, g = \rho_s\, g = K$$

This is merely a mathematical statement of the fact that at incipient fluidization, pressure forces balance gravitational forces.

If the velocity of the fluidizing gas is increased beyond the point of incipient fluidization, no further increase in the bed pressure drop is observed. This indicates that the same ΔP prevails from the incipient fluidization velocity to some higher velocity, presumably near the velocity where dilute phase fluidization begins. At gas velocities below incipient fluidization, the pressure drop relations for packed beds apply. It is conceivable that a moving slug could experience a gas velocity, relative to the moving slug, less than that required for incipient fluidization. Since the fixed bed pressure drop correlations are not simple in nature, a linear approximation will be made for purposes of simplicity. Thus approximation will be valid if physical conditions do not stray too far below the point of incipient fluidization. The approximation is the following:

$$(29)\quad -\left(\frac{\Delta P}{L}\right) = K\,\frac{(V_g - V_s)}{V_{gmf}} \qquad V_s > V_g - V_{gmf}$$

Thus the pressure force exerted on a slug is given by

$$(30)\quad \begin{aligned} F_P &= KAy && V_s \leq V_g - V_{gmf} \\ &= KAy\,(V_g - V_s)/V_{gmf} && V_s > V_g - V_{gmf} \end{aligned}$$

All elements necessary for a momentum balance have been considered.

The momentum balance is:

$$(31)\quad \frac{d}{dt}\left[\rho_s A y\left(\dot{x}-\tfrac{1}{2}\dot{y}\right)\right]=\left[\frac{K}{\rho_s}-g\right]\rho_s A y + W_1 u_1 - W_2\left[\dot{x}-\frac{W_1}{\rho_s A}\right]$$

$$V_s \leqq V_g - V_{gmf}$$

$$(32)\quad \frac{d}{dt}\left[\rho_s A y\left(\dot{x}-\tfrac{1}{2}\dot{y}\right)\right]=\left[\frac{K}{\rho_s}\left[\frac{\left(V_g-\dot{x}+\frac{W_1}{\rho_s A}\right)}{V_{gmf}}\right]-g\right]\rho_s A y + W_1 u_1 - W_2\left[\dot{x}-\frac{W_1}{\rho_s A}\right]$$

$$V_s > V_g - V_{gmf}$$

The term $\left[\frac{K}{\rho_s}-g\right]$ in Equation (31) should be equal to zero, according to Equation (28), if theory were precisely upheld, but this is not necessarily the case. It will, therefore be left in Equation (31). Since ρ_s and A are constant, the momentum balance may be reduced to:

$$(33)\quad \dot{y}\left(\dot{x}-\tfrac{1}{2}\dot{y}\right)+y\left(\ddot{x}-\tfrac{1}{2}\ddot{y}\right)=\left(\frac{K}{\rho_s}-g\right)y+\frac{W_1 u_1}{\rho_s A} - \frac{W_2}{\rho_s A}\left[\dot{x}-\frac{W_1}{\rho_s A}\right]$$

$$V_s \leqq V_g - V_{gmf}$$

$$(34)\quad \dot{y}\left(\dot{x}-\tfrac{1}{2}\dot{y}\right)+y\left(\ddot{x}-\tfrac{1}{2}\ddot{y}\right)=\left[\frac{K}{\rho_s}\left[\frac{\left(V_g-\dot{x}+\frac{W_1}{\rho_s A}\right)}{V_{gmf}}\right]-g\right]y + \frac{W_1 u_1}{\rho_s A} - \frac{W_2}{\rho_s A}\left[\dot{x}-\frac{W_1}{\rho_s A}\right]$$

$$V_s > V_g - V_{gmf}$$

These two balances, mass and momentum, suffice to describe the movements of the slug. An energy balance may also be written, but it is not independent of the mass and momentum balances.

One further assumption may be made at this point, with no experimental justification. The solids flow into and out of a slug may be considered to be equal and the same for all slugs in the system. This seems reasonable if the rate controlling event is the rate at which particles can disengage from the slug. Changes in gas velocity relative to the disengaging particles should have but little effect on disengaging rate since for all velocities in excess of the minimum fluidization velocity, particles are exposed to interstitial velocities in excess of the terminal particle velocity. The particles therefore do not fall until disengaged from the bulk of the slug. Therefore let:

$$\Theta = \frac{W_1}{\rho_s A} = \frac{W_2}{\rho_s A} \tag{35}$$

Equations (33) and (34) then become, upon substitution of Equations (35):

$$\dot{y}\left(\dot{x}-\tfrac{1}{2}\dot{y}\right)+y\left(\ddot{x}-\tfrac{1}{2}\ddot{y}\right)=\left(\frac{K}{\rho_s}-g\right)y+\Theta u_1-\Theta(\dot{x}-\Theta) \tag{36}$$

$V_s \leqq V_g - V_{gmf}$

$$\dot{y}\left(\dot{x}-\tfrac{1}{2}\dot{y}\right)+y\left(\ddot{x}-\tfrac{1}{2}\ddot{y}\right)=\left[\frac{K}{\rho_s}\left[\frac{V_g-\dot{x}+\Theta}{V_{gmf}}\right]-g\right]y + \Theta u_1-\Theta(\dot{x}-\Theta) \tag{37}$$

$V_s > V_g - V_{gmf}$

The mass balance, Equation (20), then becomes, for the case of solids inflow and solids outflow:

$$\dot{y} = 0 \tag{38}$$

There are four separate cases to be considered. Each of these cases could conceivably exist in a slugging fluid bed. Figure 2 shows each case schematically. The above equations have been written for case 4. In all four cases, a set of boundary conditions is required for the solution for slug motion. These conditions are specified as:

$$y = y_o \quad \text{when} \quad t = t_o = 0 \tag{39}$$

$$X = X_o \quad \text{when} \quad t = t_o = 0 \tag{40}$$

$$\dot{X} = \dot{X}_o \quad \text{when} \quad t = t_o = 0 \tag{41}$$

The velocity, u, is assumed to be the velocity of the particles with respect to the bed wall and hence will vary with gas velocity. However, if one remains in a region where particle terminal velocity is far greater than gas velocity, a good approximation is that u is constant and equal to the average terminal velocity of the particles in the stagnant gas. With these assumptions, all four cases can be solved.

Case 1. No solids inflow or outflow. The equations to be solved are:

The mass balance:

$$\dot{y} = 0 \tag{42}$$

The two cases of the momentum balance:

$$y\ddot{X} = \left(\frac{K}{\rho_s} - g\right) y \qquad V_s \leqq V_g - V_{gmf} \tag{43}$$

$$y\ddot{X} = \left[\frac{K}{\rho_s}\left[\frac{V_g - \dot{X}}{V_{gmf}}\right] - g\right] y \qquad V_s > V_g - V_{gmf} \tag{44}$$

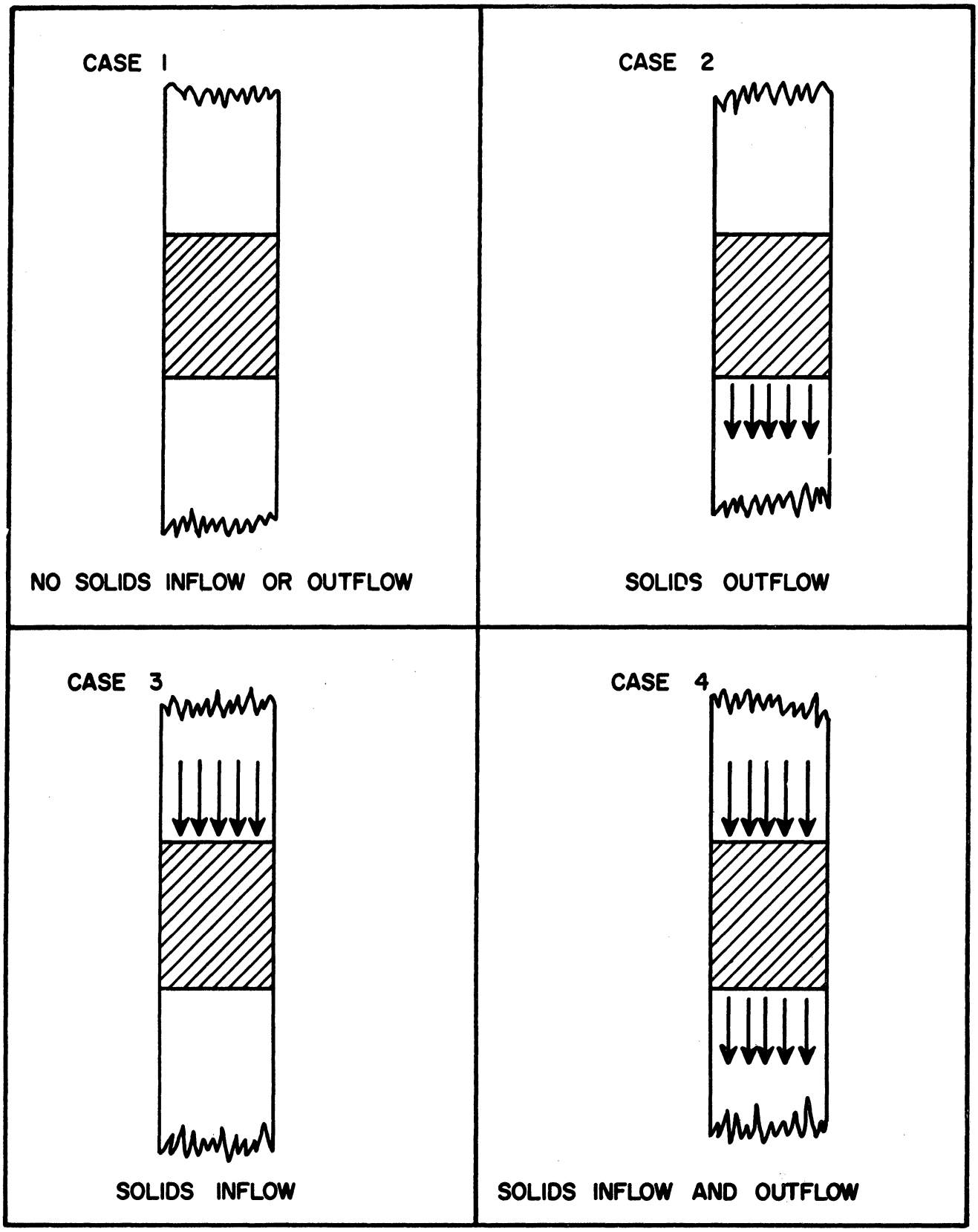

Figure 2. Four Individual Cases of Slugs Which May Exist in a Slugging Fluid Bed.

For simplicity, let $$\left[\frac{K}{\rho_s} - g\right] = c$$

The solutions of these equations yield:

(45) $$y = y_o$$

(46) $$x = x_o + \dot{x}_o t + \frac{c}{2} t^2 \qquad v_s \leqq v_g - v_{gmf}$$

(47) $$x = x_o e^{-At} + \frac{(\dot{x}_o + Ax_o)}{A}(1 - e^{-At}) + \frac{(Av_g - g)}{A^2}(e^{-At} + At - 1)$$

$$v_s > v_g - v_{gmf}$$

where $A = \dfrac{K}{v_{gmf}\rho_s}$

The details of solution are given in Appendix B.

Case 2. Solids outflow only.

In this case the mass balance is:

(48) $$\dot{y} = -\theta$$

The two forms of the momentum balance are, upon simplification:

(49) $$\ddot{x} = c + \frac{1}{2}\frac{\theta^2}{y} \qquad v_s \leqq v_g - v_{gmf}$$

(50) $$\ddot{x} = \left[\frac{K}{\rho_s}\left[\frac{v_g - \dot{x}}{v_{gmf}}\right] - g\right] + \frac{1}{2}\frac{\theta^2}{y}$$

$$v_s > v_g - v_{gmf}$$

The solution of these equations is more difficult than in Case 1, the solutions being:

(51) $$y = y_o - \theta t$$

$$(52)\quad x = x_o + (\dot{x}_o + \frac{\theta}{2})t + \frac{c}{2}t^2 + \frac{y}{2}\ln\frac{y}{y_o}$$

$$v_s \leqq v_g - v_{gmf}$$

$$(53)\quad x = x_o + \left[\frac{Av_g - g}{A}\right]t + \left[\frac{g - A(v_g - \dot{x}_o)}{A^2}\right]\left[1 - e^{-At}\right]$$

$$- \frac{1}{2}\frac{\theta}{A}\ln\frac{y}{y_o}\left[1 - e^{\frac{Ay}{\theta}}\right] + \frac{1}{2}\frac{\theta}{A}e^{\frac{Ay}{\theta}}\sum_{n=1}^{\infty}\frac{(-1)^n\left(\frac{A}{\theta}\right)^n(y^n - y_o^n)}{n\cdot n!}$$

$$v_s > v_g - v_{gmf}$$

The details of these solutions are shown in Appendix B.

Case 3. Solids inflow only.

The mass balance becomes:

$$(54)\quad \dot{y} = \theta$$

The momentum balances become:

$$(55)\quad \ddot{x} = c + \frac{\theta u_1}{y} + \frac{1}{2}\frac{\theta^2}{y} - \frac{\theta\dot{x}}{y} \qquad v_s \leqq v_g - v_{gmf}$$

$$(56)\quad \ddot{x} = A(v_g - \dot{x} + \theta) - g + \frac{\theta u_1}{y} + \frac{1}{2}\frac{\theta^2}{y} - \frac{\theta\dot{x}}{y}$$

$$v_s > v_g - v_{gmf}$$

The solution of these equations, detailed in Appendix B, is:

$$(57)\quad y = y_o + \theta t$$

$$(58)\quad x = x_o + \left[\frac{\dot{x}_o y_o}{\theta} - \frac{c y_o^2}{2\theta^2} - \frac{y_o(u_1 + \frac{1}{2}\theta)}{\theta}\right]\ln\frac{y}{y_o}$$

$$+ \frac{(u_1 + \frac{1}{2}\theta)}{\theta}(y - y_o) + \frac{c}{4\theta^2}(y^2 - y_o^2)$$

$$v_s \leqq v_g - v_{gmf}$$

$$(59)\quad X = X_0 + e^{\frac{Ay_0}{\theta}}\left[\frac{\dot{X}_0 y_0}{\theta} - \frac{D y_0}{\theta A} + \frac{D}{A^2} - \frac{E}{A}\right]\left[\ln\frac{y}{y_0} + \sum_{n=1}^{\infty}\frac{(-1)^n (A/\theta)^n (y^n - y_0^n)}{n \cdot n!}\right] + \frac{D}{\theta A}(y - y_0) + \left[\frac{E}{A} - \frac{D}{A^2}\right]\ln\frac{y}{y_0}$$

$V_s > V_g - V_{gmf}$

where $A = K/\rho_s V_{gmf}$

$D = A(V_g + \theta) - g$

$E = (u_1 + \frac{1}{2}\theta)$

Case 4. Solids inflow and solids outflow.

The mass balance in this case is given by Equation (38). The two cases of the momentum balance are given in Equations (36) and (37). Again, just the final solution of these equations will be presented, the details to be found in Appendix B.

Solution of the mass balance:

$$(60)\quad y = y_0$$

Solution of the momentum balance:

$$(61)\quad X = X_0 + \frac{\dot{X}_0 y_0}{\theta}\left[1 - e^{\frac{-\theta t}{y_0}}\right] + \frac{\alpha y_0}{\theta} t - \frac{\alpha y_0^2}{\theta^2}\left[1 - e^{\frac{-\theta t}{y_0}}\right]$$

$V_s \leqq V_g - V_{gmf}$

where $\alpha = C + \frac{\theta u_1}{y_0} + \frac{\theta^2}{y_0}$

$$(62)\quad X = X_0 + \frac{\dot{X}_0}{\gamma_1}\left[1 - e^{-\gamma_1 t}\right] + \frac{\beta}{\gamma_1} t - \frac{\beta}{\gamma_1^2}\left[1 - e^{-\gamma_1 t}\right]$$

$V_s > V_g - V_{gmf}$

where $\gamma_1 = A + \frac{\theta}{y_0}$

$\beta = A(V_g + \theta) - g + \frac{\theta u_1}{y_0} + \frac{\theta^2}{y_0}$

These equations should describe the slug in question under all circumstances. They are to be applied to a system of n slugs in a slugging fluid bed. However, the extreme complexity of these equations is discouraging, since there would be 2n of them. Further, in order to couple the equations, some assumptions must be made as to the time delay involved in the transfer of material by the raining process from a slug to its next lowest neighbor. A further complication would be the disappearance and appearance of slugs in the system; the number of slugs is observed to change with time. And, as time progresses, the equations which describe a slug can change in two ways. The first is a change from one momentum balance to another within the same case. Also, the case which applies to a given slug may change.

These reasons make it extremely doubtful that any realistic and accurate results can be obtained from this particular mathematical model. Any results would be obtained numerically at the expense of a great deal of effort. Certainly some simpler approach would be indicated if at all possible. Hence, although this approach is not necessarily the wrong one, it was abandoned.

PROPOSED MODEL FOR SLUGGING FLUID BEDS

The slug models in the unsteady state case just discussed appear unattractive for only one reason: the complexity of the mathematical description. The term unsteady state is here intended to mean that slugs accelerate and decelerate. Therefore, before becoming lost in the intricacies of mathematical analysis, it was deemed wise to begin with the most highly simplified version of the macroscopic slug model and discard simplifying assumptions as they proved invalid.

A possible set of assumptions is the following:

1. There are no radial variations in solids concentration.
2. The system consists of well defined slugs separated by "void" spaces.
3. These slugs do not accelerate or decelerate for any finite period of time.
4. There is a known process of slug generation.
5. There is a unique solids flow rate through the "void" spaces when such a flow exists.
6. Material falls through a "void" space at a velocity which is very large compared to all other velocities in the system.
7. Only one system at a time can be dealt with; that is, one bed, one type of solid, and one gas.
8. There is no friction between slug and wall.
9. There is a negligible gas pressure drop in a "void" space.
10. Gas flows through a slug at the velocity for minimum fluidization.

These assumptions will be supported at appropriate points in the following discussion. Some can be supported a posteriori only.

Let us now examine the implications of these assumptions. First of all, if the superficial (based on tube cross section) gas velocity through a slug is the minimum fluidization velocity, the pressure drop per unit length of that slug must be the pressure drop per unit length of bed at incipient fluidization. This variable will therefore be of interest in any discussion of pressure fluctuations within the bed.

Second, if there is a unique solids flow for a given system, it will be desirable to know it, a priori if possible. This variable will be of paramount interest in examining fluctuation frequencies and bed configurations.

Third, if any or all of the four possible cases of slugs discussed in the preceeding section are present in a system, one must know which case exists when and at what location.

Finally, some sort of description of slug generation must be formulated. There must exist some mechanism by which slugs come into being at the bottom of the bed; otherwise the slugging regime could not exist in a batch system.

These then are four points which must be investigated experimentally to complement the description of the behaviour of the slugs in the system. Each will be treated later in turn. However, the kernel of the overall model is the set of equations describing slug behaviour. Therefore, these equations will be developed before proceeding to examine these complementary areas.

The equations governing the motion of a slug of any of the four types mentioned proceed very easily from the assumptions. If one defines:

V_g = total superficial gas velocity

V_{gmf} = superficial gas velocity at incipient fluidization

then one may define an excess velocity:

$V_{xs} = V_g - V_{gmf}$ = superficial gas velocity in excess of that required for incipient fluidization.

This excess velocity is the component of the total gas velocity which moves through the bed as void spaces or, in large diameter beds, as bubbles. It follows that a void space which occupies the entire tube diameter must move with this excess gas velocity, provided that there is no solids flow through the void. Consequently, the solid slug above it will also slip with that linear velocity if there is no solids flow into or out of the slug.

If one now adds a solids flow through the void space, the velocity of the void space will increase proportionally, but its volume will remain the same. The volume lost by the upper bounding slug will immediately be gained by the lower bounding slug. However, the slug above the void will continue to slip at V_{xs}. The upper and lower boundaries of the slug may have an additional component of velocity proportional to the solids downflow rate.

These concepts may be formulated mathematically as follows. Let

w = solids downflow rate, gm/sec

A = tube cross section, cm^2

ρ_s = density of a slug, gm/cm^3

Define

$$\theta = \frac{W}{A\rho_s}$$

Recalling Figures 1 and 2, let us now describe each slug case.

Case 1. No solids inflow or outflow.

The mass balance, as previously, is:

$$(63)\quad \dot{y} = 0 \qquad \text{or} \qquad y = y_o$$

The velocity of the various surfaces are given by:

$$(64)\quad \dot{x} = V_{xs} \qquad \text{or} \qquad x - x_o = V_{xs}(t - t_o)$$

$$(65)\quad \dot{z} = V_{xs} \qquad \text{or} \qquad z - z_o = V_{xs}(t - t_o)$$

Case 2. Solids outflow only.

The mass balance is:

$$(66)\quad \dot{y} = -\theta \qquad \text{or} \qquad y - y_o = -\theta(t - t_o)$$

The velocities of the upper and lower surfaces are:

$$(67)\quad \dot{x} = V_{xs} \qquad \text{or} \qquad x - x_o = V_{xs}(t - t_o)$$

$$(68)\quad \dot{z} = V_{xs} + \theta \qquad \text{or} \qquad z - z_o = (V_{xs} + \theta)(t - t_o)$$

Case 3. Solids inflow only.

The mass balance is:

$$(69)\quad \dot{y} = \theta \qquad \text{or} \qquad y - y_o = \theta(t - t_o)$$

The velocities of the bounding surfaces are :

$$(70)\quad \dot{x} = V_{xs} + \theta \qquad \text{or} \qquad x - x_o = (V_{xs} + \theta)(t - t_o)$$

$$(71)\quad \dot{z} = V_{xs} \qquad \text{or} \qquad z - z_o = V_{xs}(t - t_o)$$

Case 4. Solids inflow and solids outflow.

The mass balance is:

$$(72)\quad \dot{y} = 0 \qquad \text{or} \qquad y - y_o = 0$$

The velocities involved are:

$$(73)\quad \dot{x} = V_{xs} + \theta \qquad \text{or} \qquad x - x_o = (V_{xs} + \theta)(t - t_o)$$

$$(74)\quad \dot{z} = V_{xs} + \theta \qquad \text{or} \qquad z - z_o = (V_{xs} + \theta)(t - t_o)$$

These equations represent a complete description of the configuration of each type slug as a function of time. Their ultimate use will be postponed until the four complementary areas mentioned above have been investigated.

The success or failure of the model will, as has already been mentioned, be judged on the basis of how accurately it can predict two quantities: the pressure profile of the bed as a function of time and the fluctuation frequencies of the bed. With this goal in mind, the four areas requiring investigation were studied.

BED PRESSURE DROPS AT INCIPIENT FLUIDIZATION

A. Equipment

The determination of the bed pressure drop at incipient fluidization is a relatively easy quantity to measure. The only requirements are two pressure taps, one below the bed support and one above the bed, a means of measuring gas velocity, and a manometer. The rotameters used to measure gas flow were Manostat "Predictability" flowmeters. The calibrations of these instruments is discussed in Appendix C. The manometer used was filled with tetrabromoethane and was connected differentially between the two taps mentioned above.

All flow rates were measured upstream from a sonic flow orifice (needle valve) so as to eliminate any fluctuations in the level of the rotameter float which might arise from fluctuations in the bed. This means all rotameter readings were taken at rotameter pressures at least twice the downstream pressure at the sonic flow orifice. Rotameter pressures were read from pressure gauge C2-174, the calibration of which appears in Appendix C.

The various tubes used were all preceded by a packed calming section. The intent was to distribute gas flow to the bed support as evenly as possible. The diameter of the calming section was, in all cases, three inches. The packing consisted of a 10 inch lower section of 3/4" crushed stone separated by a coarse screen from a two inch deep upper section packed with 6mm glass beads. Two inches of free space remained between the top of the packed section and the bed support.

The bed was supported by a wire cloth with 30μ mesh openings. This support was oriented as horizontally as possible. The tube was aligned as close to vertical as was possible. An expansion head topped the tube in order to prevent any solids carry over. A diagram of the apparatus appears in Figure 3.

B. Procedure.

The bed was prepared by pouring the solid into the tube through the expansion head. Bed height was measured with the solid in the resulting loose packed state. The tube was then tapped until no further settling of the solid was observed. The change of bed height with tapping was less than 5% for all solids used. The bed height at minimum fluidization also varied less than 5% from the poured height.

The remainder of the procedure is completely straightforward. The rotameter was set at a given reading and a period of a few minutes was allowed for transients to disappear. The manometer was then read.

C. Results.

It was assumed at the outset that the bed support contributed a negligible pressure drop to the measured bed pressure drop. This assumption was later verified. Figures 4 through 10 show the experimentally determined curves of total bed pressure drop versus linear

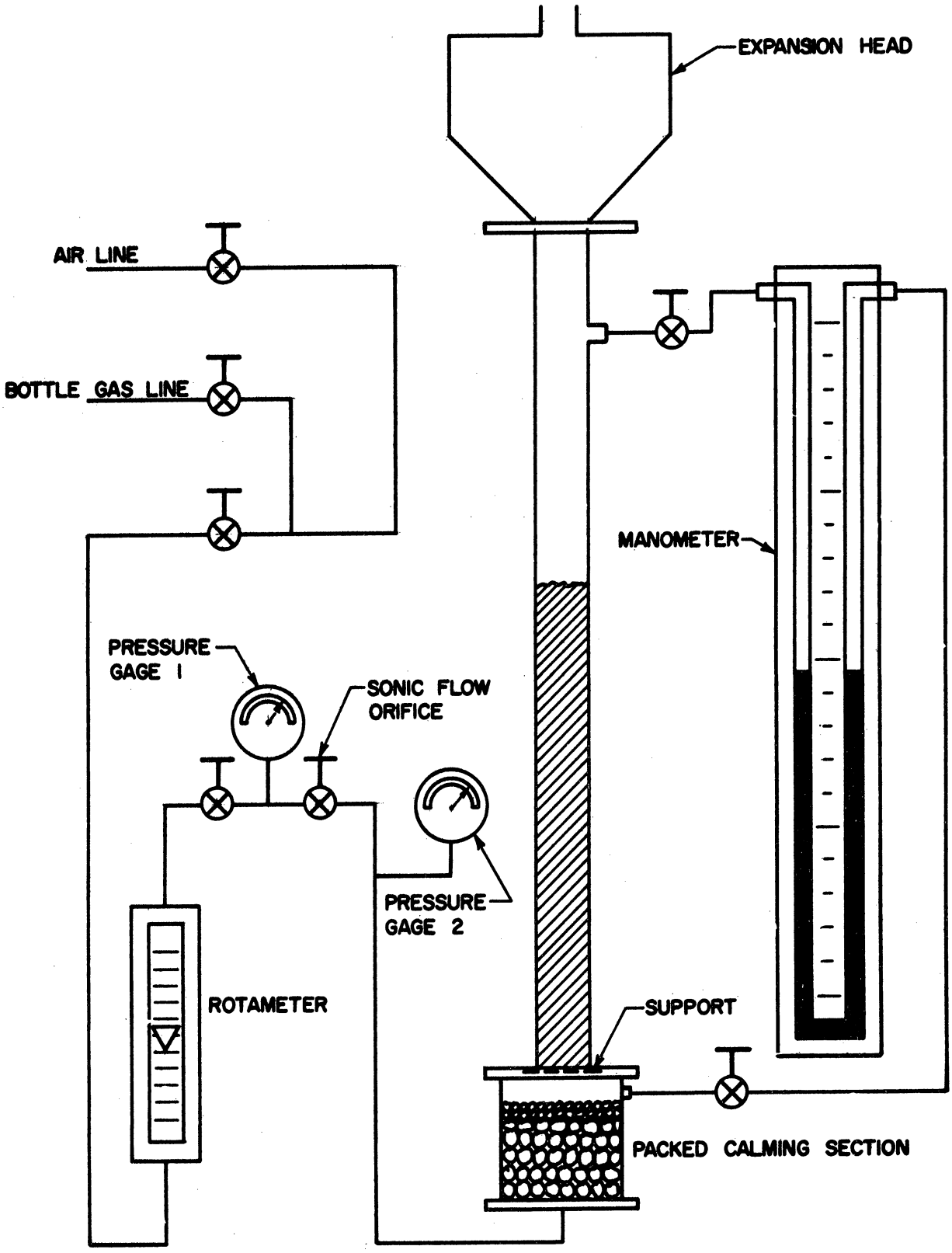

Figure 3. Experimental Equipment for Measuring Total Bed Pressure Drop.

TABLE I

Total bed pressure drop versus linear gas velocity.

System: 1. Air-sand A (100-150 mesh)
2. 2" diameter bed.
3. 74.0 cm. bed height.

Linear gas velocity at latm and 60°F. cm/sec	Total bed pressure drop, inches of tbe.*
0.00	0.00
0.90	2.3
1.30	5.4
1.85	8.6
2.40	11.0
3.60	14.7
4.80	15.3
6.00	15.5
7.45	15.8
10.20	16.2

*tbe. tetrabromoethane. One inch tbe.=0.107 psig.

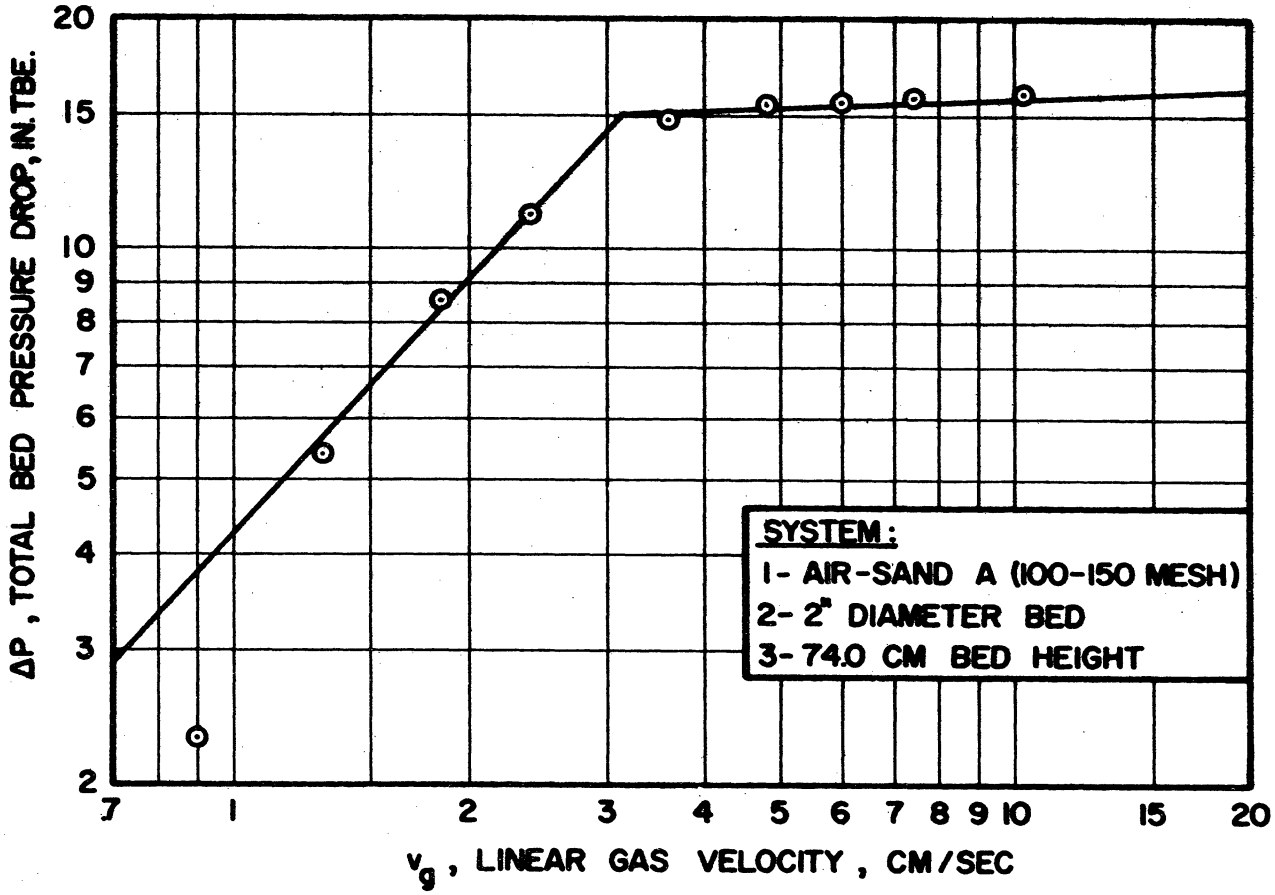

Figure 4. Total Bed Pressure Drop Versus Linear Gas Velocity.

TABLE II

Total bed pressure drop versus linear gas velocity.

System: 1. Helium-Sand A. (100-150 mesh)
2. 2" diameter bed.
3. 72.0 cm. bed height.

Linear gas velocity at latm and 60°F. cm/sec	Total bed pressure drop, inches of tbe.
0.00	0.00
0.30	1.2
1.10	3.7
2.40	9.3
3.90	13.6
5.60	14.4
7.30	14.8
9.10	15.0

BLANK PAGE

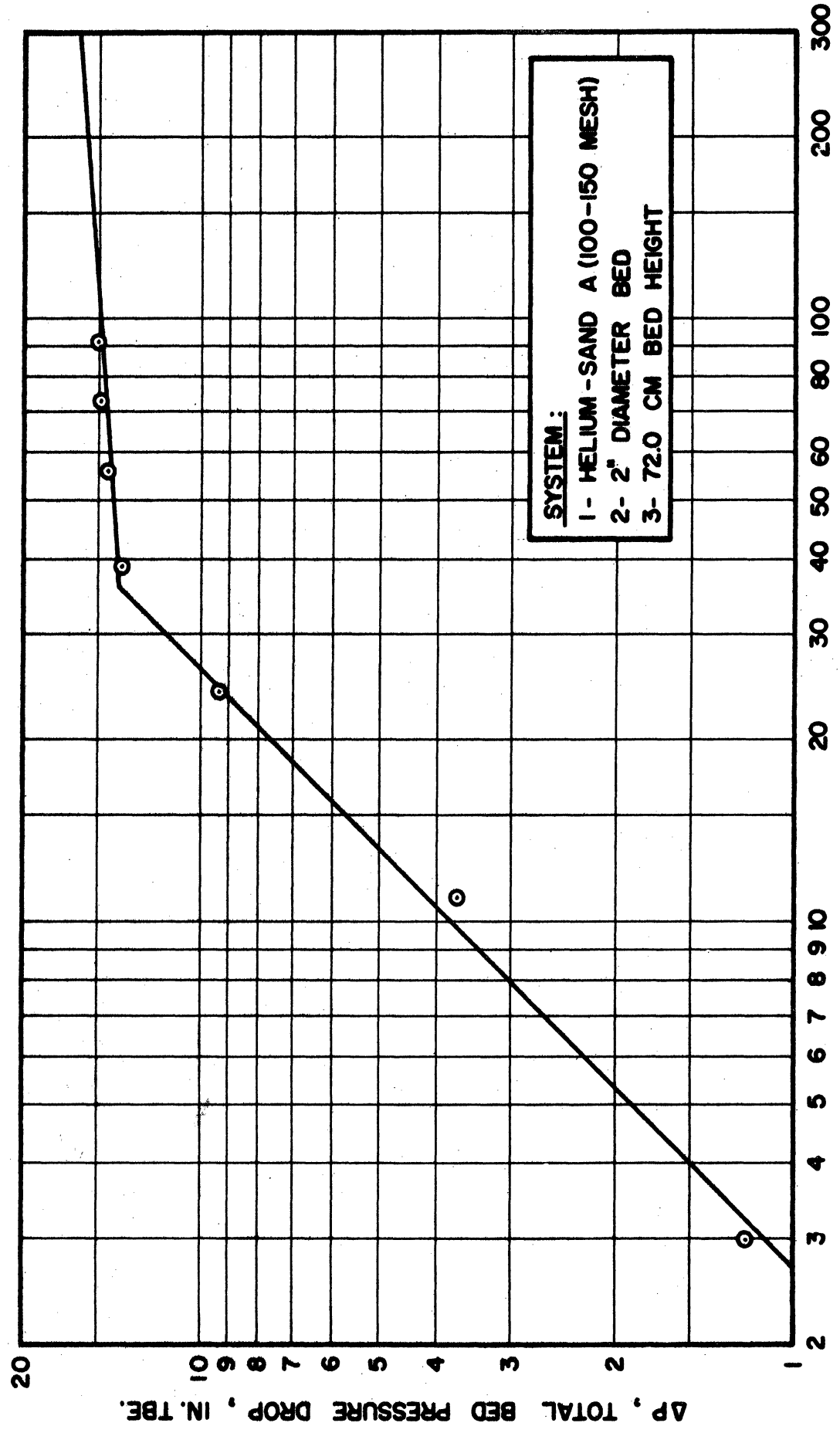

Figure 5. Total Bed Pressure Drop Versus Linear Gas Velocity.

TABLE III

Total bed pressure drop versus linear gas velocity.

System: 1. Air-Sand A (100-150 mesh)
2. 1" diameter bed.
3. 21.2 cm. bed height.

Linear gas velocity at latm and 60°F. cm/sec	Total bed pressure drop, inches of tbe.
0.00	0.00
0.19	0.38
0.30	0.83
0.44	1.36
0.59	1.91
0.77	2.53
1.00	3.25
1.28	3.92
1.58	3.82
1.73	3.92
2.06	4.08
2.31	4.10
2.64	4.14
3.04	4.20
3.44	4.26

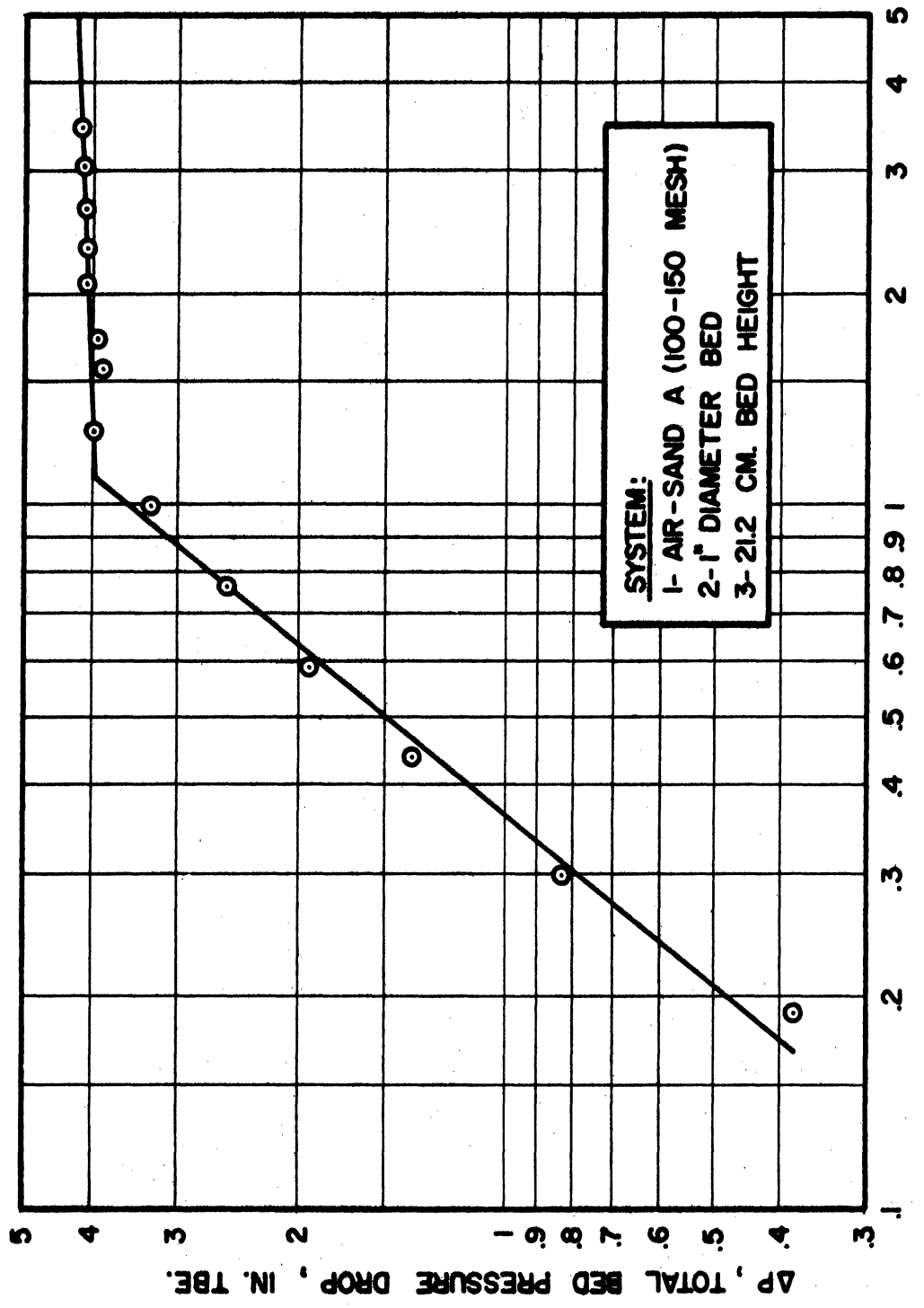

Figure 6. Total Bed Pressure Drop Versus Linear Gas Velocity.

TABLE IV

Total bed pressure drop versus linear gas velocity.

System: 1. Air-Sand A (100-150 mesh)
2. 1" diameter bed.
3. 58.0 cm. bed height

Linear gas velocity at latm and 60°F. cm/sec	Total bed pressure drop, inches of tbe.
0.00	0.00
0.92	2.55
1.60	8.10
2.42	13.48
3.50	11.88
4.83	12.60
6.04	13.10

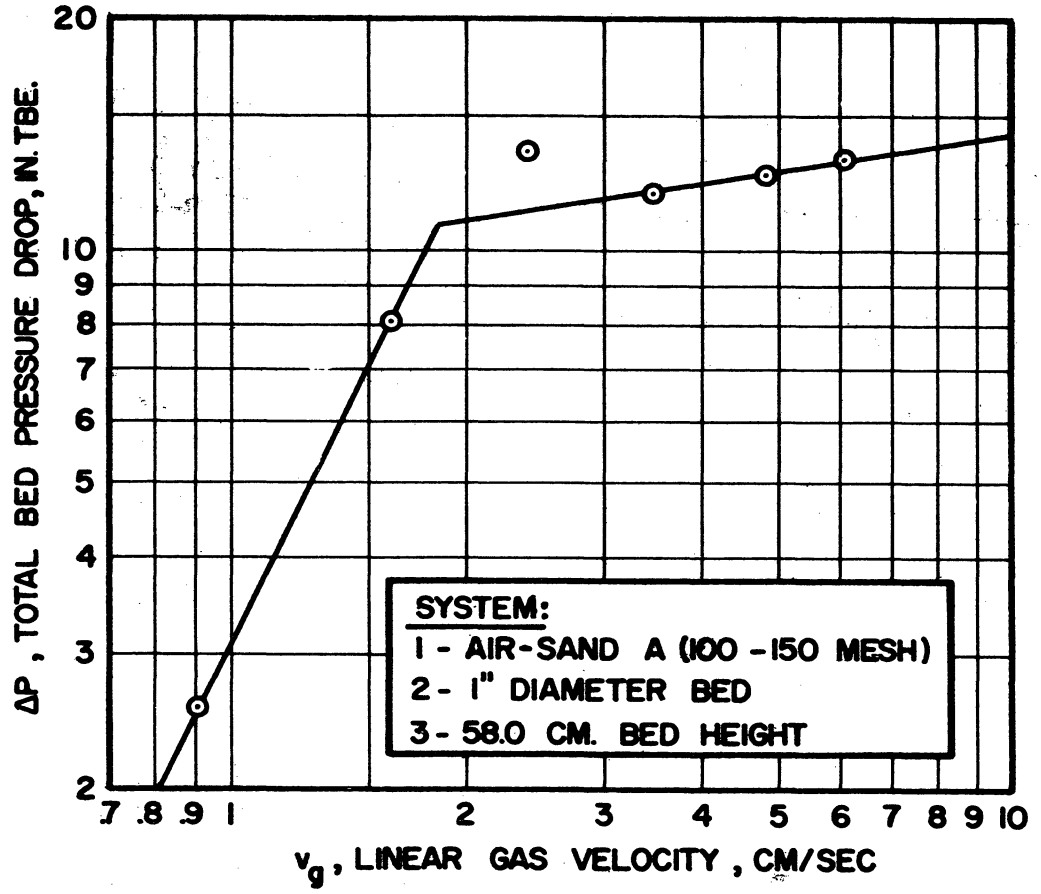

Figure 7. Total Bed Pressure Drop Versus Linear Gas Velocity.

TABLE V

Total bed pressure drop versus linear gas velocity.

System: 1. CO_2-Sand A. (100-150 mesh)
2. 1" diameter bed.
3. 42.0 cm. bed height.

Linear gas velocity at latm and 60°F. cm/sec	Total bed pressure drop, inches of tbe.
0.00	0.0
0.72	2.1
1.26	6.0
1.91	8.7
4.65	8.9
8.85	9.2

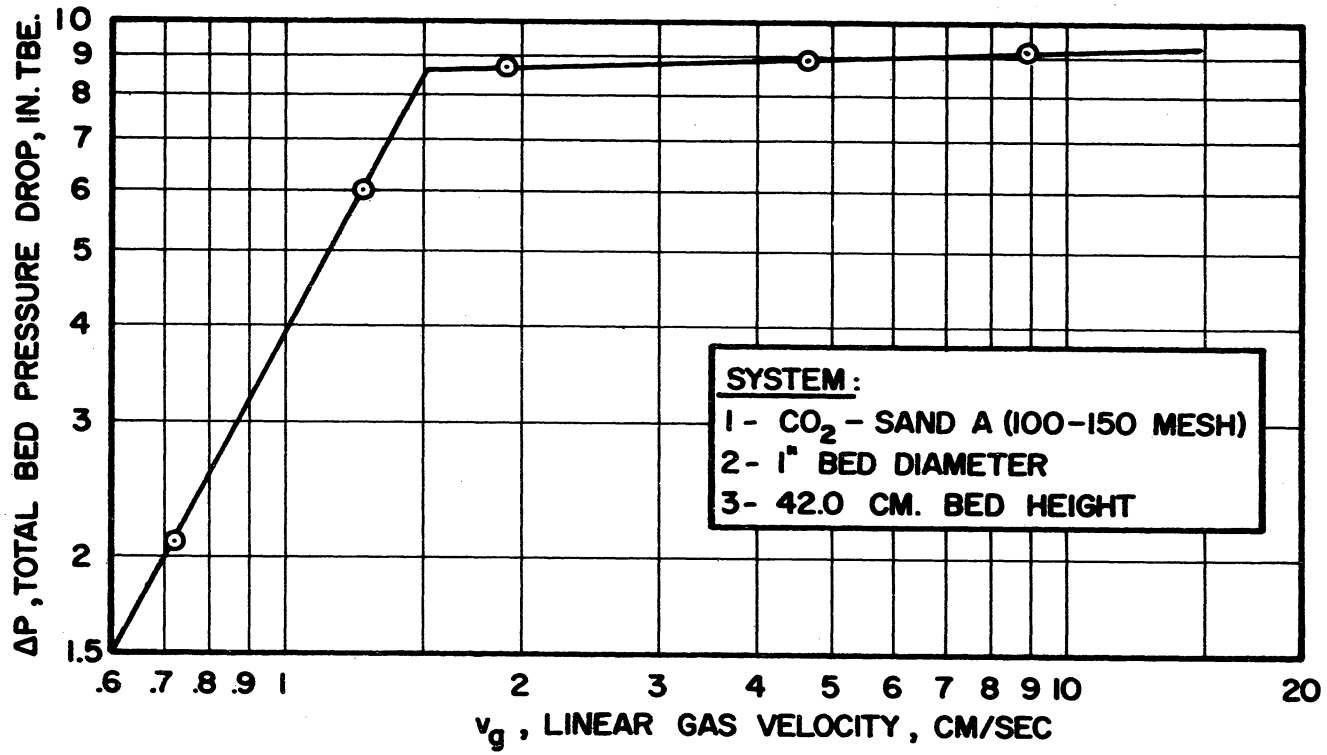

Figure 8. Total Bed Pressure Drop Versus Linear Gas Velocity.

TABLE VI

Total bed pressure drop versus linear gas velocity.

System: 1. Helium-Sand A. (100-150 mesh)
2. 1" diameter bed.
3. 42.0 cm. bed height

Linear gas velocity at latm and 60°F. cm/sec	Total bed pressure drop, inches of tbe.
0.00	0.00
2.08	1.7
3.64	4.05
5.53	6.85
7.94	8.60
13.48	9.50
19.5	9.80
25.6	9.80

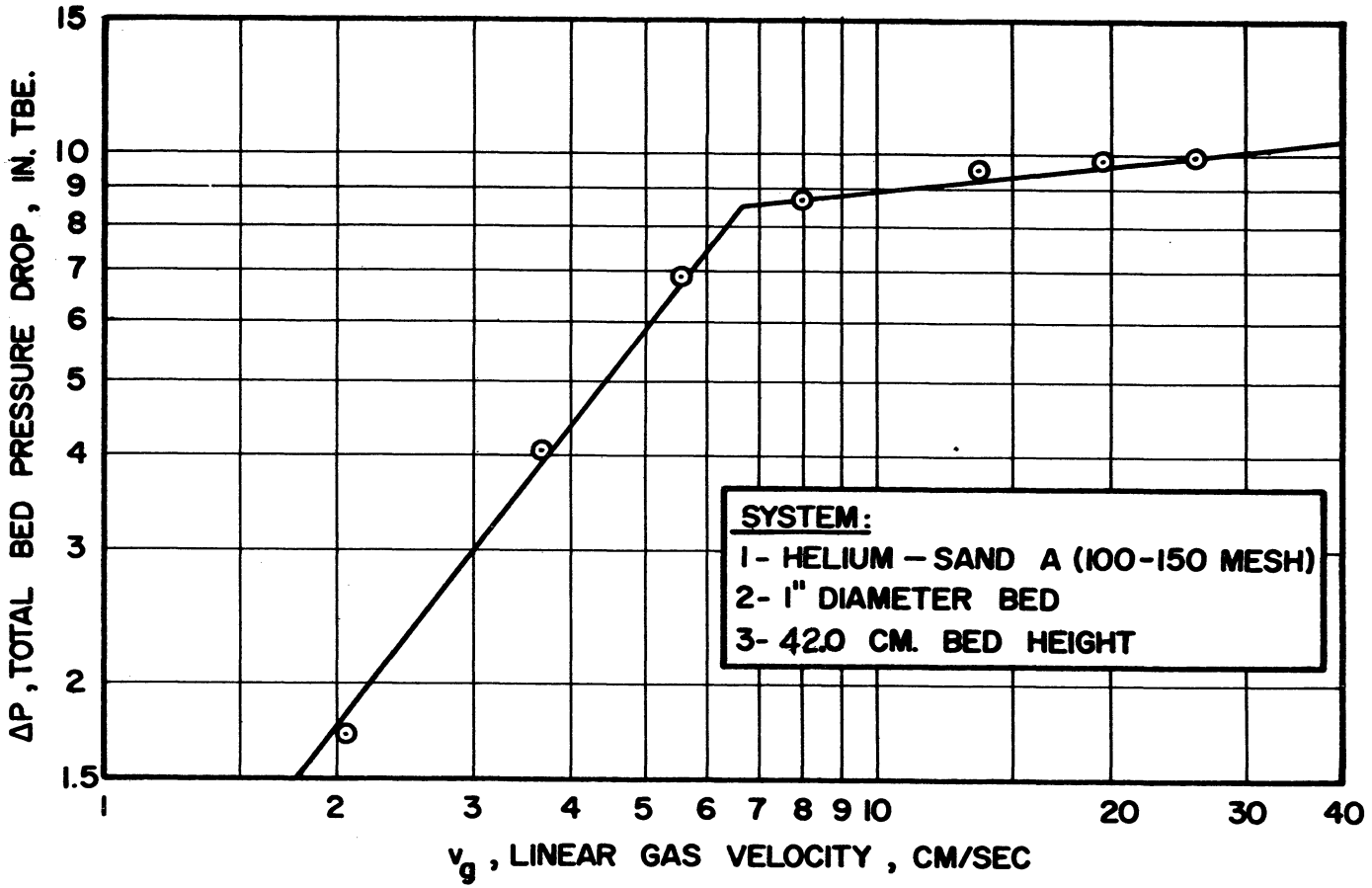

Figure 9. Total Bed Pressure Drop Versus Linear Gas Velocity.

TABLE VII

Total bed pressure drop versus linear gas velocity.

System: 1. Air-Sand B. (monazite)
2. 1" diameter bed
3. 33.0 cm. bed height

Linear gas velocity at latm and 60°F. cm/sec	Total bed pressure drop, inches of tbe.
0.00	0.00
1.04	2.66
1.55	4.65
2.14	7.55
3.36	11.80
5.73	12.00
8.32	12.55
10.92	12.65

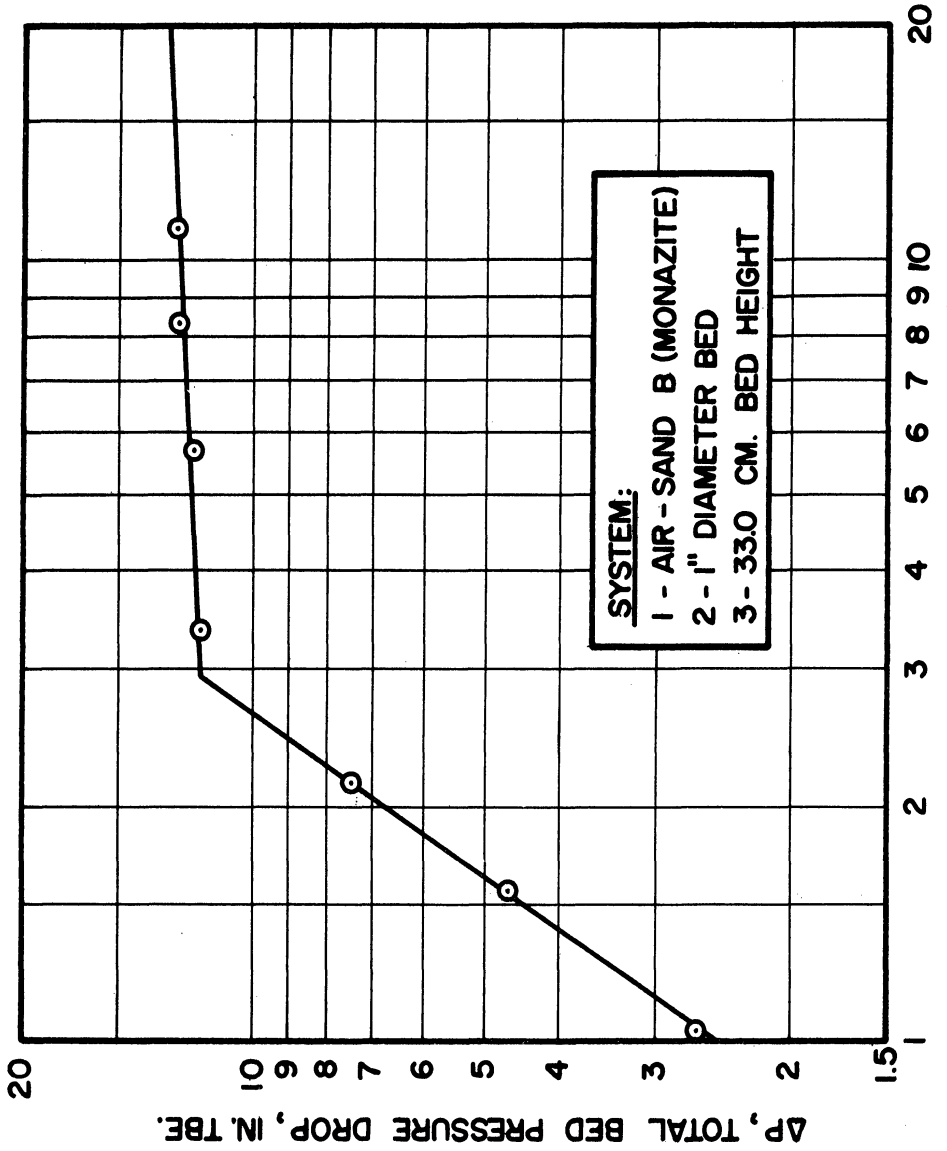

Figure 10. Total Bed Pressure Drop Versus Linear Gas Velocity.

gas velocity. The incipient fluidization velocity is quite apparent on each of these curves.

A simple check on the accuracy of these curves and at the same time on the assumption of zero pressure drop across the bed support can be made. The pressure drop at incipient fluidization should equal the weight of the bed per unit bed cross sectional area. This should be true of all gases. If one plots pressure drop at incipient fluidization versus bed height, the intercept at zero bed height will be the pressure drop due to the bed support. The slope of such a curve should be $\rho_s g/g_c$, in appropriate units. Figure 11 shows the data and theoretical curve for sand A (100-150 Mesh) and zero support resistance. It is apparent that the assumption of zero support resistance is valid. Table IX lists all pressure drops per unit bed length at incipient fluidization and minimum fluidizing velocities for all systems.

TABLE VIII

Total Bed Pressure Drop at Incipient Fluidization versus Bed Height for 100-150 Mesh Sand.

Gas	Bed Diameter in.	Bed Height cm.	Pressure Drop in. tbe.
Air	1.00	21.2	3.95
Helium	1.00	42.0	8.50
CO_2	1.00	42.0	8.60
Air	1.00	58.0	10.92
Helium	2.00	72.0	13.80
Air	2.00	74.0	15.00

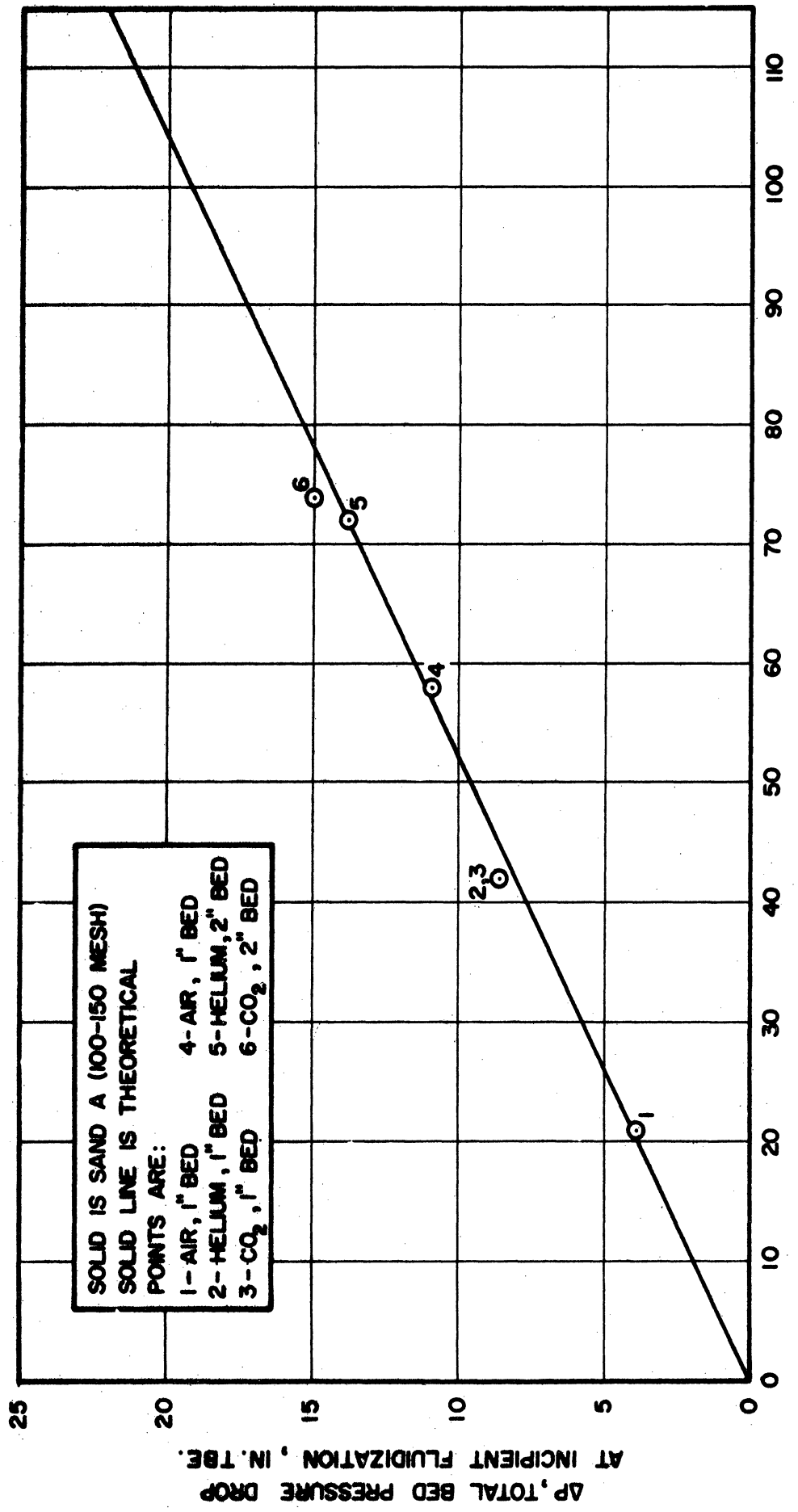

Figure 11. Total Bed Pressure Drop at Incipient Fluidization Versus Bed Height

TABLE IX

Incipient Fluidization Data for Systems Studied.

Gas	Bed Diameter in.	Bed Height, cm.	Solid	Vgmf, cm/sec	Pressure Drop per unit length, psi/cm
Air	1.00	21.2	Sand A	1.10	0.0199
Helium	1.00	42.0	Sand A	6.60	0.0217
CO_2	1.00	42.0	Sand A	1.52	0.0219
Air	1.00	58.0	Sand A	1.82	0.0202
Helium	2.00	72.0	Sand A	3.60	0.0206
Air	2.00	74.0	Sand A	3.14	0.0217
Air	1.00	33.0	Sand B	2.95	0.0383

SOLIDS DOWNFLOW RATES

The rate at which solids flow through void spaces is the most important variable in the characterization of slugging gas-solid fluid beds. Considerable effort was spent in determining precisely what conditions prevail in such systems. The first guess was that the solids downflow rate would vary with gas velocity; this was shown to be incorrect. Because slugs move at the excess velocity of the gas, v_{xs} , the lower surface of the slug is always exposed to a relative velocity equal to that at incipient fluidization.

I. Bin Flow Measurements.

A. Equipment

The first measurements were taken in the two inch diameter bed. The only additions to the equipment shown in Figure 3 were a slide valve at the expansion head and a photoelectric sensing device coupled to an oscillographic recorder.

The slide valve was designed to divert the gas flowing up the column out of the side of the column when closed to confine the solids to the expansion head. When the slide valve was opened, the gas was diverted up through the expansion head. This presumably exposed the solids at the throat of the expansion head to the velocities encountered by solid slugs in the tube.

The photocell measured the incident light from a projection lamp after two traverses of the tube via a mirror. The electrical output of the photocell was continuously recorded on a Sanborn

Twin-Viso oscillographic recorder. The output of photocell was not calibrated to measure solids density accurately; the only desired information was the time of fall of a known quantity of solids contained in the expansion head.

A diagram of this equipment is shown in Figure 12.

B. Procedure

The desired gas flow was set, the flow being diverted by the slide valve to the atmosphere. The expansion head was filled with solids sufficient to fill the tube to some point below the photocell arrangement. The oscillograph chart was started and the slide valve opened. The falling solids changed the transmittance characteristics of the tube and contents and provided a measure, qualitative since no calibrations were made, of the solids density of the tube. Figure 13 shows a trace of light transmitted versus time for a typical run.

C. Results

The results of these measurements for a 100-150 mesh sand in a two inch tube are shown in Figure 14. The solids downflow at zero gas velocity in similar systems has been investigated [7,8]. Kelly[8] reports that the flow of solids through 2 inch orifices follows the equation:

$$(75) \quad W = 0.156D^{2.84}$$

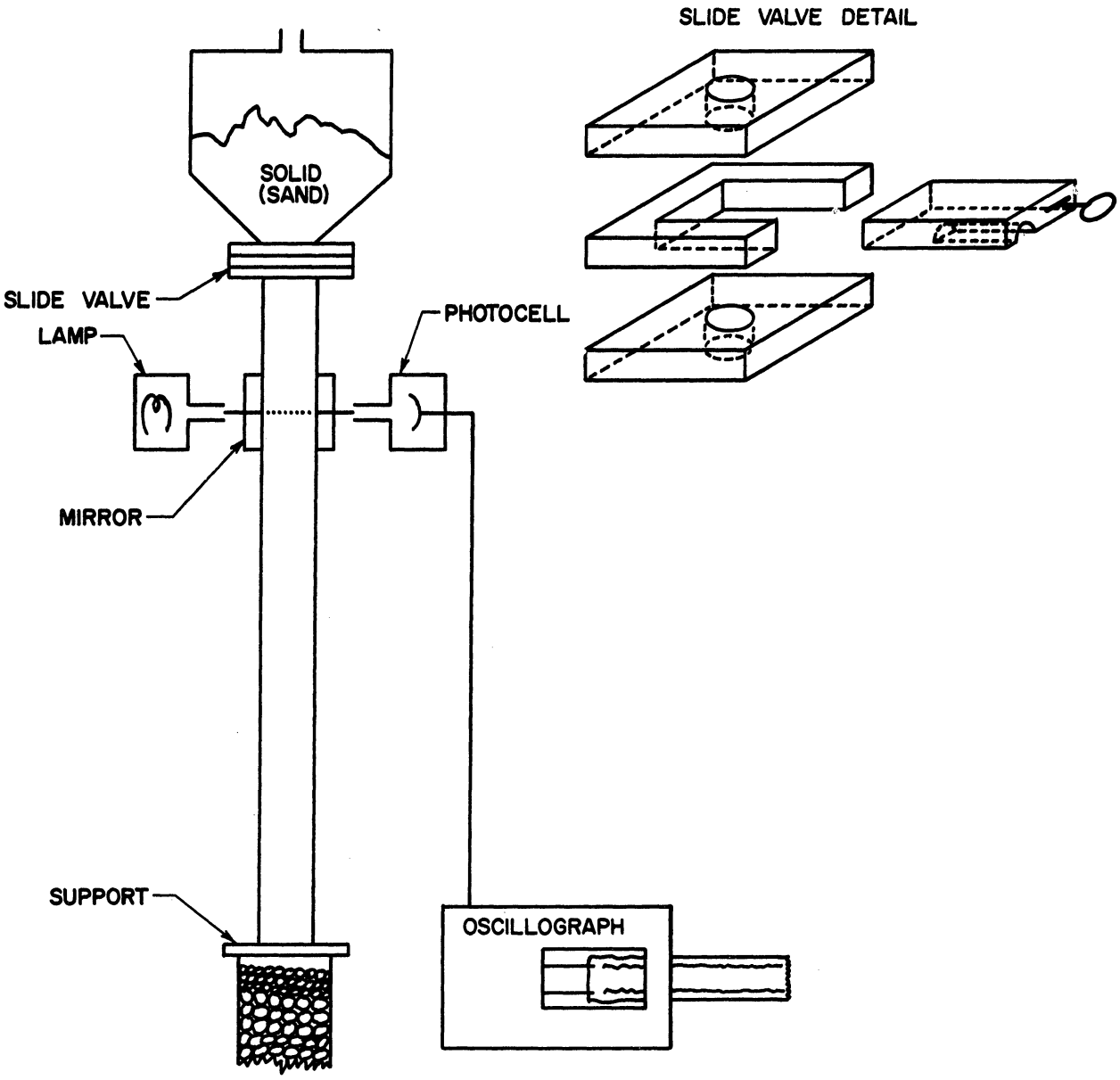

Figure 12. Apparatus for Measuring Solids Downflow Rates.

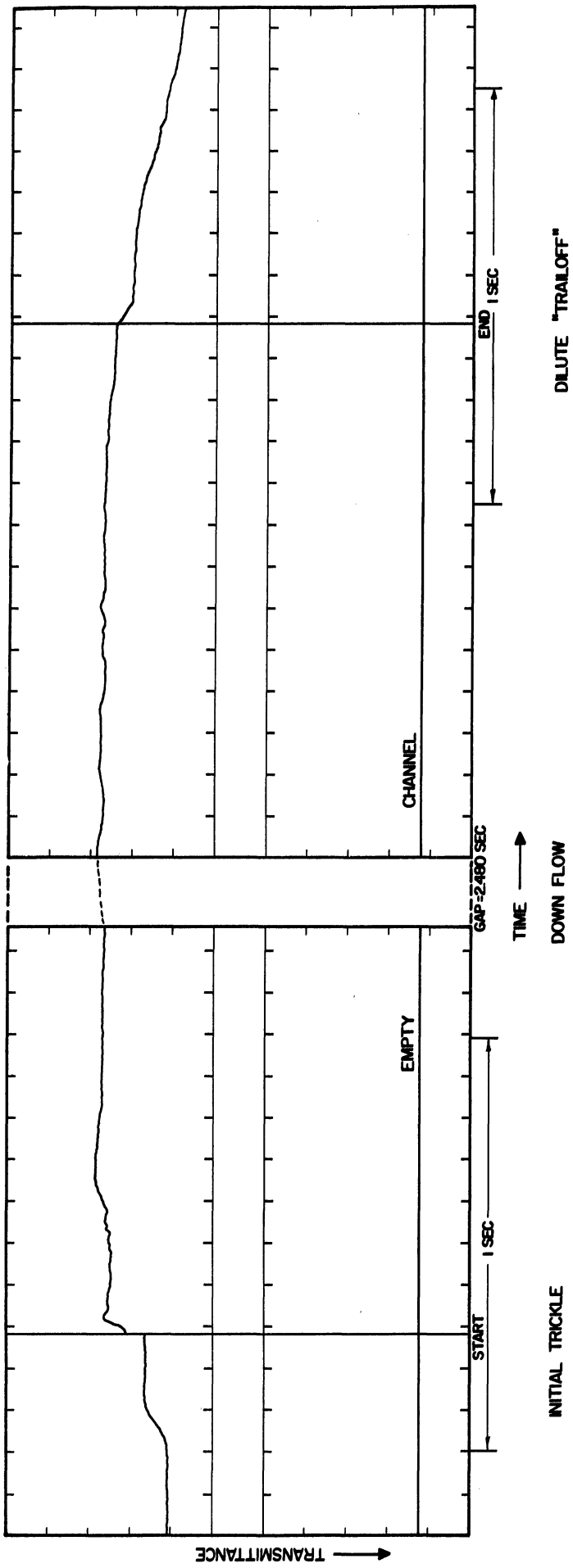

Figure 13. Measurement of Solids Downflow Rate. Typical Oscillograph Record of Falling Solids Optical Density. Conditions: No Gas Flow, 74.7 cm of Settled Solids in 2.0 inch Tube After Run Completion. Scale: 1 cm = 0.1010 sec. Run Duration: 5.170 sec.

TABLE X

Solids Downflow Rate versus Gas Velocity.

System: 1. Air-Sand A (100-150 Mesh)
2. 2" Diameter Tube.
3. Bin flow technique.

Gas Velocity, cm/sec	Solids Downflow Rate gm/cm^2 sec
0.0	20.0
0.0	19.6
0.0	20.8
1.0	18.9
2.0	19.6
3.25	26.2
4.2	27.2
5.7	24.4
6.0	29.1
6.0	29.8
7.4	23.5
8.2	20.4
8.7	21.0
11.5	15.3

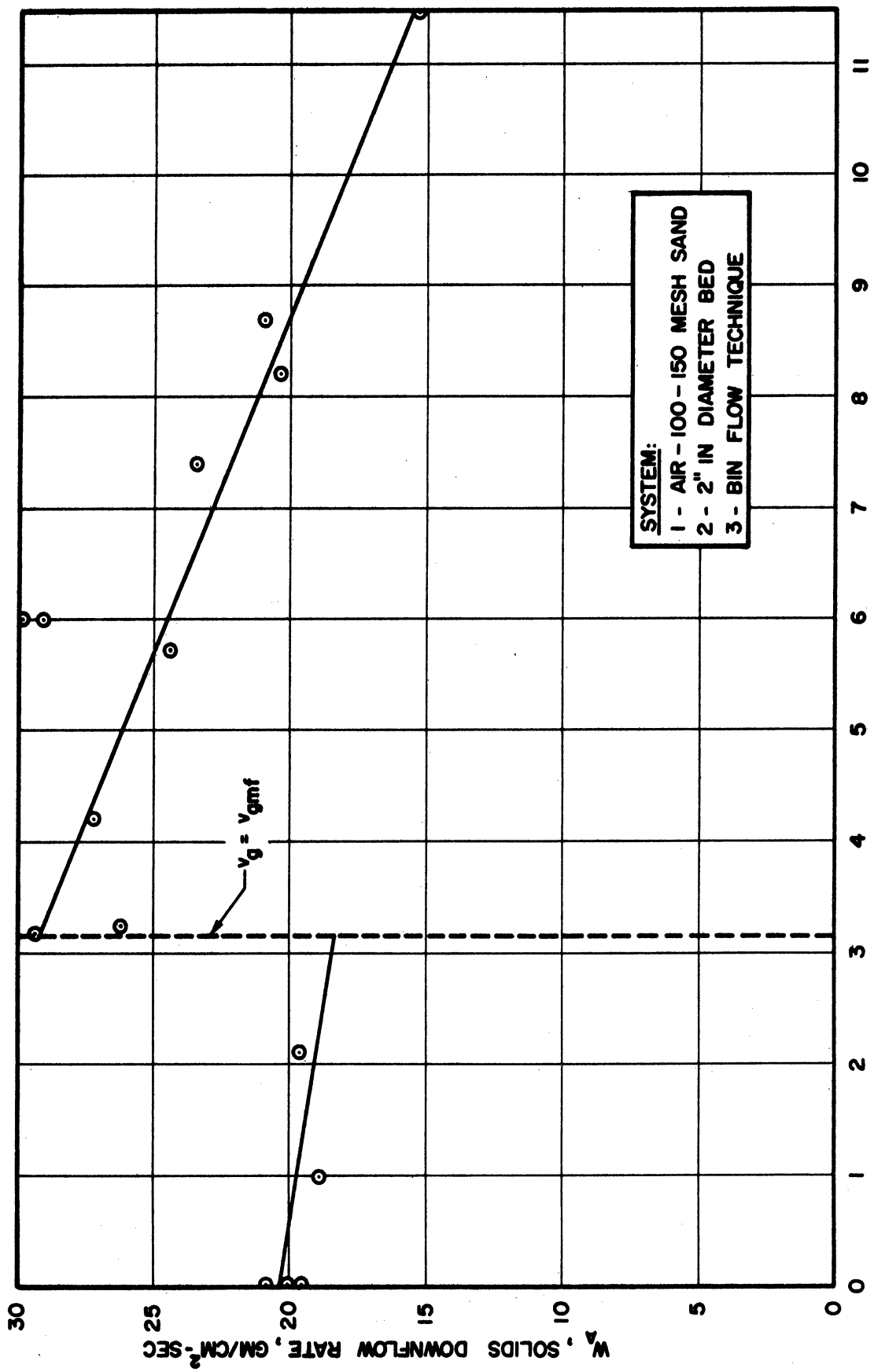

Figure 14. Solids Downflow Rate Versus Gas Velocity.

where D is in inches and W is in pounds per second. This yields, for the two inch orifice used, a flow rate of 24.5 gm/cm^2 sec. This compares favorably with the observed value of 20.5 gm/cm^{2}sec. The discrepancy probably lies in the fact that Equation (75) is written for bead or pelletized catalyst, which may have differed significantly from the sand used in this study.

As the gas flow rate is increased from zero to the velocity for minimum fluidization, the solids downflow rate drops, most likely due to increased drag on particles as they separate from the bulk. At the velocity of minimum fluidization there is a marked increase in solids downflow rate. Further increases in gas velocity cause a decrease in solids flow.

The two data points in Figure 14 at gas velocities of 6.0 cm/sec are noted to be considerably higher than all other points. The reason for this high solids flow rate is that some grease from the slide valve found its way into the solids and caused agglomeration of solids. The solids used were replaced whenever this occurred after the first incident.

D. Conclusions

Two important points may be made as a result of these bin flow tests. The first is that solids flow tends to decrease with increasing gas velocity both above and below incipient fluidization. The second is that a sizable increase in solids flow occurs at the velocity of incipient fluidization. This increase is due, in all probability, to the

increase in the freedom of particle motion at this velocity. A particle which is free from forces exerted by its neighbors is able to disengage from the bulk more easily. The important result is the value of w_a at the maximum, as will be seen.

II. Pressure Profile Measurements.

A logical question arises following the completion of these bin flow measurements. What relation is there between the solids downflow rates measured with bin and slide valve to the actual solids flow rates which prevail in a slugging fluid bed? The answer to this question was sought before proceeding with more bin flow tests. Pressure-time records were used to determine solids flow rates in slugging beds.

A. Equipment

The apparatus used for these measurements is that shown in Figure 15. Two pressure taps were placed in the tube at heights of 60.0 and 75.8 cm. above the bed support. Each tap consisted of a $\frac{1}{4}$" pipe to $\frac{1}{4}$" copper tubing tee with a medium mesh screen across the tube side leg. One tube leg, the downward oriented leg, was used as a trap to collect solids which entered the tap through the screen. This leg was emptied periodically. The upper leg led to a tee which permitted two pressure connections to one tap. One connection was made through a pet cock to one side of a differential pressure pickup. The other side of the pickup was connected via

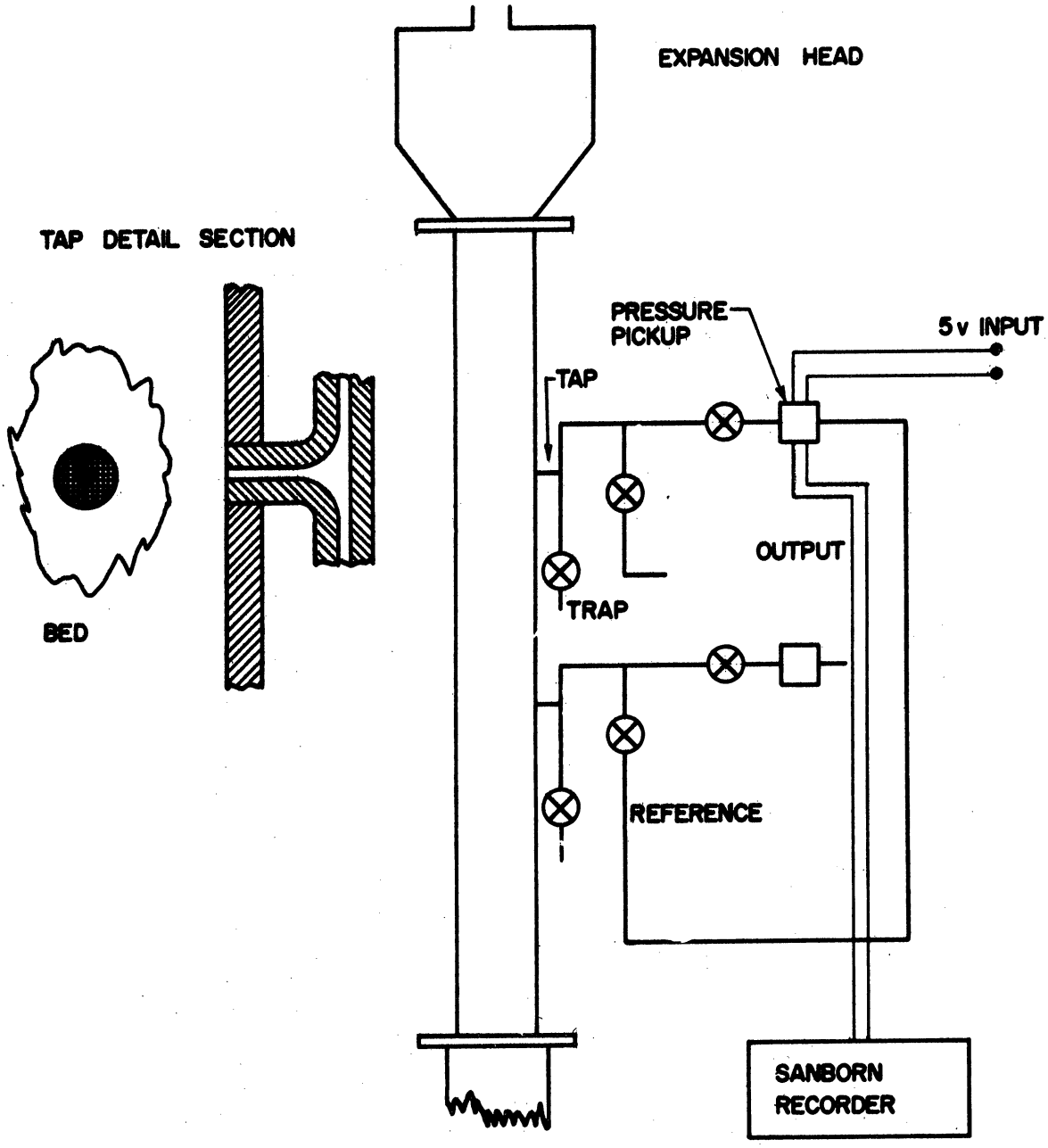

Figure 15. Equipment Used for Measuring Solids Downflow Via Pressure Drop in Slugging Fluid Bed.

rubber tubing with two pinch clamps to one connection on the lower tap. For these measurements, the extra pressure connection at each tap was closed and unused. In other applications, these extra connections led to other pickups.

The strain gage pressure pickups used were CEC model 4-315, $\pm$ 1 psi differential transducers. The pickup used in these measurements was number 2172, the calibration of which appears in Appendix C. Appendix C also contains other pertinent information on this pressure pickup such as zero shift with temperature, linearity, hysteresis, etc.

A constant 5 volt D. C. excitation produced, through the transducer, an electrical output which was recorded on the Sanborn Twin-Viso recorder.

B. Procedure

The proper valves were opened to permit operation of the transducer. The gas flow rate was adjusted to the desired value and the bed allowed to reach steady state operation (5 minutes). Then the pickup excitation source was switched on and a one minute recording of the pickup output was made.

C. Results

A sample oscillographic recording is shown in Figure 16.

Since the pressure drop measured was at all times in a zone of solids downflow, the slopes of the observed pressure curve yield, under the assumptions of the postulated model, a measure of solids downflow. Consider first a decreasing pressure differential. This will

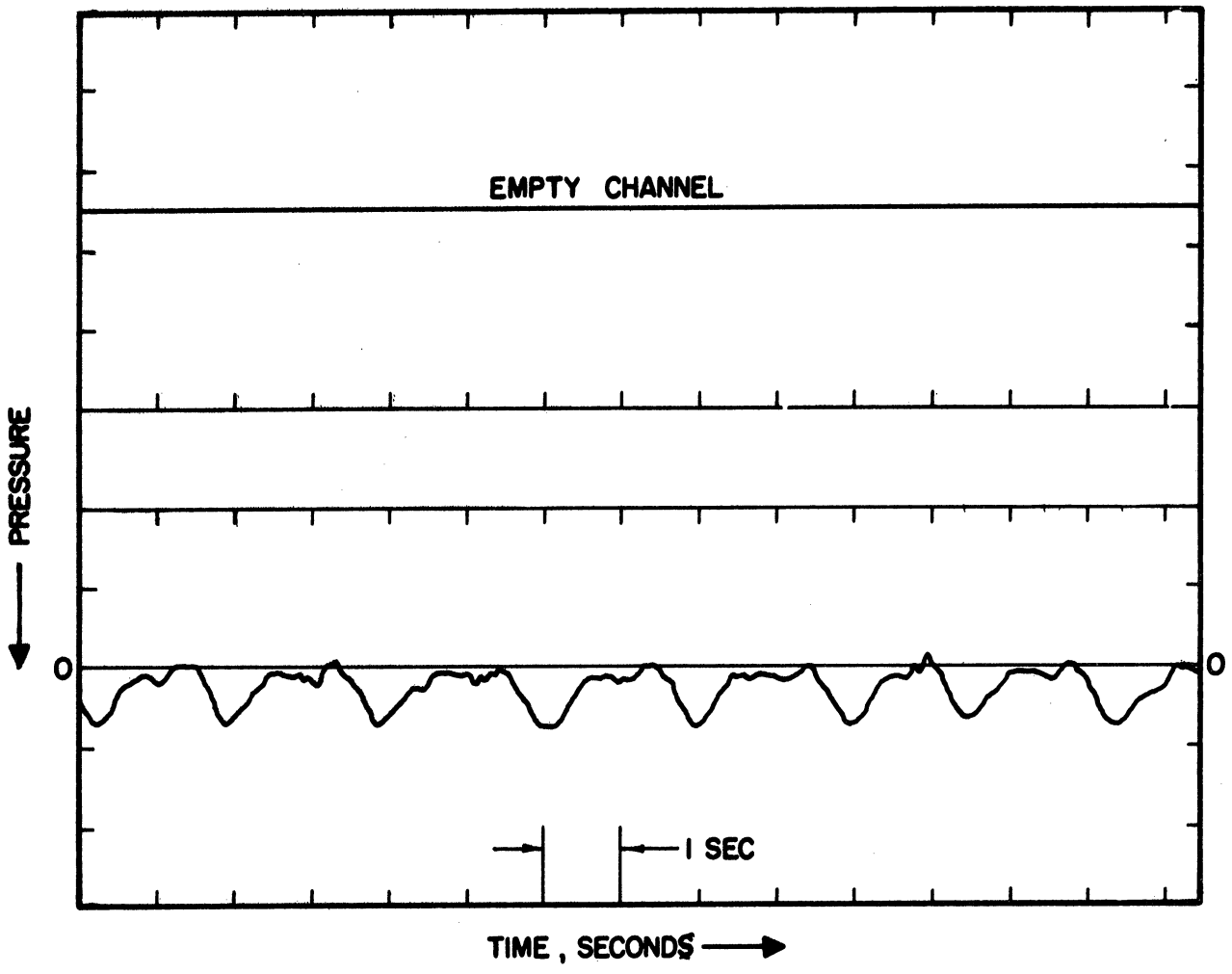

Figure 16. Oscillograph of Pressure Variation Between Two Taps 15.8 cm Apart Near the Top of a Slugging Fluid Bed. Solid is 100-150 Mesh Sand. Gas: Helium. Gas Velocity: 10.9 cm/sec in 2.0 Diameter Tube. Lines at the Right are for Slope Measurement.

be due to the upward movement of a slug-over-void interface through the zone between the pressure taps. As the void moves upward, the amount of solids between the taps decreases. If the total pressure difference is attributed to a slug at conditions of incipient fluidization, then the pressure difference is a measure of the slug length between taps. If the top of the slug is above the top tap, then the rate of decrease of pressure is proportional to the rate of upward motion of the interface. But the proposed model gives this rate as:

$$(76) \quad \dot{z} = V_{xs} + \theta$$

The excess gas velocity is easily calculated from

$$(77) \quad V_{xs} = V_g - V_{gmf}$$

Thus θ may be determined and converted, by use of solids density, to w_a, solids downflow rate.

Next consider an increasing pressure differential. This is due to a void-over-slug interface moving into the zone between taps. The model gives this rate:

$$(78) \quad \dot{x} = V_{xs} + \theta$$

Therefore, the analysis of increasing pressure differentials is similar, except for sign, to the analysis of decreasing pressure differentials.

Figure 17 shows the results of these measurements for 100-150 mesh sand in a 2.0 inch diameter tube for air and helium. It appears

TABLE XI

Solids Downflow Rate versus Gas Velocity.

Operational Pressure Drop Technique

Gas	Gas Velocity cm/sec	Downflow Rate gm/cm^2 sec
Air	7.0	31.5
Air	10.0	31.9
Air	13.0	35.1
Helium	9.1	32.8
Helium	10.9	37.1
Helium	14.7	32.1
Helium	18.0	34.6

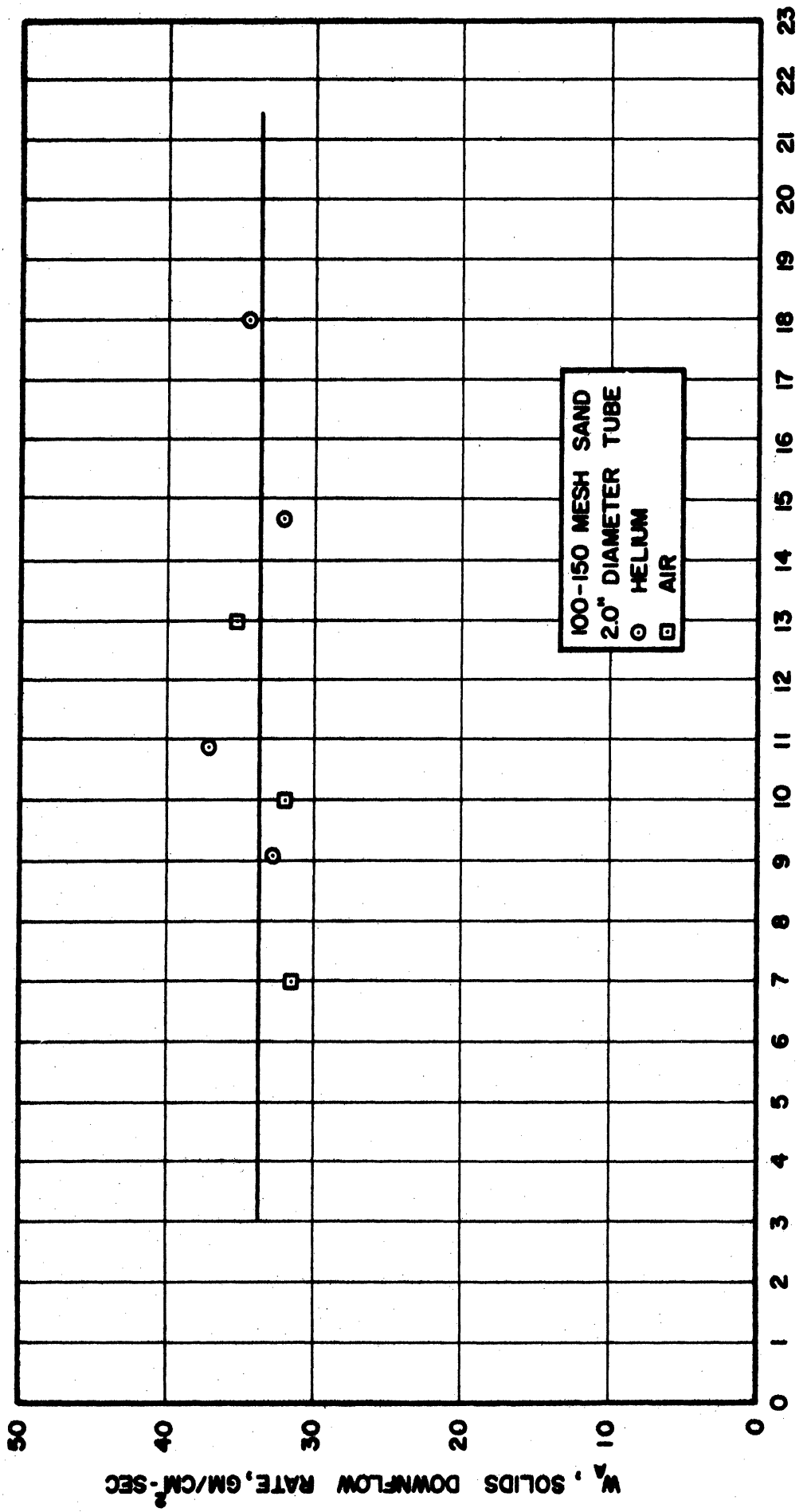

Figure 17. Solids Downflow Rate Versus Gas Velocity. Pressure Measurement Technique.

that there is no change in w_a with gas velocity. For this reason all subsequent measurements of w_a or θ were made at only one gas velocity, the velocity at minimum fluidization.

The data at this point are inconclusive as to whether or not the gas used affects solids downflow. Certainly the variation between air and helium is slight.

D. Conclusions

These results lead to several important conclusions. There are:

1. Slugs slip with respect to the tube wall at the excess gas velocity v_{xs}. This is true necessarily in the bed zone studied.

2. No acceleration or deceleration of slugs is present. The linearity of the pressure curves points this out. Assumption 3 of the proposed model is thus verified for the bed section studied.

3. There is a unique solids downflow rate. This verifies assumption 5 of the proposed model for the bed section studied.

4. There is a negligible pressure drop in void spaces. This is true because the pressure trace returns to the base line when only falling solids occupy the zone between taps (see Figure 16). Again this only holds at present for the bed section studied. This verifies assumption 9 of the model under consideration.

5. The agreement between bin flow measurements and pressure drop measurements of w_a indicates that the lower interface of a slug, and hence the slug itself, is exposed to a relative velocity the same as the velocity for incipient fluidization. Assumption 10 of the model is thus verified for the bed section studied.

III. Effect of Operating Variables on Solids Downflow Rate.

With gas velocity ruled out as a variable, the remaining variables of the gas used and tube diameter were investigated briefly. Carbon dioxide, helium and air were used to fluidize 100-150 mesh

sand in a 1.0-inch-diameter Plexiglas tube. Air and this same sand were also checked in a 1.0-cm.-diameter glass tube. Finally, the system air-monazite sand was studied in a 1.0-inch Plexiglas tube. In every case, except the 1.0-cm. tube runs, both bin-flow and pressure-curve techniques were used to obtain solids downflow rates.

A. Equipment

1. The apparatus for pressure measurement is the same as that previously discussed, with one exception. The screen over the pressure tap was replaced with a very thin glass-wool plug for measurements in the 1.0-inch-diameter bed.

2. The apparatus for photoelectric measurements was altered slightly to yield more information. Two light beams in these experiments made only one traverse each of the tube. The photocells and their respective sources were located near the bottom of the bed and were separated by a distance of 17.0 cm. Thus the solids optical density was measurable at two separate locations.

The slide-valve arrangement already described was used for bin-flow measurements for the one-inch bed. A section of 1-cm. rubber tube and pinch clamp was used for controlling solids flow in the 1-cm. bed. Several pin holes in the rubber tube below the pinch clamp diverted gas flow to the atmosphere until the clamp was opened.

The bins used were changed for convenience. A section of 3 inch Plexiglas pipe served as the hopper for measurements in the one-inch bed; a glass funnel performed the same function for the one centimeter diameter bed.

The bed supports in both instances were changed to porous glass wool plugs. No calming section was used. Figures 18 and 19 show these arrangements.

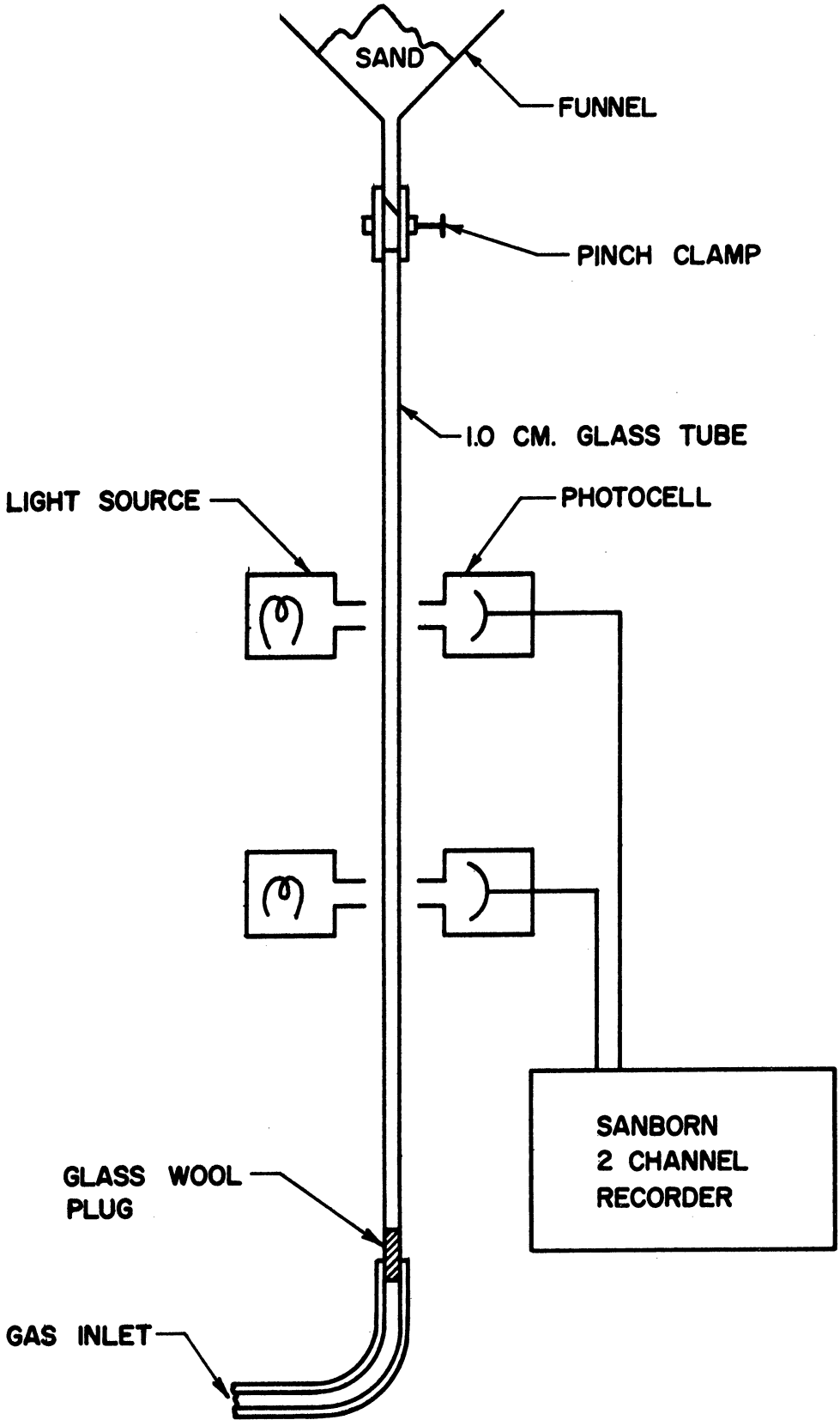

Figure 18. Equipment for Measuring Solids Downflow in a 1.0 cm. Glass Tube.

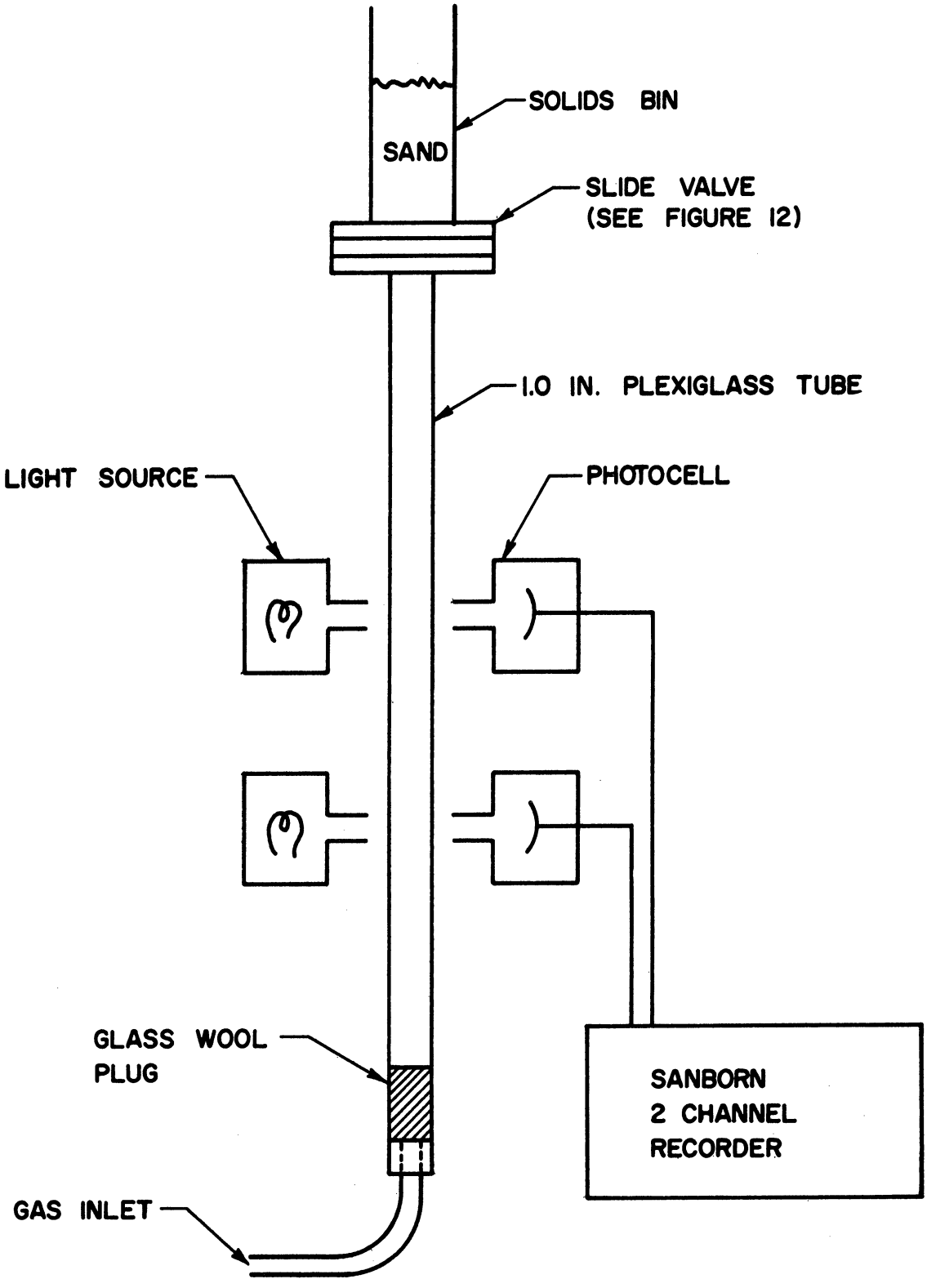

Figure 19. Equipment for Measuring Solids Downflow in a 1.0 inch Plexiglass Tube.

B. Procedure

The procedure for determining solids downflow rate from pressure measurements had already been outlined.

The bin flow procedure operated as follows. When the solids were released, falling solids interrupted both light beams to a certain extent. Fluctuations in the light transmitted by the column of falling solids were observed. When the tube filled with solids in the light beam, these fluctuations ceased. Therefore, the time delay between the cessation of transmittance fluctuations in the two photoelectric measuring points will give the value of solids downflow. The distance between beams divided by this time delay is exactly the value θ, which may be converted to w_a.

C. Results

The results of bin-flow experiments in the 1.0-cm. glass tube will be discussed first. The solids, upon release from the bin, fall first through the upper light and then through the lower light beam. Before reaching the upper beam, the solids have fallen over 200 cm., and therefore should be close to terminal velocity. The distance between beams divided by the time delay between initial beam interruptions is therefore a good measure of particle terminal velocity. A typical oscillograph showing this delay is shown in Figure 20. The value of terminal velocity determined in this way was 120 cm/sec. This compares quite favorably with the value calculated from drag correlations for single spheres of 134 cm/sec. The average mesh size was taken as the diameter for purposes of this calculation.

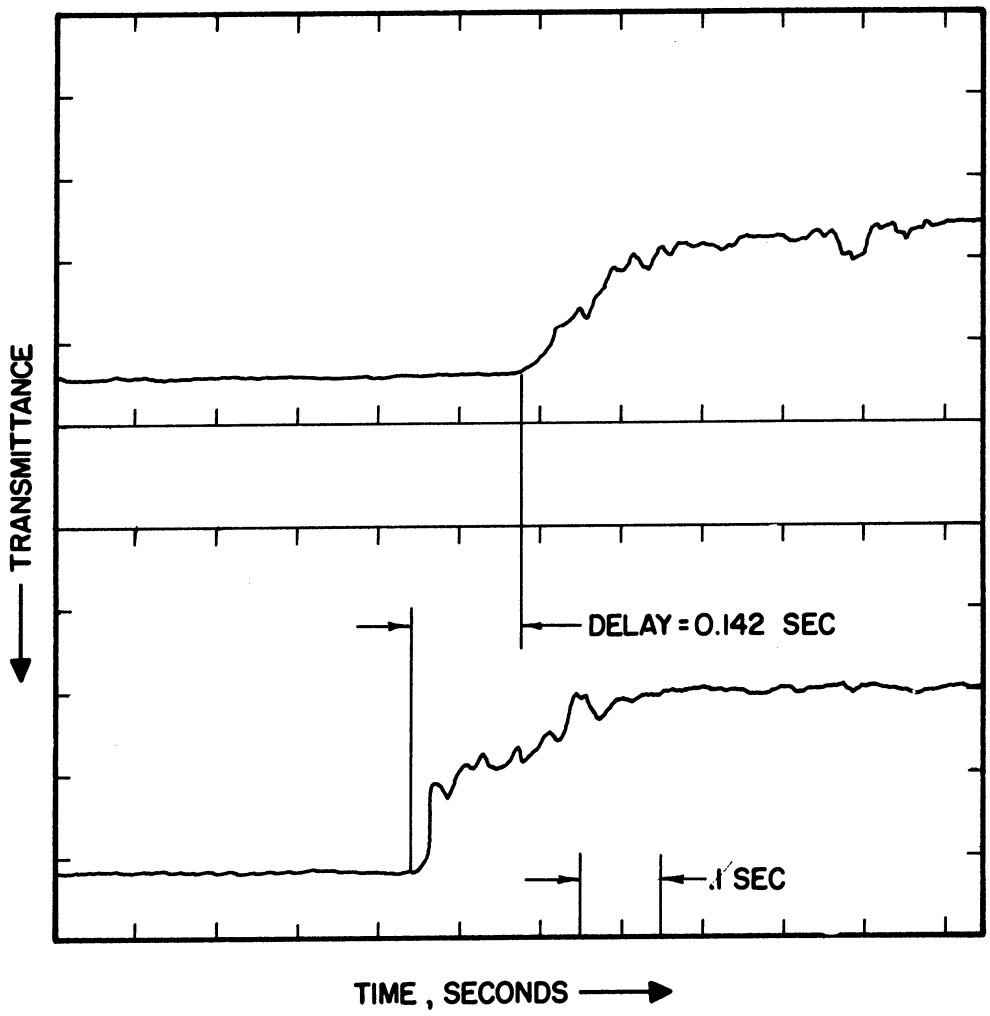

Figure 20. Determination of Particle Terminal Velocity. System: 100-150 Mesh Sand in Air in a 1.0 cm Glass Tube. Distance Between Photo Beams: 17.00 cm.

Solids downflow rates determined by both procedures for nearly all tube diameters, gases, and solids are shown in Table XII.

Three variables are present which may affect the solids downflow rate. These are:

1. A variable characterizing the solid.
2. A variable characterizing the gas.
3. A variable characterizing the tube.

Since this study was not intended to examine the complex problems of solids characterization, only a brief excursion was made in this direction. The two solids considered were 100-150 mesh sand and 100-150 mesh monazite sand. The former, sand A, had a bulk density of 1.44 gms/cm^3, the latter, sand B, 2.98 gm/cm^3. These solids appeared identical under a microscope. The particles were smooth and fairly regular. Figure 21 shows a plot of w_a versus apparent solid density, the only solid variable of consequence. Normally two data points are insufficient, but the plot shows, as expected, that the origin is also a point on the curve.

The variable which best characterizes the gas is the particle Reynolds number at incipient fluidization. The velocity for minimum fluidization is used because it has been shown that this is the velocity to which the disengaging particles at the bottom of a slug are exposed. The resultant effect of particle Reynolds number on w_a is shown in Figure 22. As expected, the increase of particle Reynolds number decreases the solids downflow rate w_a, although very slightly. This plot also demonstrates the effect of the most important variable, bed diameter.

TABLE XII

Summary of Observed Solids Downflow Rates.

Bed Diameter, cm.	Gas	Solid	w_a gm/cm^{2}sec.	Technique
5.08	Air	Sand A	29.5	Bin flow
5.08	Air	Sand A	32.8	Pressure
5.08	Helium	Sand A	34.1	Pressure
2.54	Air	Sand A	26.4	Bin flow
2.54	Air	Sand A	24.7	Pressure
2.54	Helium	Sand A	23.5	Bin flow
2.54	Helium	Sand A	22.8	Pressure
2.54	CO_2	Sand A	18.4	Bin flow
2.54	CO_2	Sand A	21.4	Pressure
2.54	Air	Sand B	53.4	Pressure
1.00	Air	Sand A	12.2	Bin flow

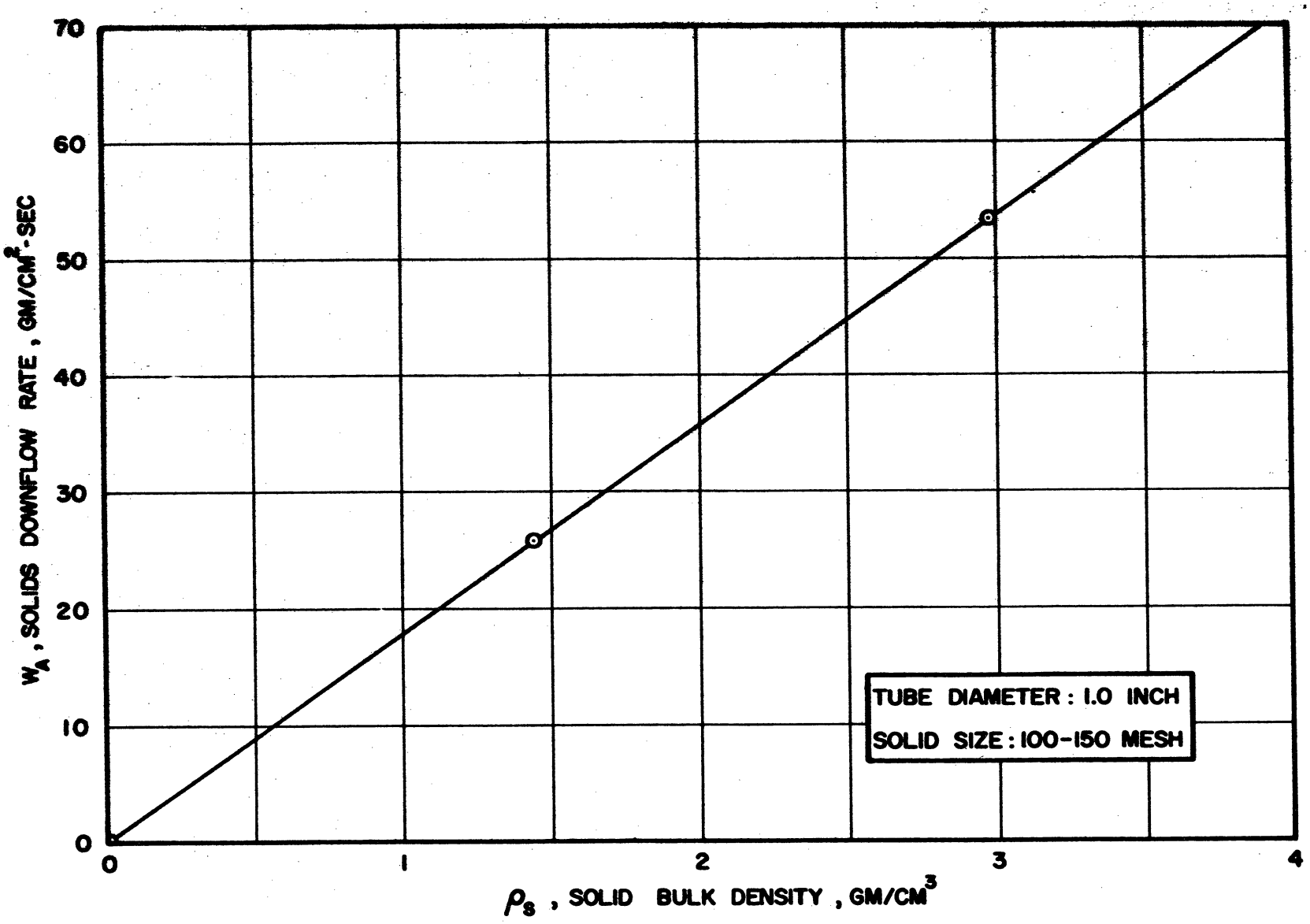

Figure 21. Solids Downflow Rate Versus Solid Density.

TABLE XIII

Solids Downflow Rate versus Particle Reynolds Number at Incipient Fluidization.

Bed Diameter, in.	Gas	Re_p	$\bar{w}_a$ gm/cm^{2}sec.
1.0	Helium	0.0665	23.2
1.0	Air	0.0875	25.5
1.0	Air	0.145	25.5
1.0	CO_2	0.238	19.9
2.0	Helium	0.0361	34.1
2.0	Air	0.249	31.2

Solid used: 100-150 Mesh Sand A.
$\rho_s = 1.44$ gm/cm^3 bulk.

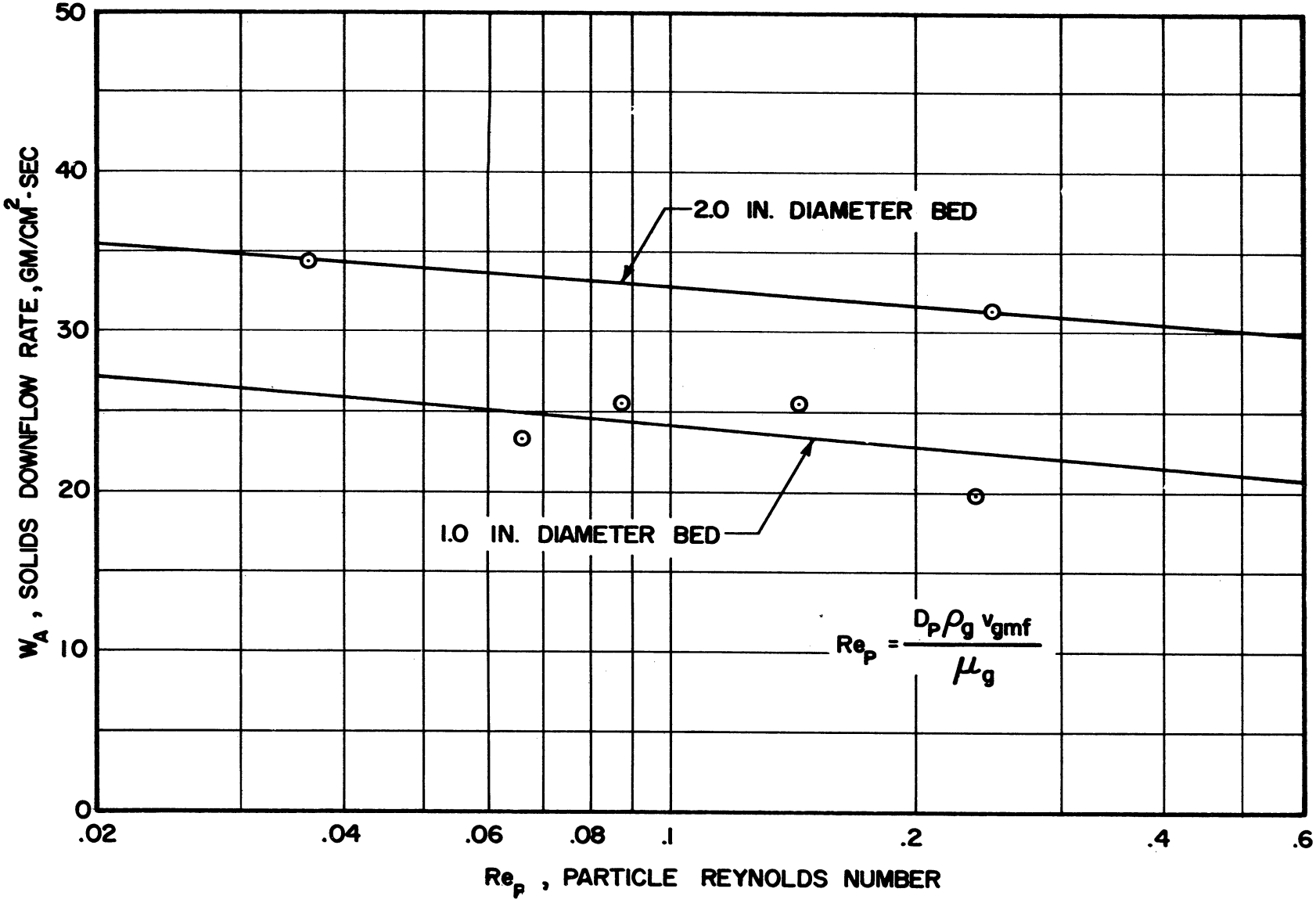

Figure 22. Effect of Reynolds Number on Solids Downflow Rate.

Figure 23 shows the effect of bed diameter on solids downflow rate. This curve exhibits a tendency to level off at larger bed diameters. This curve must of necessity pass through w_a equal to zero when the bed diameter equals particle diameter. Since the diameter of a particle is very small, this curve appears to pass through the origin.

D. Conclusions

Since the terminal velocity of a particle is much greater than all other system velocities, assumption 6 of the proposed model is verified. The largest impressed gas velocity was of the order of 40 cm/sec, which is much smaller than the observed terminal velocity for Sand A of 120 cm/sec. This conclusion permits one to assume that solids transfer from slug to slug is very fast.

The bin flow technique for measuring solids downflow is seen to be a reasonably accurate means of predicting w_a. Pressure measurements give nearly the same values. This indicates that one need not operate a slugging system in order to know w_a; it can be measured with auxiliary equipment.

The results of Figure 21 lead to the conclusion that solids downflow is directly proportional to solids density. The data available is not great in number, but the results are not to be denied. This curve definitely passes through the origin, showing solid density to be a very significant variable. On the other hand, the properties of the gas used seem to have but a weak effect on w_a. The slight

TABLE XIV

Effect of Bed Diameter on Solids Downflow Rate.

Gas	Bed Diameter cm.	w_{A_2} gm/cm^{2}sec
Air	5.08	31.2
Helium	5.08	34.1
Air	2.54	25.5
Helium	2.54	23.2
CO_2	2.54	19.9
Air	1.00	12.2

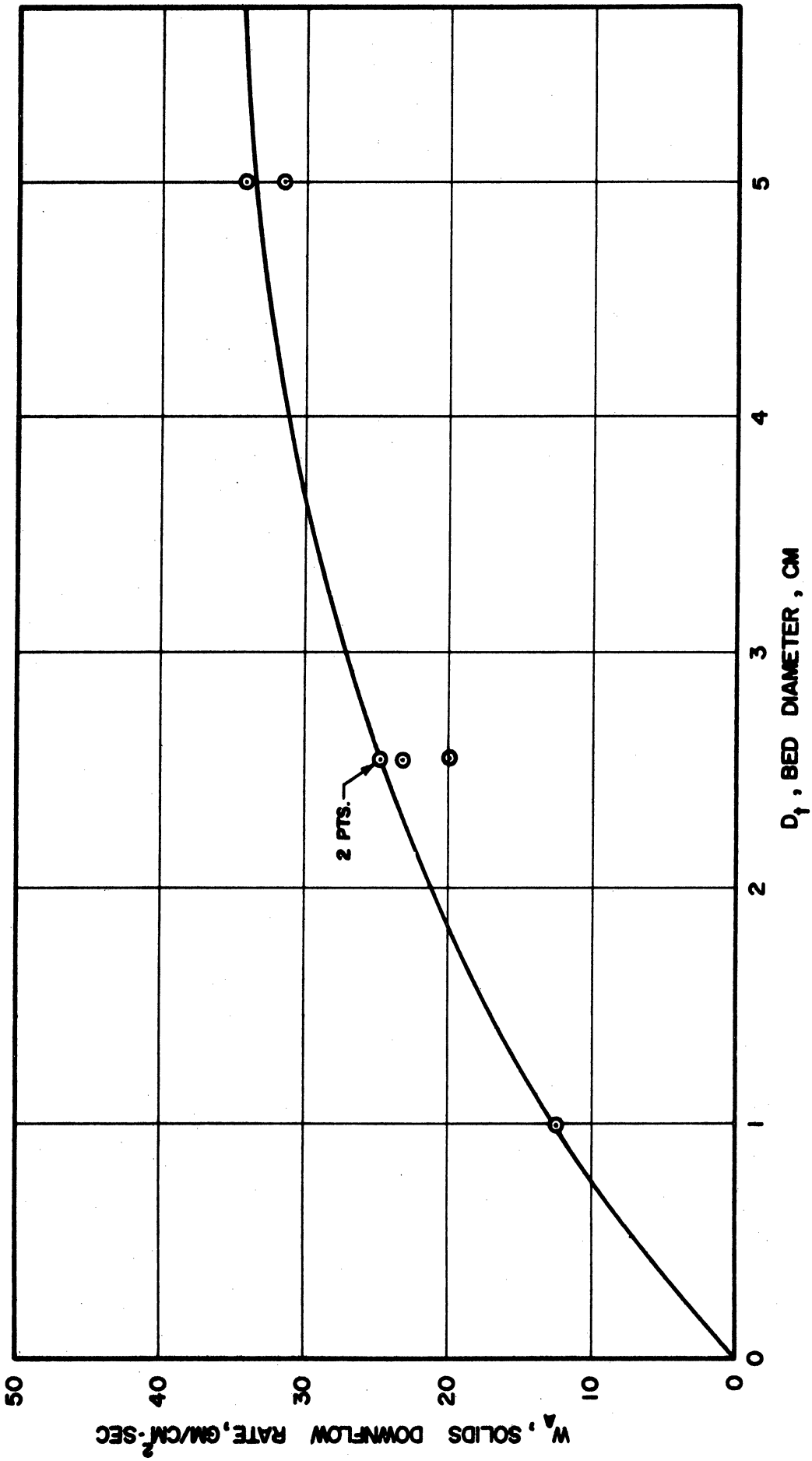

Figure 23. Effect of Bed Diameter on Solids Downflow Rate.

decrease in w_a with increasing particle Reynolds number can be attributed to increased drag on the disengaging particles. Bed diameter has a strong effect on w_a, indicating that bed geometry plays an important role in small beds. It is quite probable that there is some critical diameter above which w_a is not affected by changes in bed diameter. The large equipment required to explore larger diameters made such a study impractical. These results point to an expression for w_a of the form.

$$(79)\quad w_A = A\rho_s f_1(Re_p) f_2(D_t) f_3(\text{SOLID SHAPE})$$

The character of f_1 and f_2 has already been demonstrated. The function f_3 has always been a very difficult one, and, as stated earlier, beyond the scope of this work. The manner in which solid density enters if interesting because it means that the previously defined quantity, θ, is independent of solid density:

$$(80)\quad \theta = A f_1 f_2 f_3$$

Two conclusions regarding the study of solids downflow are worthy of further emphasis. They are:

1. There is a unique solids downflow rate for a given system.
2. This downflow rate may be determined without operating the actual system; i.e., it may be determined with auxiliary equipment.

BED CONFIGURATION

This section deals with the type of slugs which exist at various elevations in a slugging fluid bed. There are the four possibilities listed in the proposed model. Certainly the top slug in any system must be a case 2 slug, that is a slug with material outflow from the bottom. The remainder of the slugs, however, may in theory fall into any of the four cases described.

A. Equipment

The equipment has already been described in preceding sections; no instrumentation was used.

B. Procedure

There were three events of note which recurred periodically at three statistically varying elevations. The first of these was the maximum elevation of the top of the bed. The top surface of the slug rose upward until the top slug disappeared because of solids outflow. The second was the stabilization of the lower interface of the slug below the top slug. The term stabilization is here intended to mean the cessation of solids outflow from this interface. The location of this interface at the moment of stabilization is the quantity of interest. The third quantity was the elevation at which bubbles, originating at the distributor, grew to occupy the whole bed cross section, thus creating a slug and a void space. As will be seen these three elevations serve to characterize the bed and completely determine the case of all slugs in the system.

The procedure therefore consisted of measuring these three elevations as functions of gas velocity. Because statistical variations were present, approximately 30 measurements of each level at each velocity were taken for each system. The average value is reported. A glass marking wax crayon was used to mark the elevation of the event. The average of the readings was thus visually apparent.

Results.

The three levels mentioned above are given by:

H_T = maximum height of the top of the bed

H_M = height of the lower interface of the slug below the top slug when solids cease to fall from this interface.

H_B = height at which bubbles formed at the distributor grow to occupy the entire tube.

All heights are measured from the bed support. Figures 24 to 32 show the results of these measurements. These three "level curves", H_T, H_M, and H_B versus velocity serve to characterize the bed configuration.

The region between the stabilized interface and the top of the bed always contains two slugs. The top slug always has outflow only. The second slug is a case 4 slug when at lower bed elevations. When the lower interface reaches H_M, it becomes a case 3 slug-one with inflow only. An occasional particle was observed to fall from this "stable" lower interface, but this "dripping" was of no consequence.

There existed in every system a bubbling zone at the bottom of the bed. These bubbles grew to the size of the bed at the elevation

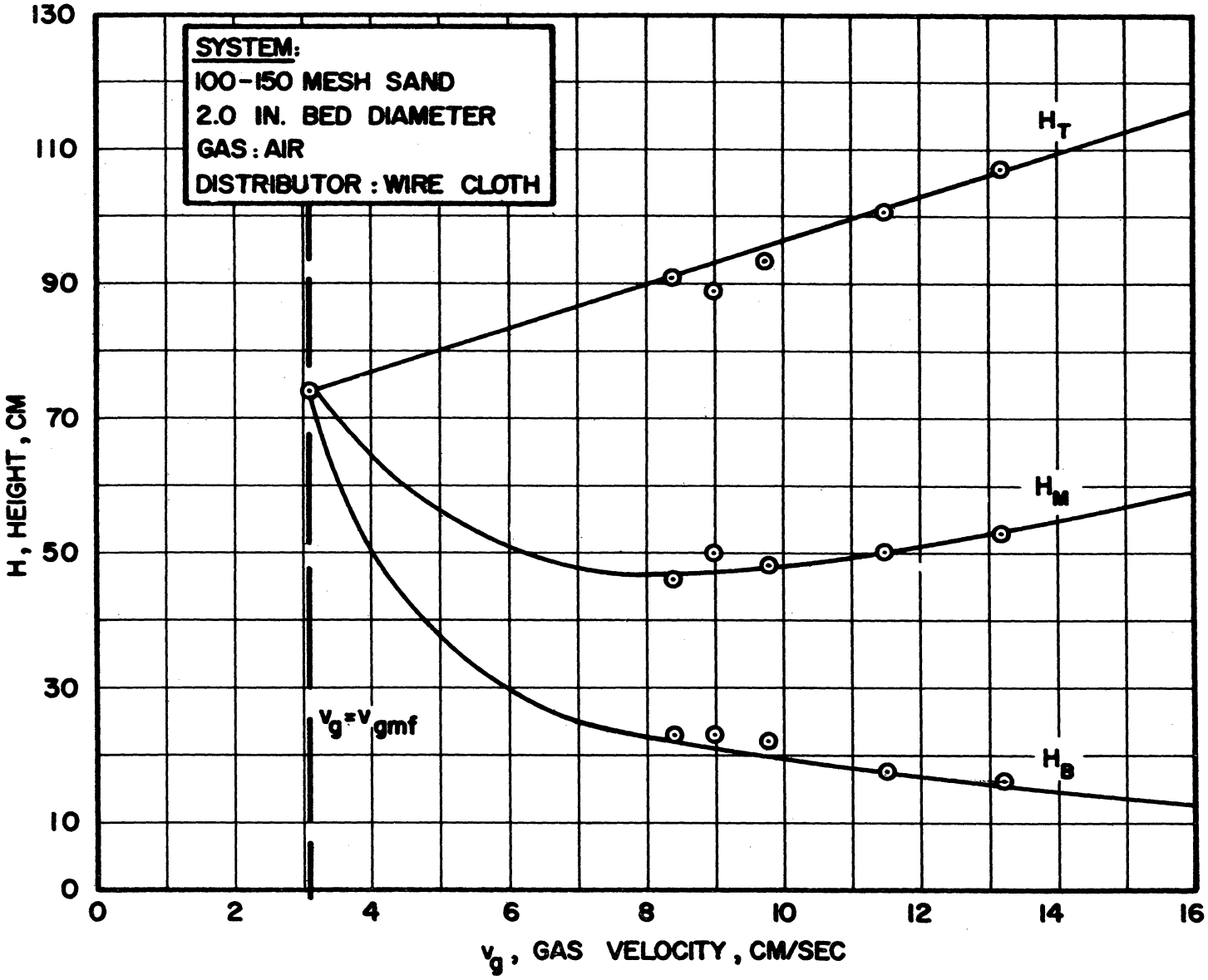

Figure 24. Level Curves for 100-150 Mesh Sand.

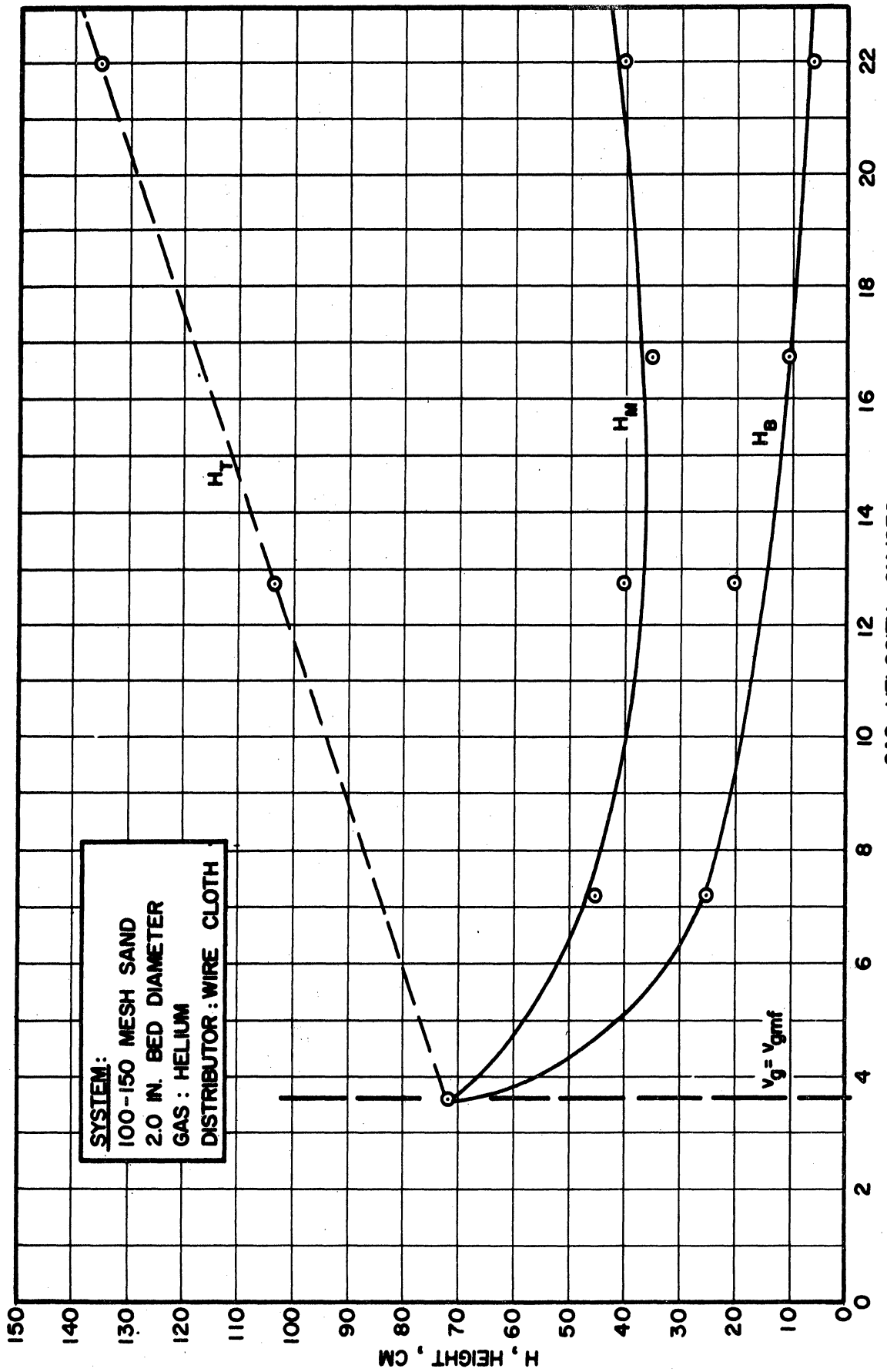

Figure 25. Level Curves for 100-150 Mesh Sand.

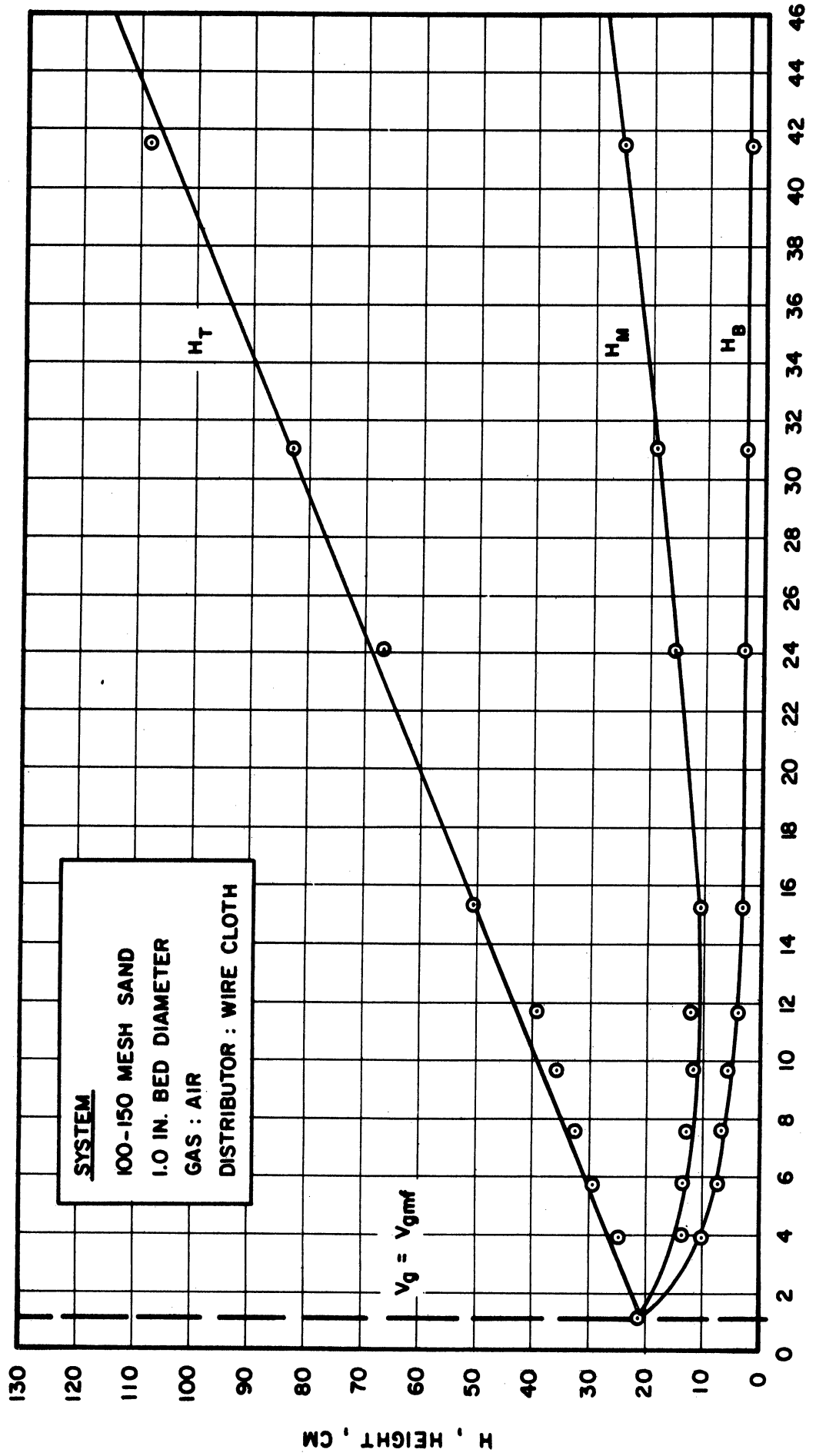

Figure 26. Level Curves for 100-150 Mesh Sand.

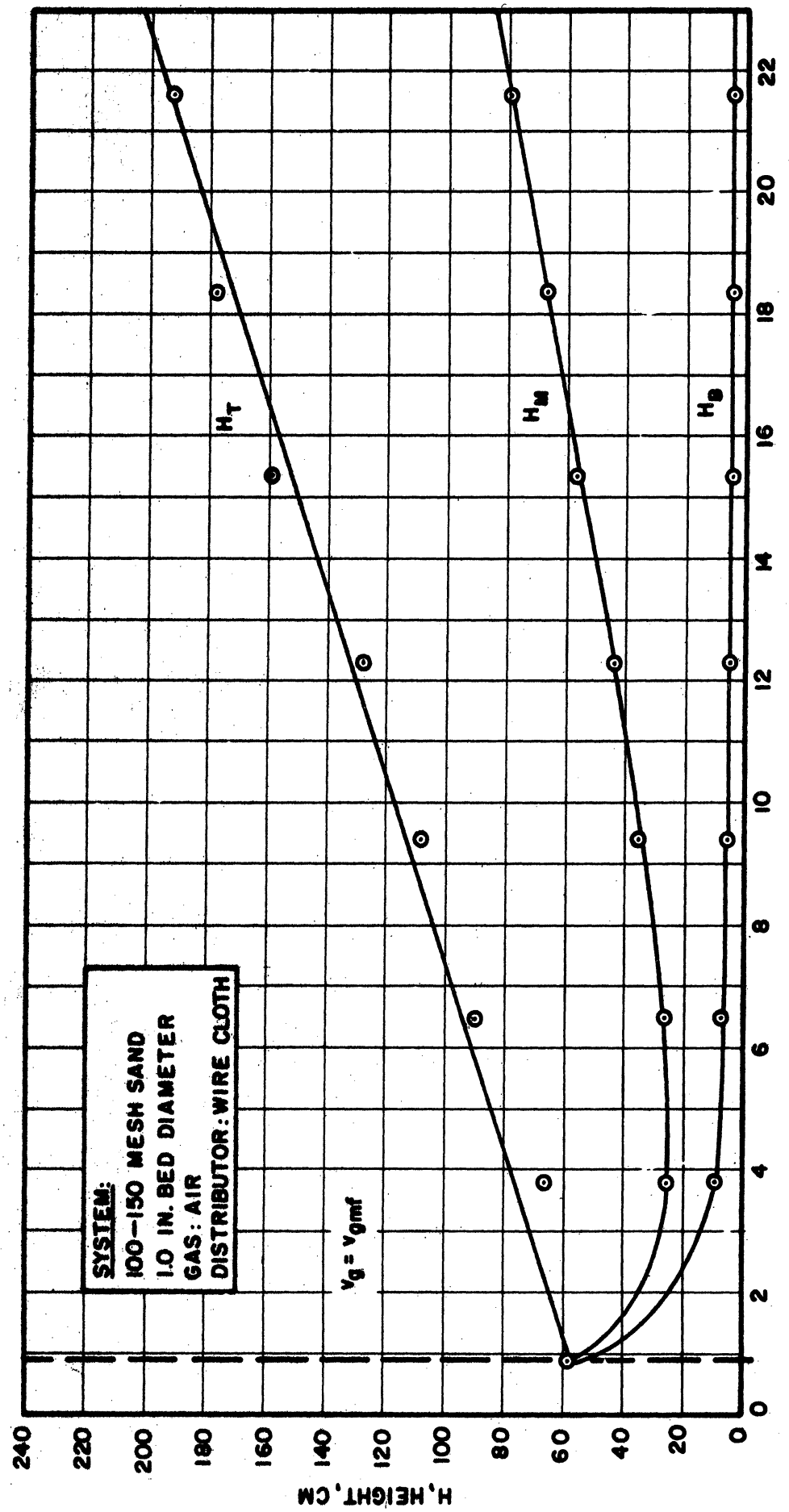

Figure 27. Level Curves for 100–150 Mesh Sand

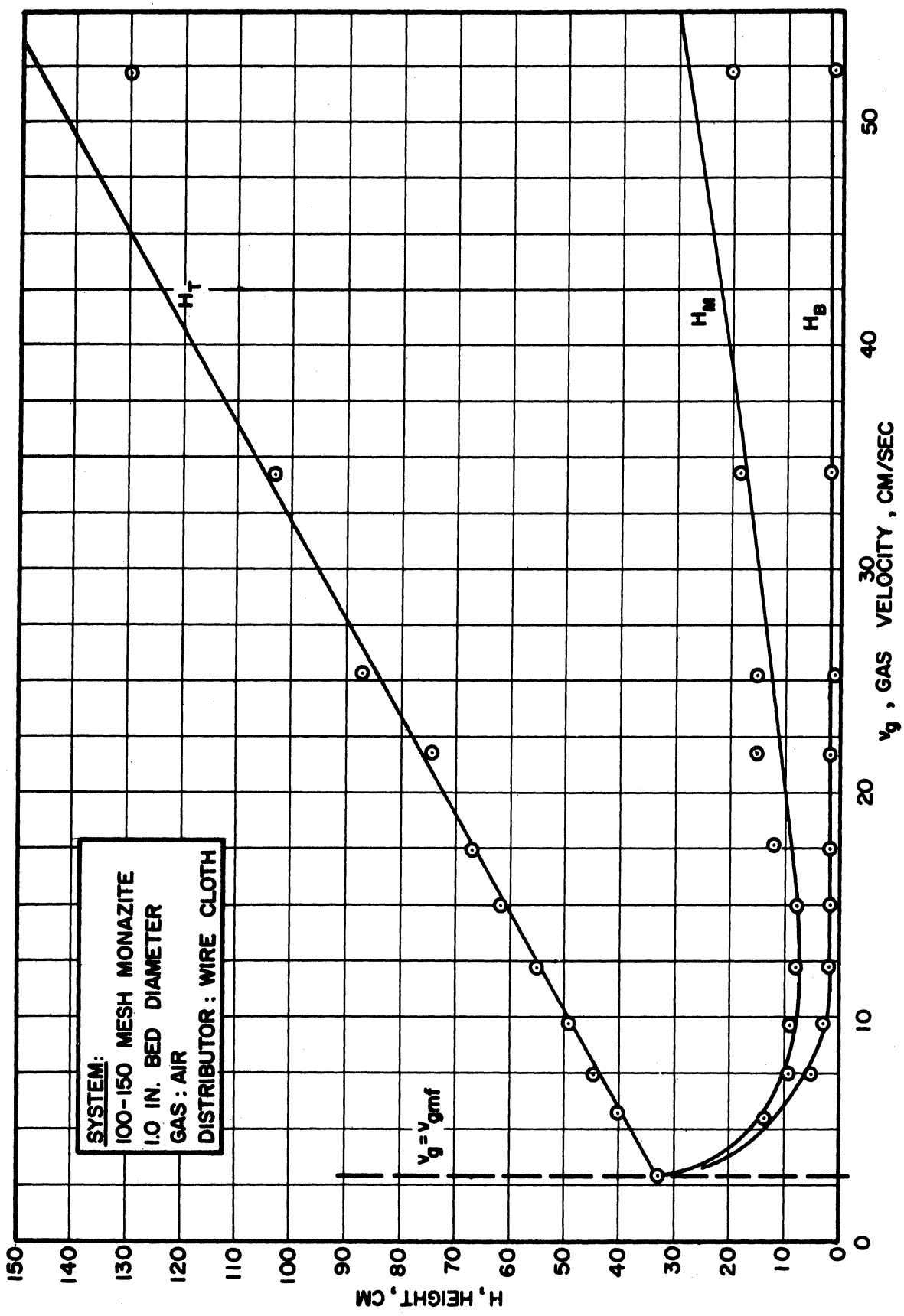

Figure 28. Level Curves for 100-150 Mesh Monazite.

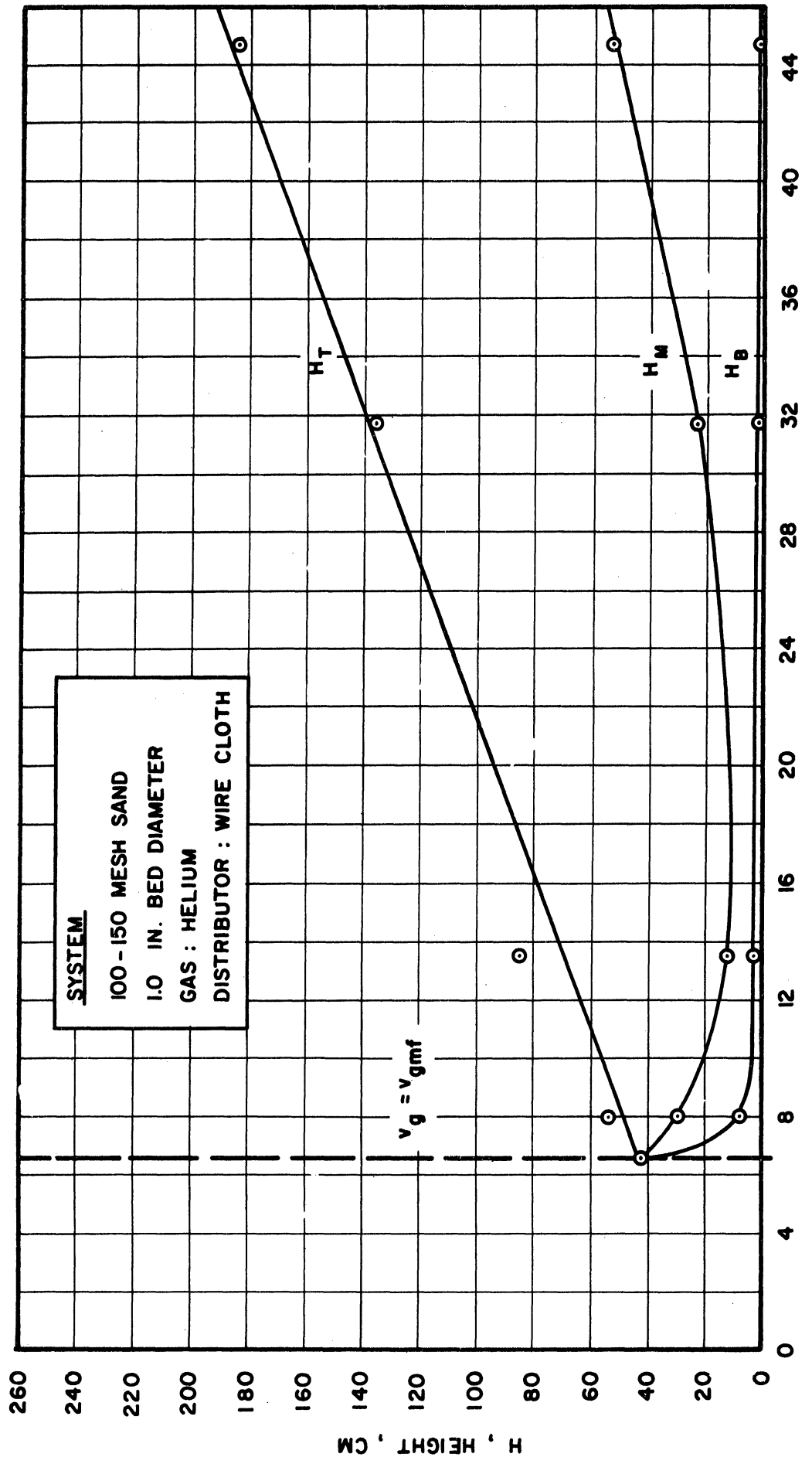

Figure 29. Level Curves for 100-150 Mesh Sand.

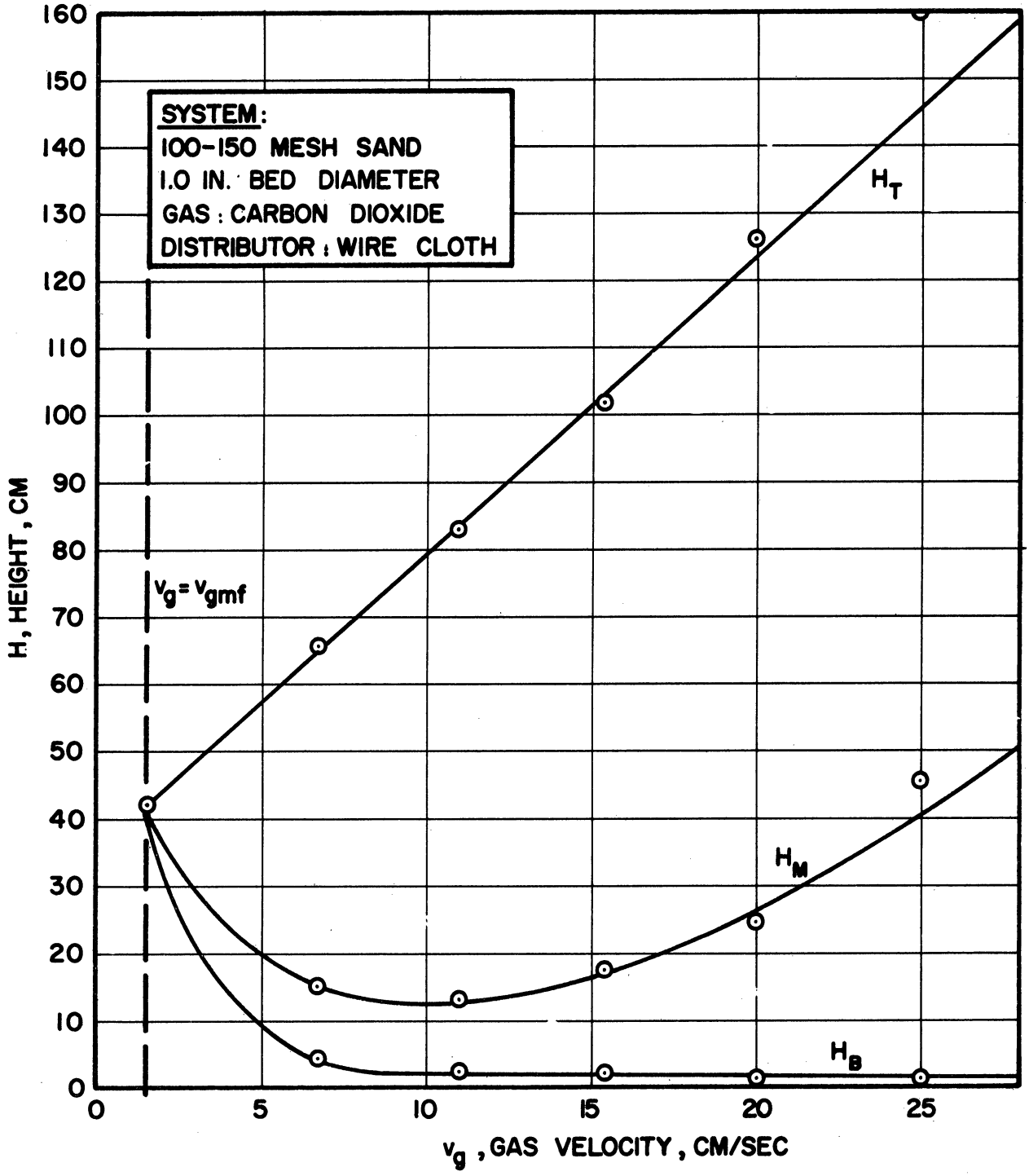

Figure 30. Level Curves for 100-150 Mesh Sand.

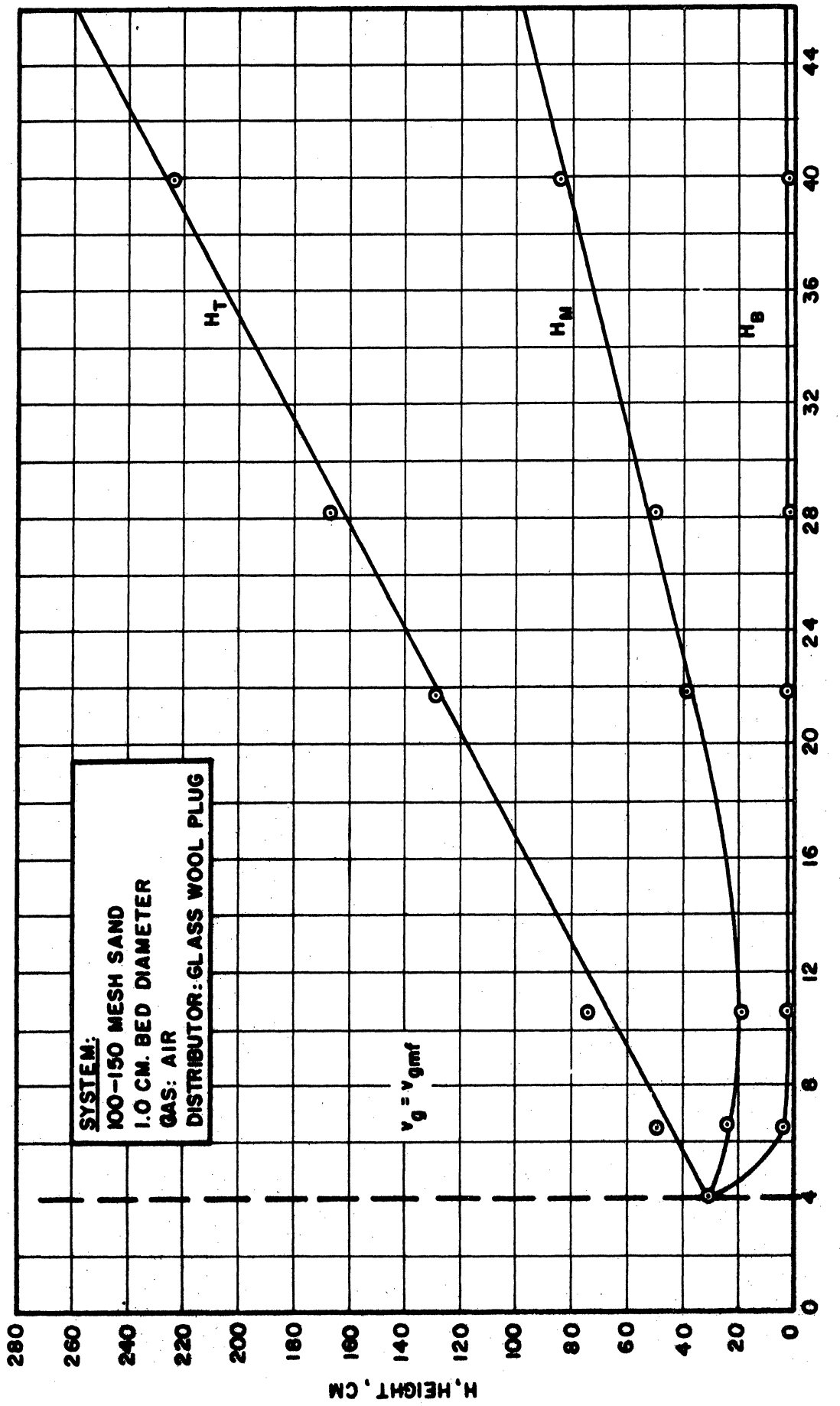

Figure 31. Level Curves for 100-150 Mesh Sand.

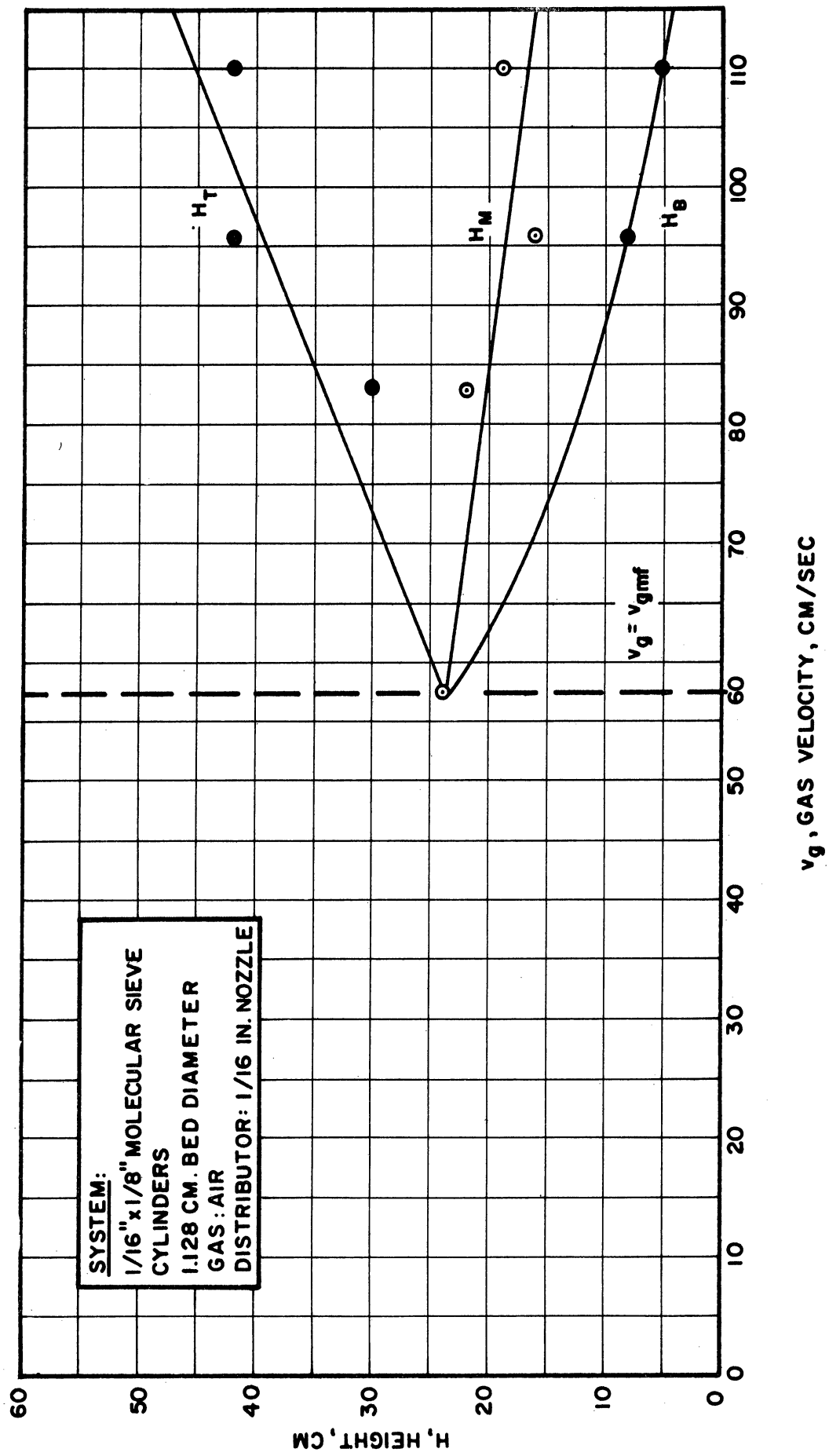

Figure 32. Level Curves Versus Velocity for 1/16" x 1/8" Molecular Sieve Cylinders.

designated H_B, thus creating a void space and a slug. If H_M was not too low, one or more slugs existed between the bubbling zone and the stable interface. The third slug from the top exists as a case 2 slug throughout most of its history. All slugs between the third and the bubbling zone were case 4 slugs. Figure 33 show pictorially the situations discussed above.

The shapes of the level curves for the systems studied are all similar. The curves in Figure 24 are the only ones which deviate in any respect. In this case a bubbling region preceded the slugging region as velocity was increased. The result is that the curves are translated to the right.

Conclusions.

The bubbling zone will be covered in the following section. The results of this section show that the bubbling zone occupies a small fraction of the total bed height.

The stabilization of the lower interface of the second slug can be explained in terms of drag forces. Nearly all drag correlations are of the form

$$F_D = A \rho_g V_g^2 \tag{81}$$

An entirely reasonable assumption for gases is that the product $\rho_g V_g$ is constant throughout the bed. It will vary from void space to slug. Hence F_D depends on gas velocity, which varies from point to point in the bed. The stable interface would then occur

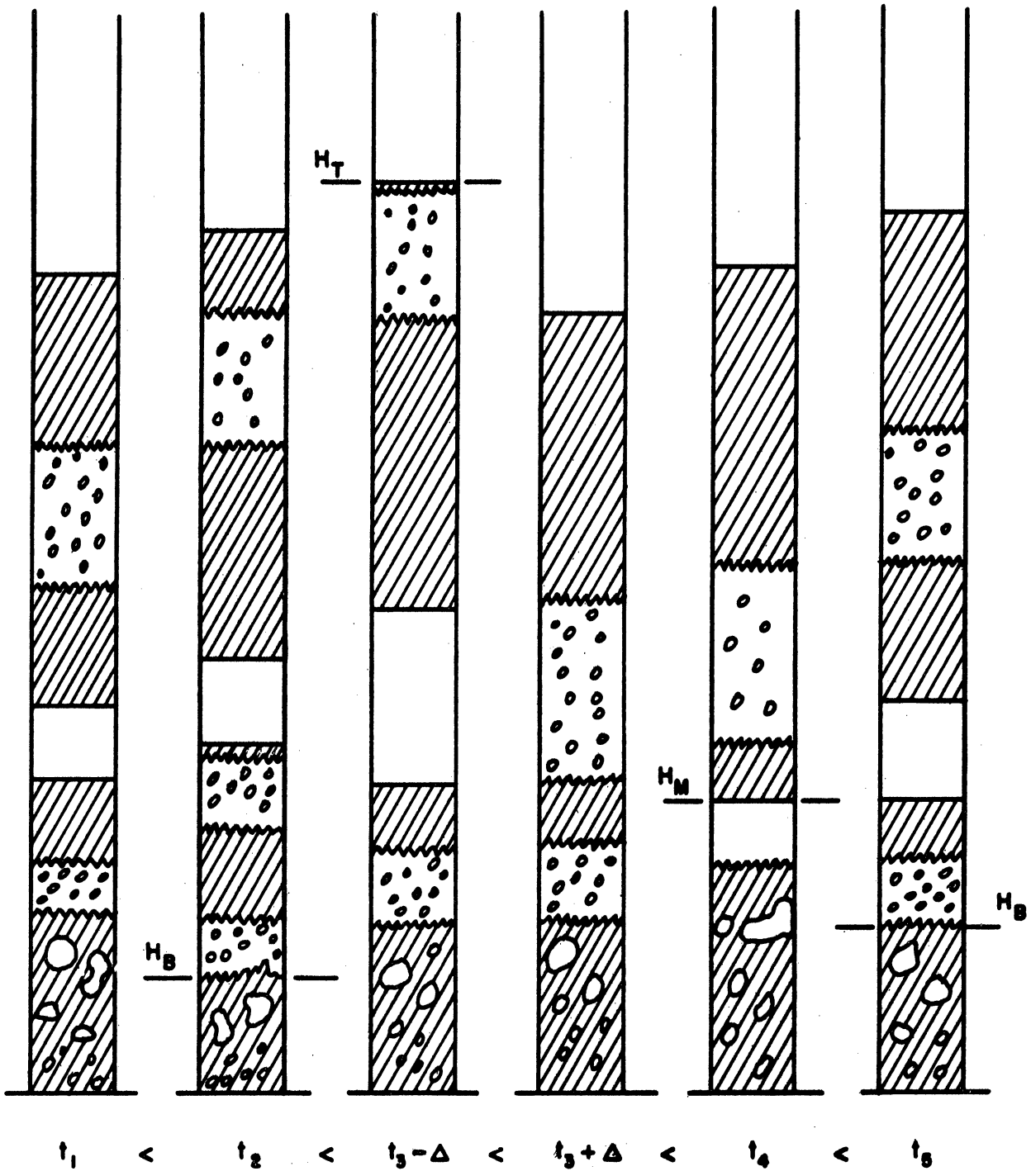

Figure 33. Illustration of Bed Configuration Versus Time. Physical Meaning of H_T, H_M, H_B. Not to Scale.

at the point in the bed where the gas velocity is such as to exert terminal drag on the particles of a lower slug surface. This is possible if the free cross section of the lower surface is low enough to yield the high interstitial velocity required for terminal drag. Existing drag correlations predict precisely where in the bed this event will occur.

This configuration is not particular to any one solid or bed support. Nozzles, porous plugs and wire cloth were all used as distributors without any noticeable change in the level curves. One therefore concludes that the bed support is relatively unimportant in determining bed configuration. Neither size nor density of solid would appear to be important, since the level curves for monazite and molecular sieve cylinders did not deviate in shape from the curves for the 100-150 mesh sand.

Thus the type of slugs existing in a system is known once the level curves for the system are known. No correlative techniques could be found which allowed a good prediction of these curves. The variables of bed diameter, bed height, gas properties and solid properties all affect these curves. Some comments can be made however. The H_T curve slope is a strong function of bed diameter, as is shown in Figure 34. The height of the bed for determining these slopes is the fractional increase in static bed height. The effect of increasing bed diameter is to decrease this slope. Since the H_T curve should pass through the point of incipient fluidization, this slope correlation allows a fair prediction of the H_T curve.

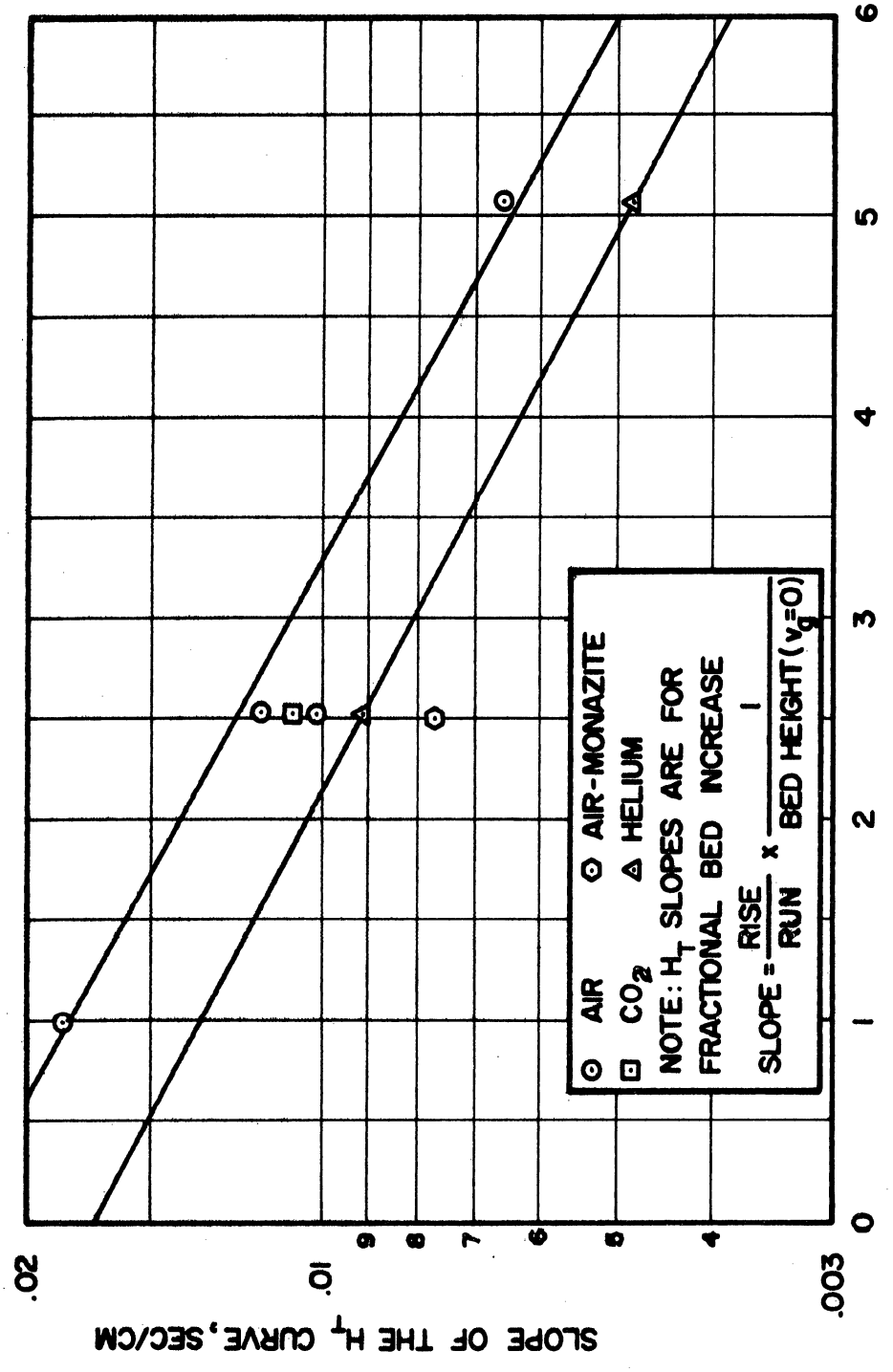

Figure 34. Effect of Bed Diameter on Slope of the H_T Curve.

The level H_B, the top of the bubbling zone of the bed, in all cases drops as velocity increases. It very quickly approaches a height corresponding to $H_B/D_t \cong 2$. This, for most slugging beds, is an insignificant part of the bed.

The H_M curves presents the greatest difficulty. Figure 35 shows a plot of the ratio of H_M to static bed height at the minimum of the H_M curve versus the velocity at that minimum. Considerable scatter is apparent. It is impossible to generalize at all from these data.

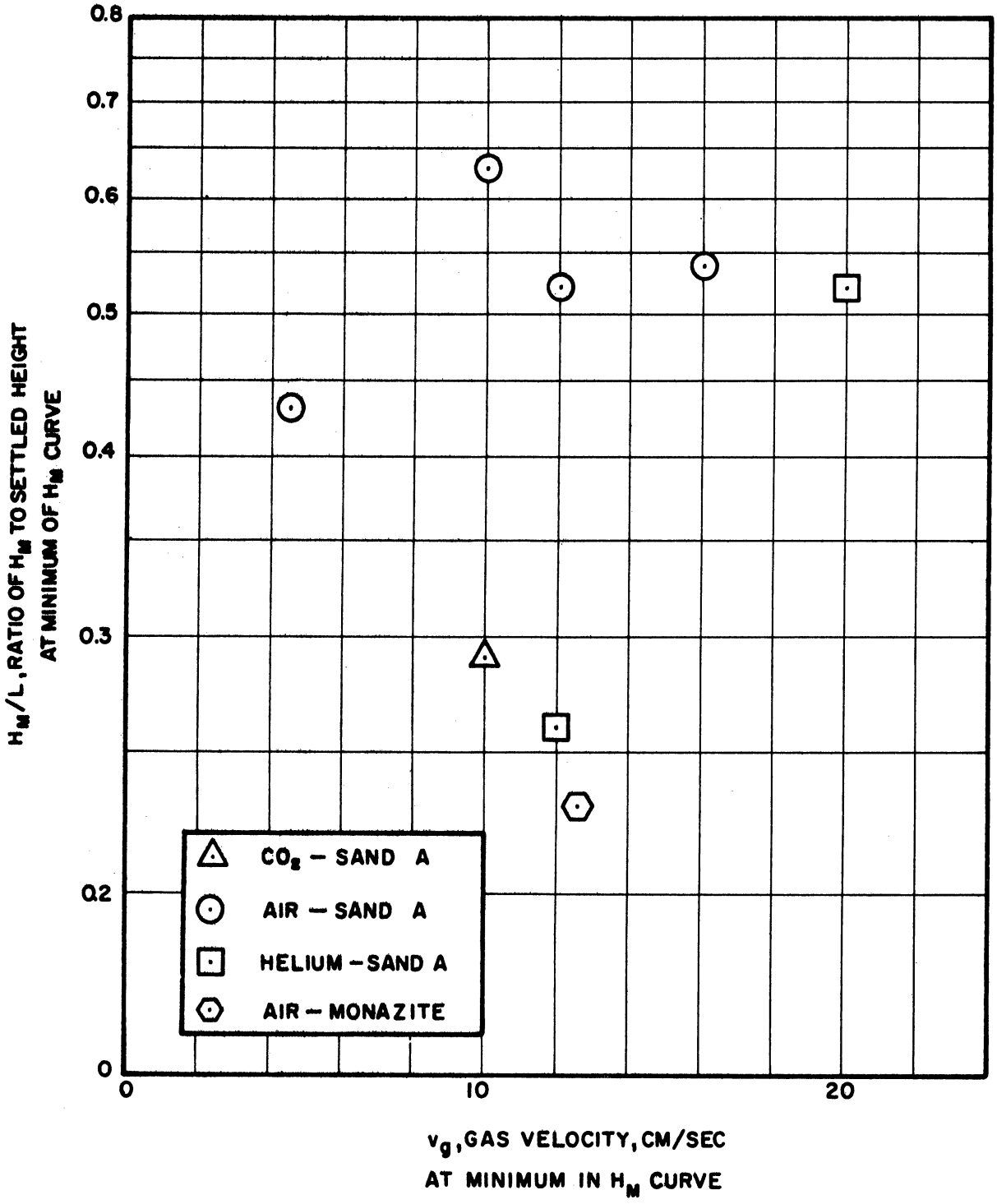

Figure 35. Location of Minimums in H_M Curves.

SLUG GENERATION

The mechanism of slug generation is a statistical process in that slugs of varying lengths are generated. The height at which slugs form has been treated in the preceding section. The two remaining questions are, then, what is the length of a slug when it forms and by what distance is it separated from the bubbling portion of the bed?

Let us treat the separation problem first. Suppose a slug of length y_o has just been formed. This means that the bottom bubbling section of the bed at some prior instant was H_B plus y_o. These additional solids, of length y_o, must have built up due to solids downflow. This rate is known to be Θ cm/sec. Therefore the time required to obtain length y_o is given by y_o/Θ. In this length of time gas will have been creating void spaces in the form of bubbles. Since the rate of gas flow in excess of the minimum fluidization velocity has been shown to proceed through the slugging portion of the bed as void spaces, it is reasonable to assume that this excess gas proceeds through the bubbling zone as bubbles. It is also reasonable that there is a relatively constant bubble holdup in that zone. If this is the case, then the excess gas which entered the bed during the interval y_o/Θ must be located beneath the newly formed slug. The separation of this slug from the bubbling zone will therefore be $V_{xs}y_o/\Theta$.

The second point, the size of the generated slugs, strongly suggests that some minimum length of bed above the level H_B will be

stable in that a slug can be formed which does not immediately disintegrate. There has been some work done in this area. Zenz and Othmer[12] state that the length-to-diameter ratio of slugs in slugging fluid beds may be used as a measure of the tangent of the angle of internal friction, α, for the fluidized solid. A reasonable value for α for the sands used in this study appears to be 64° [12] This value seems to be characteristic of sands in general. The tangent of this angle is 2.045. This then means that the bubbling section of bed should terminate at an elevation of $H_B = 2.0D_t$. This was verified visually. A generated slug in a 5.08 cm. bed was approximately 10 cm. in length. There is some variation in y_o observed. An arbitrary method for accounting for such variation is to assume that the generated slug lengths are normally distributed about a mean of $y_o=2D_t$ with some arbitrary standard deviation, σ. Experience dictates a value of $\sigma = 0.2D_t$. The slug generation mechanism suggested is therefore the random selection of consecutive values from such a distribution.

USE AND VERIFICATION OF PROPOSED MODEL

I. Prediction of Bed Configuration.

Procedure and Results

The model proposed, together with the information already obtained, make possible the prediction of total bed configuration as a function of time. The first step in the procedure is to determine all measured variables in the system. A numerical example will be carried out to illustrate the technique.

Bed diameter: 2.00"

Bed support: wire cloth

Solid: 100-150 mesh sand

Bulk solid density: 1.44 gm/cm^3

Mean particle size: 120 microns

Gas velocity: 7.00 cm/sec

Fluidizing velocity: 3.14 cm/sec

Excess gas velocity: 3.86 cm/sec

Solids downflow rate: 31.5 gm/cm^2 sec

Buildup velocity, Θ : 21.9 cm/sec

Bubbling zone height, H_B: 25 cm

Stabilization level, H_M: 48 cm

Maximum rise, H_T: 86 cm

Let us begin with an initial bed configuration chosen arbitrarily. The bed behaviour will be worked out for a sufficient period of time to allow the solution to reach a steady state. Refer to Figure 33.

Numbering slugs from the top down, this initial configuration is assumed to be:

Slug 1.	$x_1 = 80$ cm	
	$y_1 = 12$ cm	Case 2
	$z_1 = 68$ cm	
Slug 2.	$x_2 = 66$ cm	
	$y_2 = 20$ cm	Case 4
	$z_2 = 46$ cm	
Slug 3.	$x_3 = 44$ cm	
	$y_3 = 10$ cm	Case 4
	$z_3 = 34$ cm	
Bubbling zone.	$x_B = 32$ cm	
	$y_B = 32$ cm	
	$z_B = 0$ cm	

The slug generation height, $H_B + y_o$, is chosen from a random set of such numbers with mean 10 cm. and standard deviation 1 cm. Such a number for the first generation is 11 cm.

At this point, let us recall the equations governing slug movement. These are:

Case 1 slug. No material inflow or outflow.

$$Y = Y_o$$
$$X = X_o + V_{xs}(t - t_o)$$
$$Z = Z_o + V_{xs}(t - t_o)$$

Case 2 slug. Material outflow only.

$$y = y_o - \theta(t-t_o)$$
$$x = x_o + v_{xs}(t-t_o)$$
$$z = z_o + (\theta + v_{xs})(t-t_o)$$

Case 3 slug. Material inflow only.

$$y = y_o + \theta(t-t_o)$$
$$x = x_o + (v_{xs} + \theta)(t-t_o)$$
$$z = z_o + v_{xs}(t-t_o)$$

Case 4 slug. Material inflow and outflow

$$y = y_o$$
$$x = x_o + (v_{xs} + \theta)(t-t_o)$$
$$z = z_o + (v_{xs} + \theta)(t-t_o)$$

These equations will govern the movement of the assumed slugs until (1) one of the slugs changes from one case to another, (2) a slug disappears, or (3) a slug is generated. When one of these events occurs, one must review the system and reassign a new case, possibly the same as before, to every slug. At this point, the values of x_o, y_o, z_o and t_o are also changed appropriately. For the example at hand, we have:

$$\theta + v_{xs} = 25.76$$

Since only three slopes apply to all x, y and z curves, a graphical solution is the least tedious route. Figure 36 indicates this graphical solution. The heights x_1 and z_1 change according to the prescribed slopes until t = 0.09 seconds. At this time the lower surface of the second slug has reached H_M = 48 cm. Hence the slug

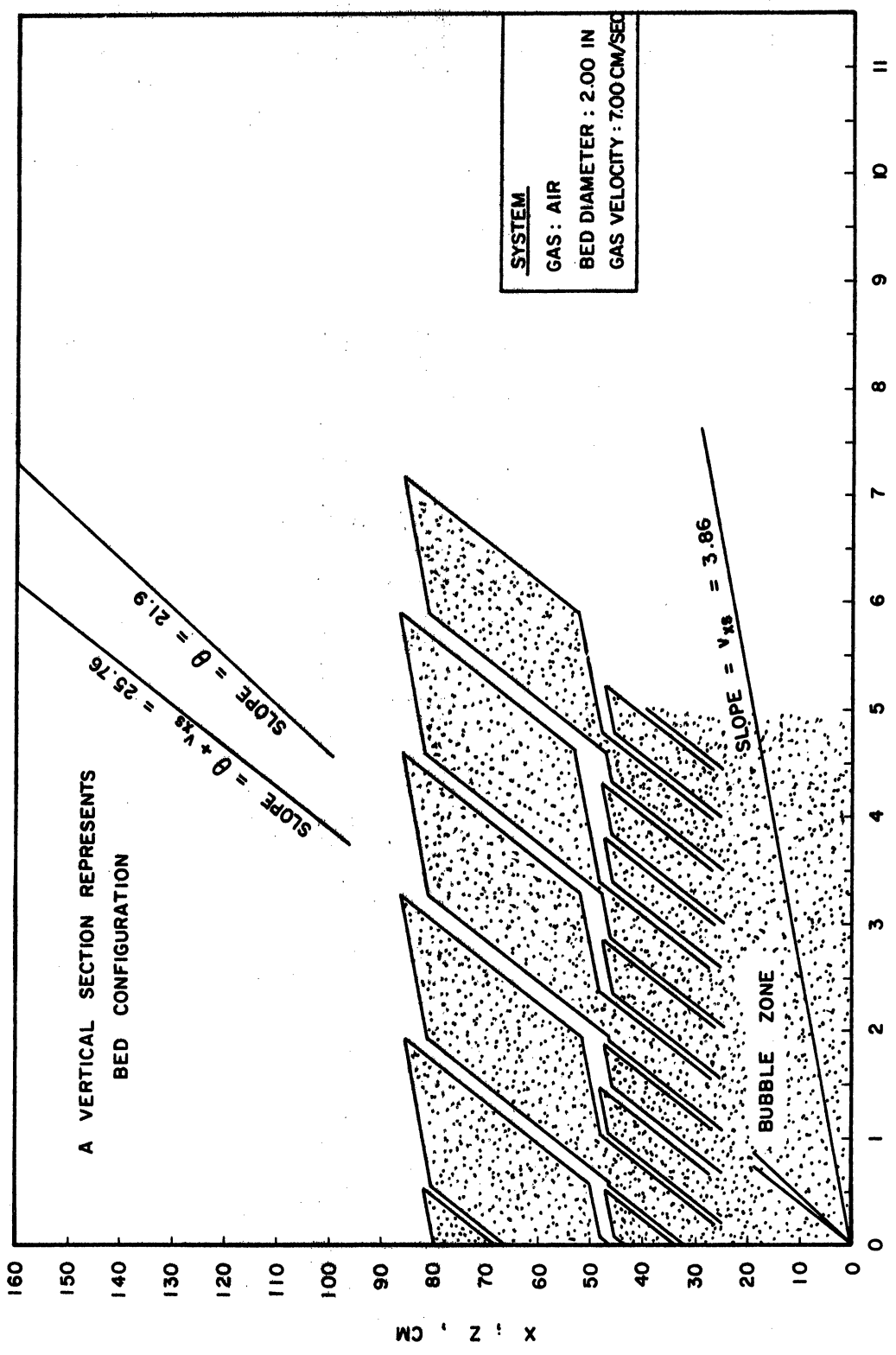

Figure 36. X, Height of the Top of a Slug, and Z, Height of Bottom of a Slug, Measured From Bed Support, Versus Time. Shaded Area is High Solids Density. These Curves Predict:

H_T = 86 cm

f = 1.35 sec

types change to :

Slug 1 - Case 2

Slug 2 - Case 3

Slug 3 - Case 2

The slugs change according to the prescriptions for these cases until t = 0.20 seconds. At that time a new slug is generated and the slug types are then:

Slug 1 - Case 2

Slug 2 - Case 3

Slug 3 - Case 2

Slug 4 - Case 4

At the instant before generation, the bubbling zone had attained a height of 37 cm. After generation, the height reverted to 25 cm. with a new 11 cm. slug in the system. The bottom surface of this slug is moved upward an appropriate distance to account for the excess gas which must have accumulated beneath the slug during its generation. This distance is the separation of two lines of slopes $V_{XS}+\Theta$ and Θ, drawn from the point of height H_B = 25 cm. at the instant of the previous generation, at the time of this generation.

The system obeys this new set of rules until t = 0.52 seconds. At that time the third slug disappears and the first or top slug disappears. This is a coincidence, not the usual occurrence. The system now changes to:

Slug 1 - Case 2

Slug 2 - Case 3

Figure 36 shows this general procedure carried out for five full cycles of the bed. Due to a fortunate choice of initial configurations, this is sufficient to obtain the steady state variation in bed configuration.

This example demonstrates the use of the model and auxiliary information for the prediction of bed configuration as a function of time. Two results are immediately apparent. The maximum height to which the bed should rise is 86 cm. in Figure 36, comparing very well with the observed H_T of 86 cm. Second, the period of one fluctuation, measured peak to peak, is predicted to be 1.35 second. This compares well with the observed period of 1.44 seconds.

Conclusions.

Sufficient visual observations had been made at this point to qualitatively verify assumptions one and two of the proposed model. There existed, in the systems observed no radial variations outside of the bubbling zone. Slugs and void spaces are clearly distinguishable.

The model has been shown to be a fairly simple one to use to predict a fairly complex phenomenon-bed configuration. It remains to be seen whether or not it can accurately predict bed behaviour.

II. Period of fluctuations.

Procedure and Results.

There is a second method of predicting the period of bed fluctuations in the zone between H_M and H_T which is much less tedious

than the above procedure. One requires an estimate of the maximum length of the top slug in the system. The best experimental method for obtaining this estimate is to measure H_M and H_T. The fraction $(H_T-H_M)/H_T$ is a measure of the fraction of the expanded bed height which lies in the zone of the two uppermost slugs. It is therefore an estimate of the expanded length of the top slug in the system at the moment of its formation. To translate this to the true maximum length of the top slug, one need only multiply by the static bed height:

$$(82) \qquad Y_{1,max} \doteq \frac{H_T - H_M}{H_T} \cdot L$$

Once this estimate of $Y_{1,max}$ has been obtained, the period of upper bed fluctuation is easily obtained. The only way that this top slug can disappear is via solids downflow. This solids downflow rate is known; it is Θ. Therefore the time for disappearance which is the period, is given by

$$(83) \qquad \tau = Y_{1,max}/\Theta$$

In the example being considered, one finds

$$Y_{1,max} = \frac{86-48}{86} \cdot 74 = 32.7 \text{ cm}$$

hence

$$\tau = 32.7/21.9 = 1.49 \text{ sec}$$

which again agrees quite well with the observed period of 1.44 seconds. This procedure will be referred to as the shortcut procedure. Figures 37 through 44 show the curves predicted by this

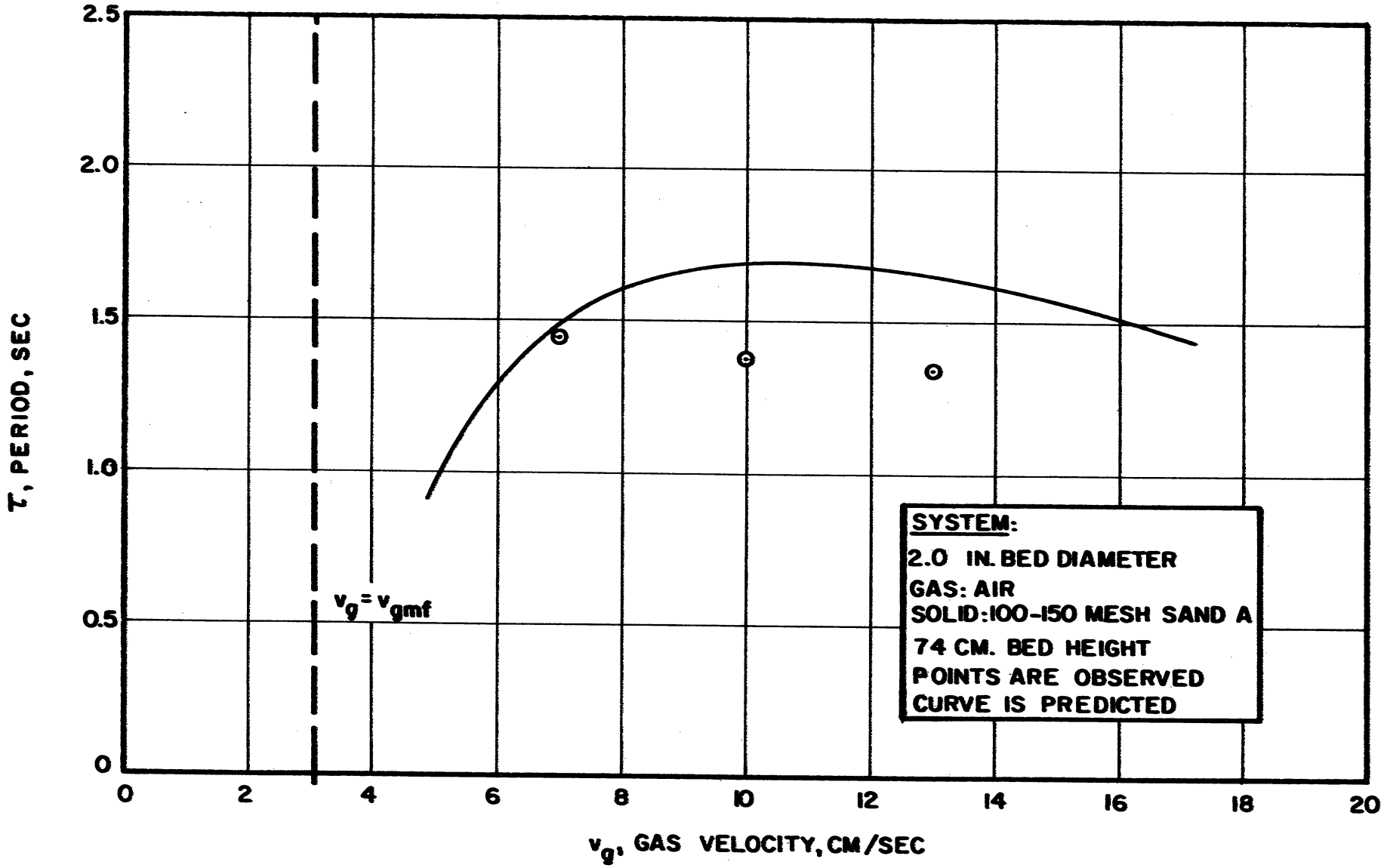

Figure 37. Upper Bed Fluctuation Period Versus Gas Velocity.

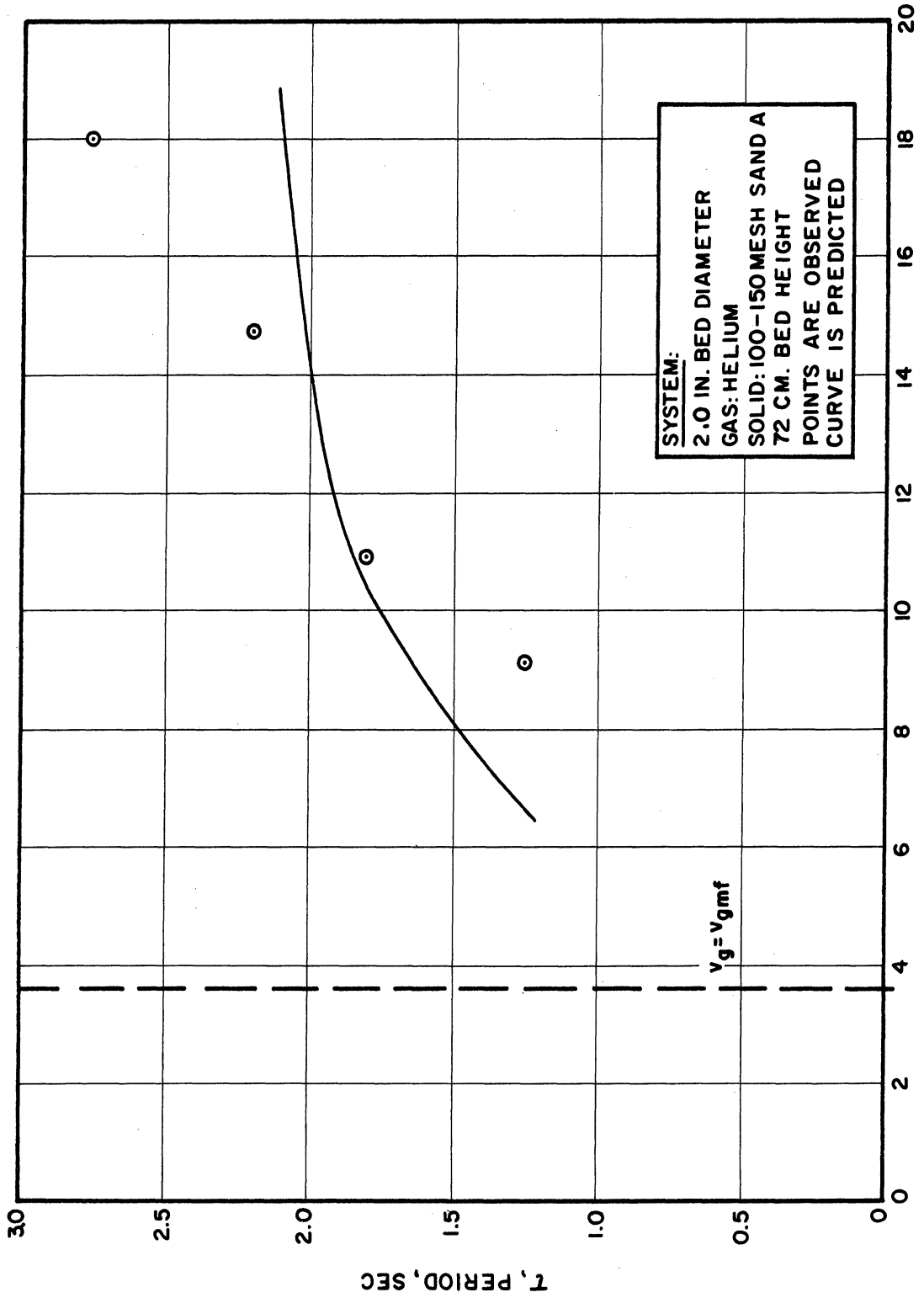

Figure 38. Upper Bed Fluctuation Period Versus Gas Velocity.

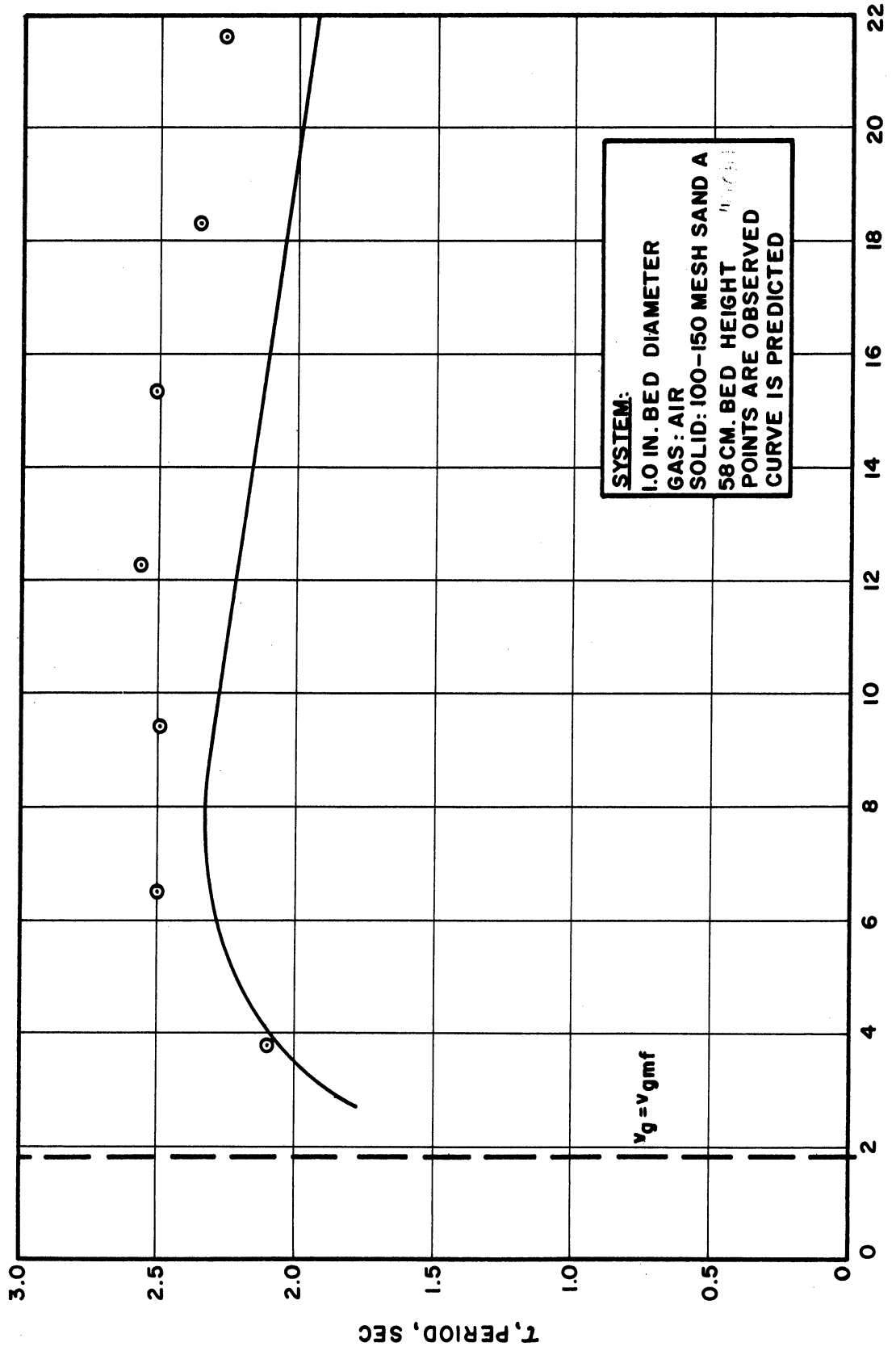

Figure 39. Upper Bed Fluctuation Period Versus Gas Velocity.

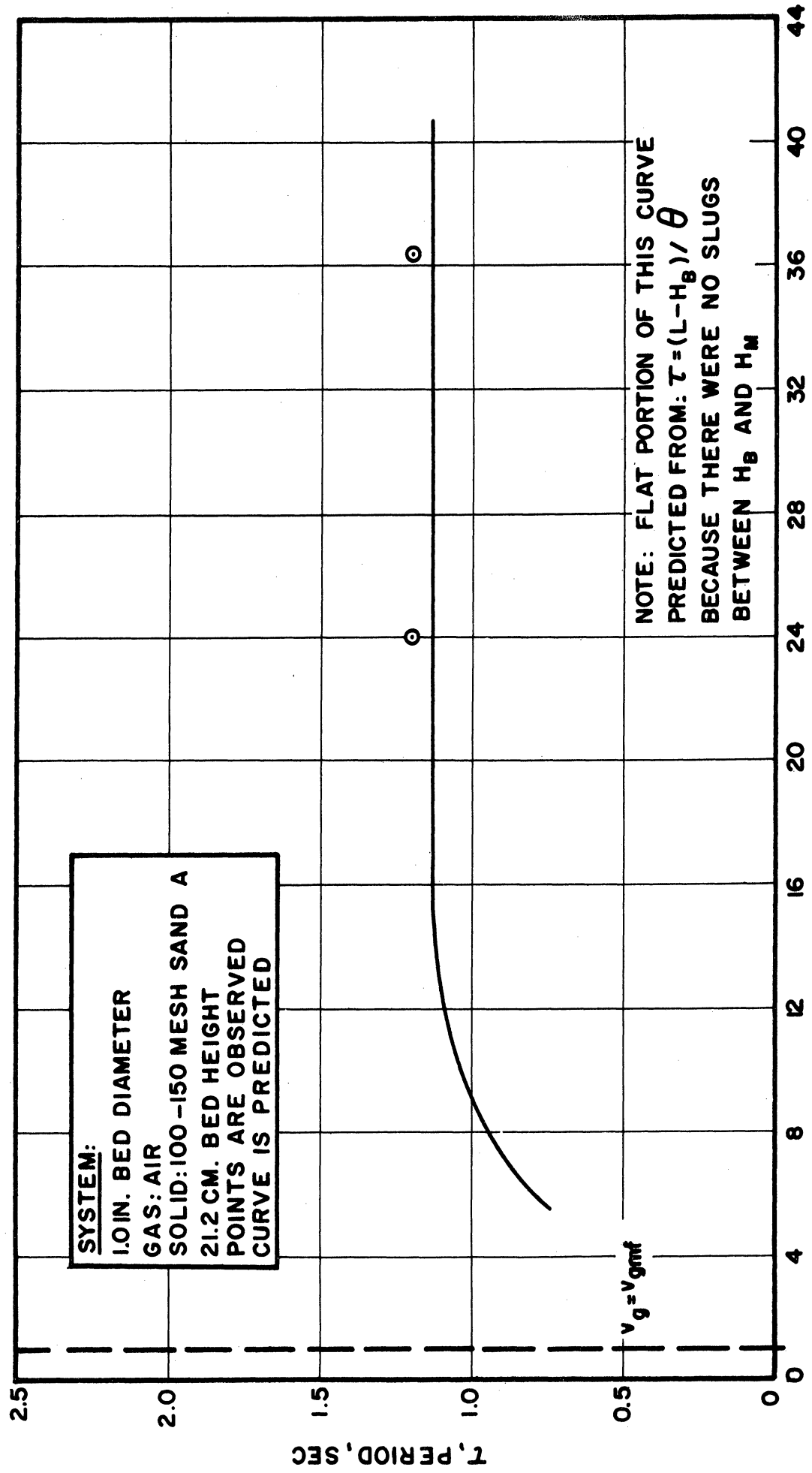

Figure 40. Upper Bed Fluctuation Period Versus Gas Velocity.

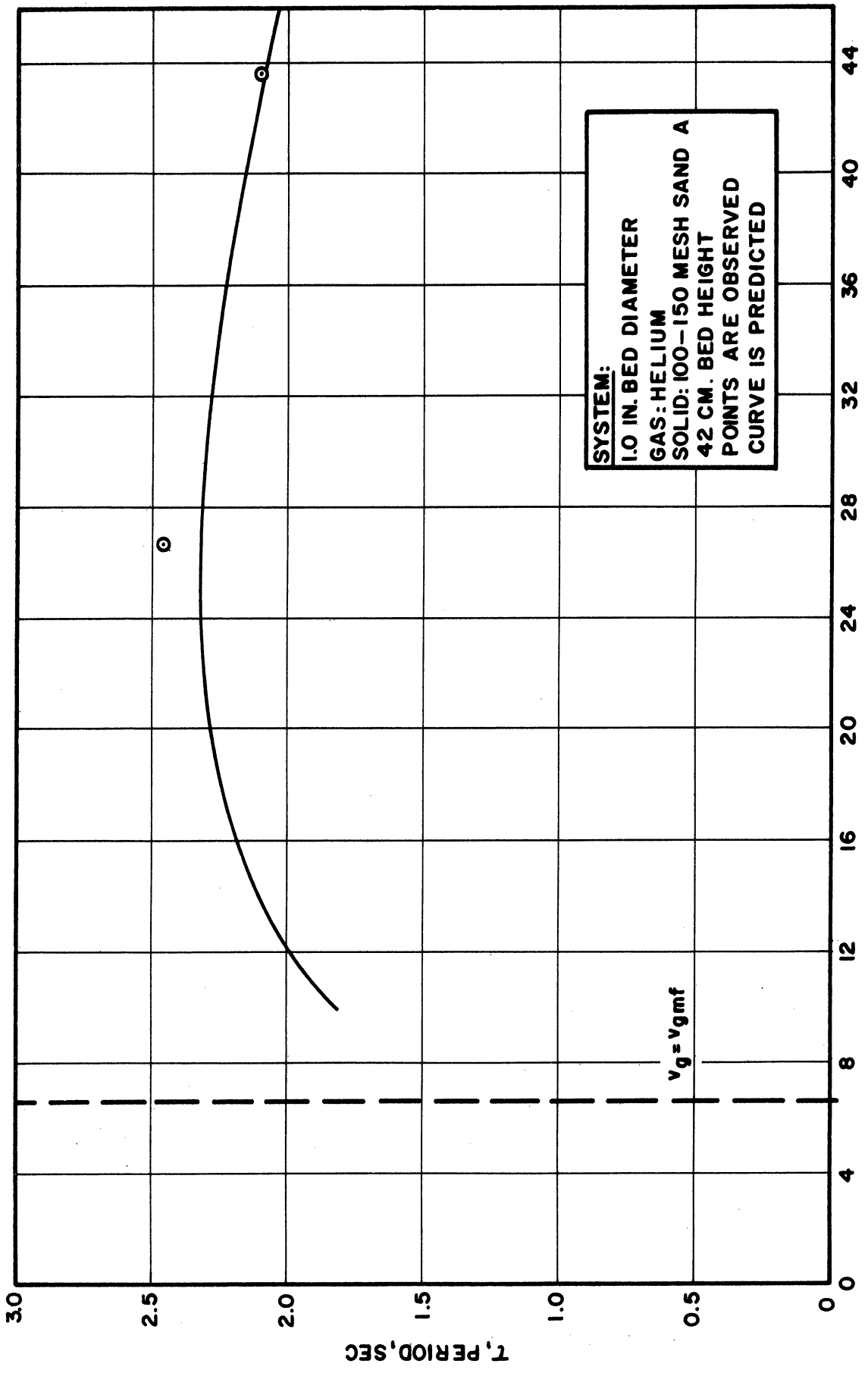

Figure 41. Upper Bed Fluctuation Period Versus Gas Velocity.

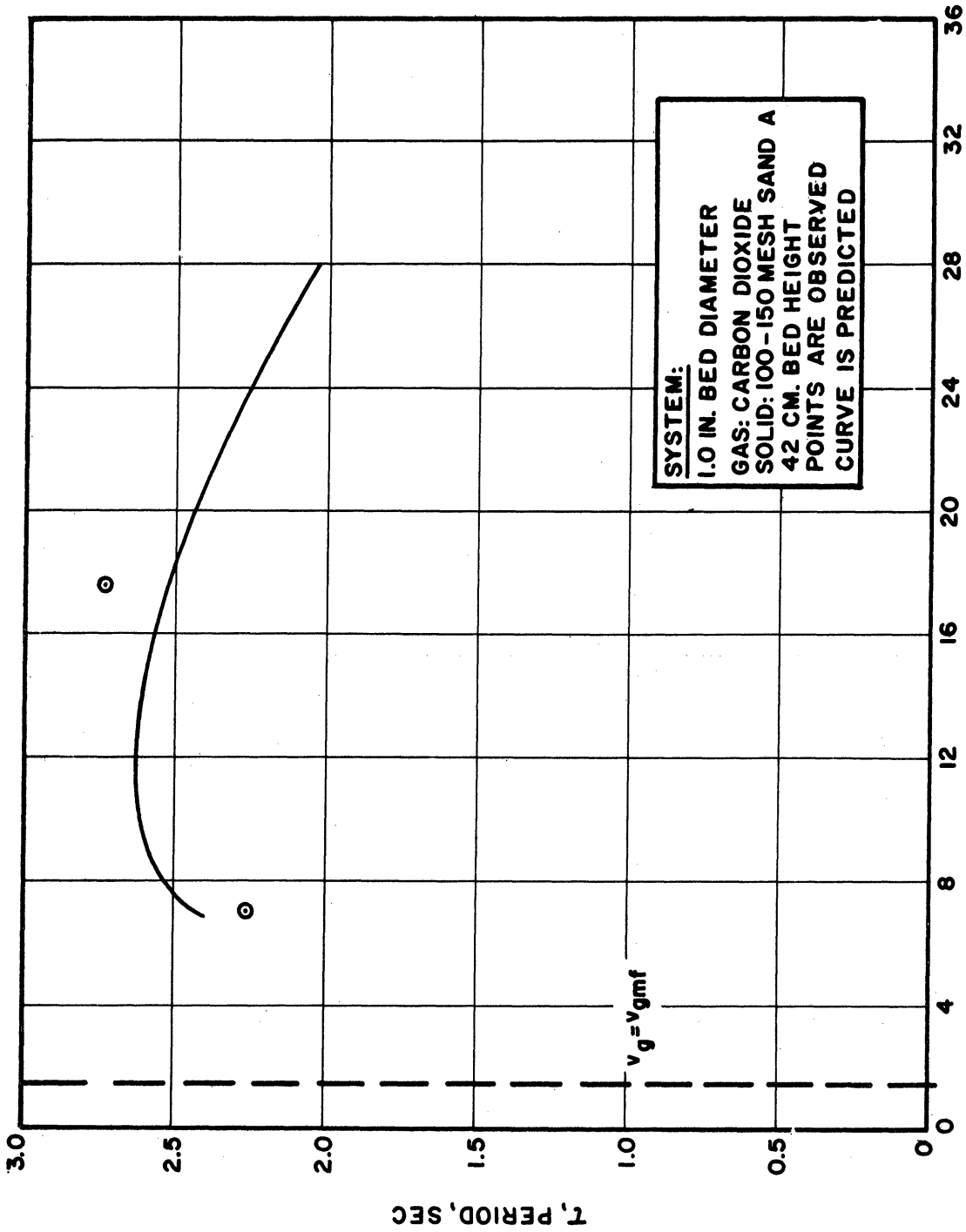

Figure 42. Upper Bed Fluctuation Period Versus Gas Velocity.

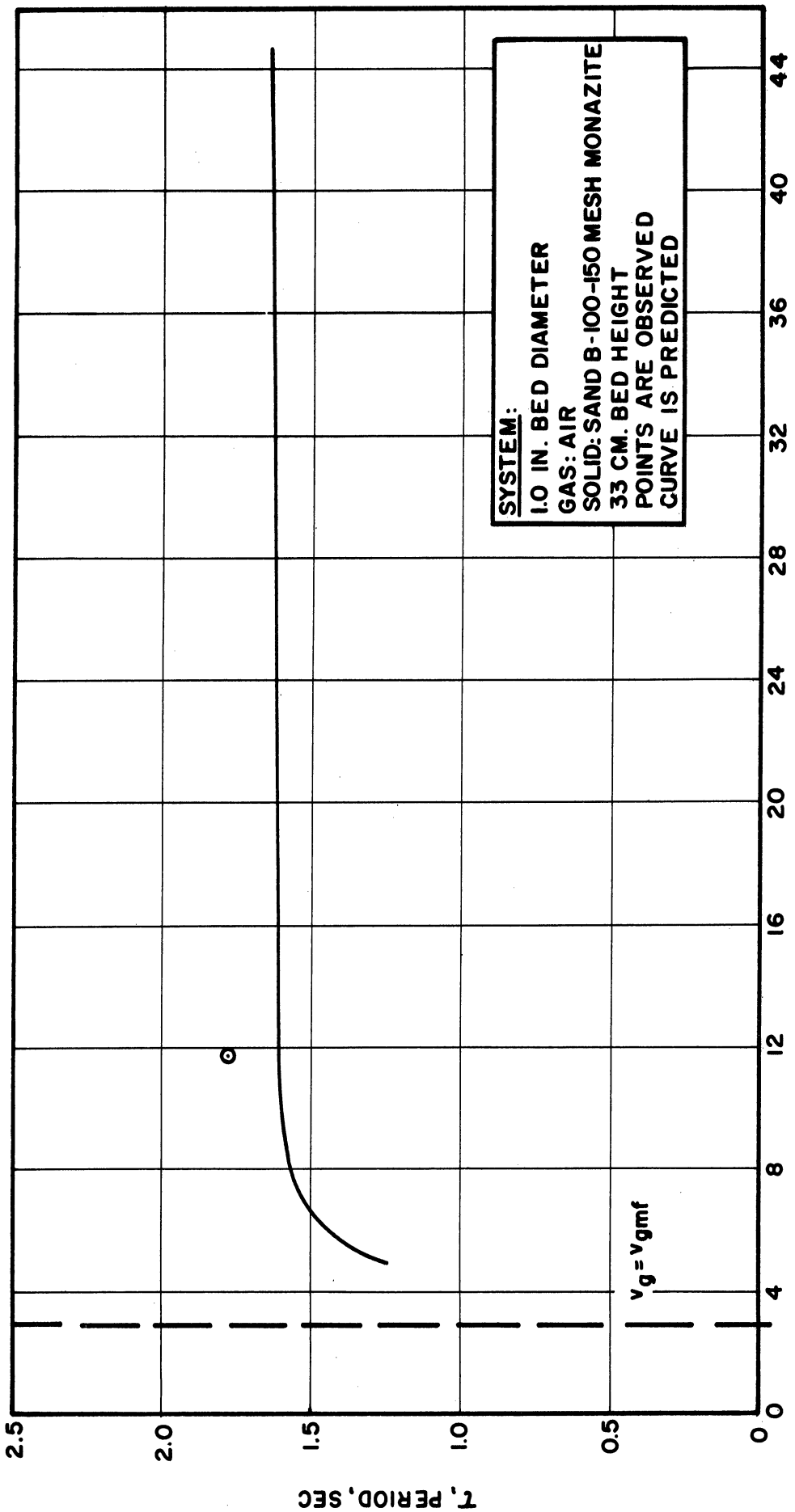

Figure 43. Upper Bed Fluctuation Period Versus Gas Velocity.

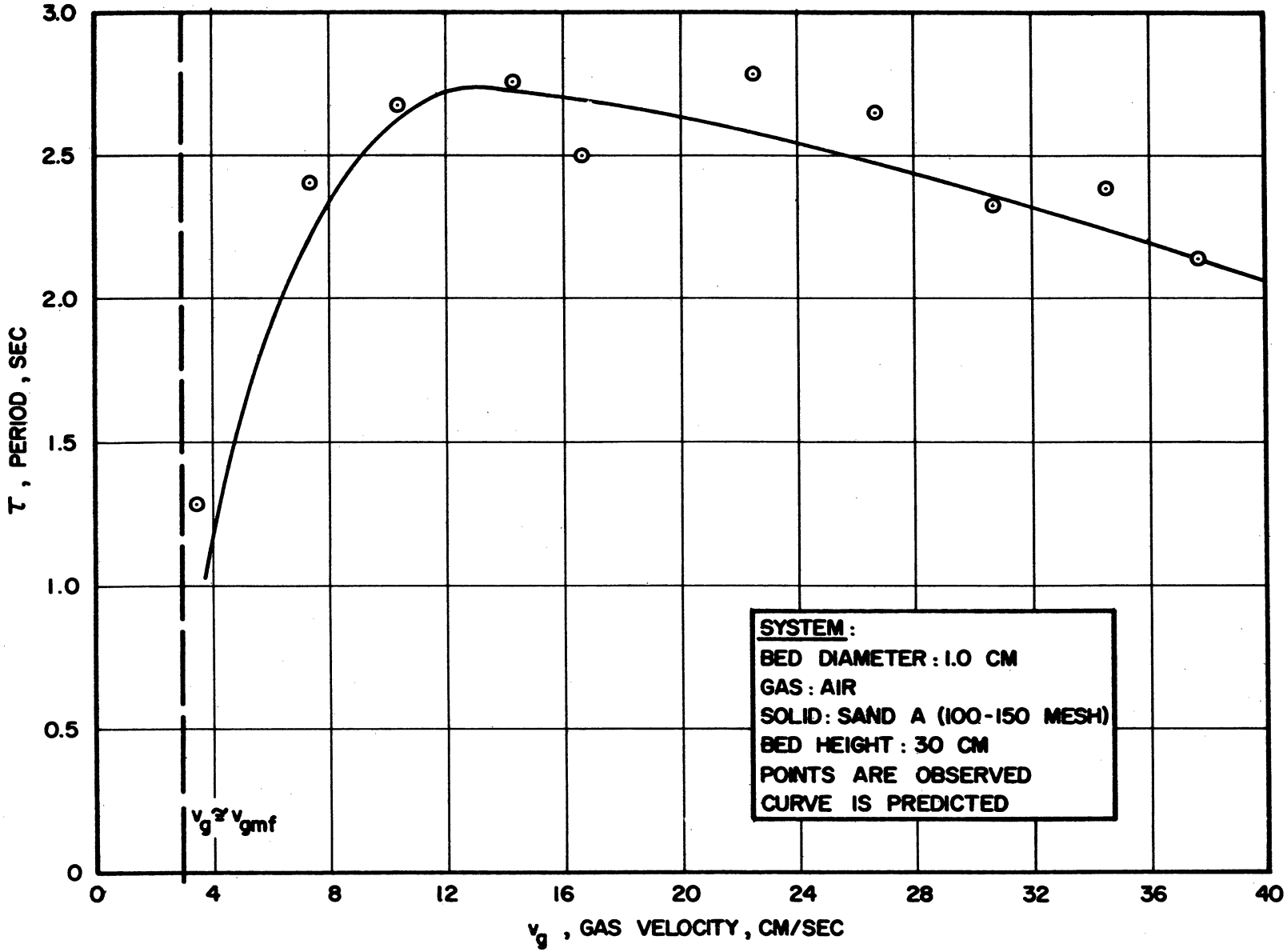

Figure 44. Upper Bed Fluctuation Period. Versus Gas Velocity.

shortcut procedure for period versus velocity. The observed data are also shown on these plots. This period applies to the upper section of the bed, that region bounded by H_T and H_M. This constitutes from 40 to 95% of the bed, a good average figure being 75%. The remainder of the bed is a region of bubbling and of small slugs. No attempt has been made to correlate these period data since all components of the period, H_T, H_M, and θ, have been correlated in previous sections.

The measurement of period was done in two ways. The first was visual observation coupled with a high speed strip chart and marker. Each time a maximum was observed in the upper bed surface, the strip chart was marked. An average over 30 or more readings was recorded. The second method was the measurement of peak to peak distances on a pressure-time recording of the upper section of the bed. This type of measurement will be discussed in more detail in the succeeding section.

Conclusions.

The good agreement between the predicted and observed periods supports the model used to arrive at the prediction. All the assumptions which go into this estimate of period are thereby verified.

III. Pressure Profiles.

Prediction from Model.

An acid test of the model is the use of it to attempt a prediction of bed pressure profiles. The prediction of configuration

serves as the basis for determining pressures. Let us recall assumption 10 of the proposed model. This concept is that gas flows through a slug at the velocity for minimum fluidization. If this is true, then the pressure drop per unit length of such a slug must be the pressure drop per unit length of bed at the point of incipient fluidization. This fact, coupled with the supported hypothesis (assumption 9) of no pressure drop in a void space, is enough to enable one to calculate pressures from the bed configuration.

Let us return to the example begun in the discussion of bed configuration. One more piece of information is necessary; the pressure drop per unit length at incipient fluidization:

$$\frac{\Delta P}{L} = 0.0217 \text{ psi/cm}$$

Suppose now that we wish to compute the pressure difference between two taps located 60 cm and 75.7 cm above the bed support at a time of 2.0 seconds. Referring to Figure 36, we find that at that instant the entire region between taps is filled with solids in the form of a slug. The pressure differential will therefore be:

$$\Delta P = 0.0217 \times 15.7 = 0.343 \text{ psi}$$

Proceeding in this manner, one can establish the pressure differential between these taps as a function of time.

Suppose that such a pressure versus time recording is available. A much easier check on the accuracy of the model than working out the bed configuration, and then pressures, is available. The first check is on the observed frequency of slugging. This has already been checked and verified. The second check is on the slopes of the pressure-time

curves. These slopes must fall into three categories for the slugging zone. They must either arise from an interfacial increase slope of V_{xs}, θ, or of $V_{xs} + \theta$, the only three cases allowed in the model. Therefore measurement of the slopes of the pressure-time curve must be one of the following three:

1. $V_{xs}(\Delta P/L)$
2. $(V_{xs}+\theta)(\Delta P/L)$
3. $\theta(\Delta P/L)$

Measurement of slopes then, in conjunction with period, provides a check on the model. In practice the third one occurs only at the extreme bottom of the bed and is not measured.

Experimental Procedure.

The apparatus for measuring pressure-time curves had been shown in Figure 15. The only modification used for this work was the addition of more pressure taps. The gases used in these experiments were humidified by bubbling through approximately 10 inches of water in order to minimize electrostatic effects. This technique proved completely effective. The experimental procedure is discussed in the section on the pressure technique for measuring solids downflow rate.

Results.

The first result to be discussed is the agreement between the predicted pressure-time curves and the experimentally observed curves for two different gases in a 2.00 inch diameter tube. Figures 45

and 46 show predicted and observed pressure-time curves for air-sand A in a 2.00 inch tube at a gas velocity of 7.00 cm/sec. Figure 47 shows the "noise" produced at the bottom of the bed due to the bubbling action.

At this point it would be in order to disgress for a moment and explain a feature of all oscillographic pressure-time records produced in this study. None of these records, it will be observed, have any specified units for the ordinate. The units are mullivolts. The characteristic curve for the particular pressure transducer used, together with the calibration of the Sanborn recorder permitted all values taken from these curves to be translated into pressure-time data. These in turn can be converted via the quantity $\Delta P/L$ to velocity data: Θ, v_{xs}, etc. This will be done in all cases preceding and succeeding without further comment. The transducer characteristics are shown in Appendix C. The Sanborn recorder was always calibrated for a sensitivity of 5.00 millivolts per ordinate centimeter.

Figure 48 shows the results of pressure-time measurements at two other air velocities for the 2.00" bed of 100-150 mesh sand.

Figure 49 shows pressure records at three elevations in the system of 100-150 mesh sand in a 2.00" diameter bed fluidized with helium at a velocity of 30.2 cm/sec. It is seen that these curves are extremely regular. Figures 50 and 51 show typical profiles of this same system at different gas velocities.

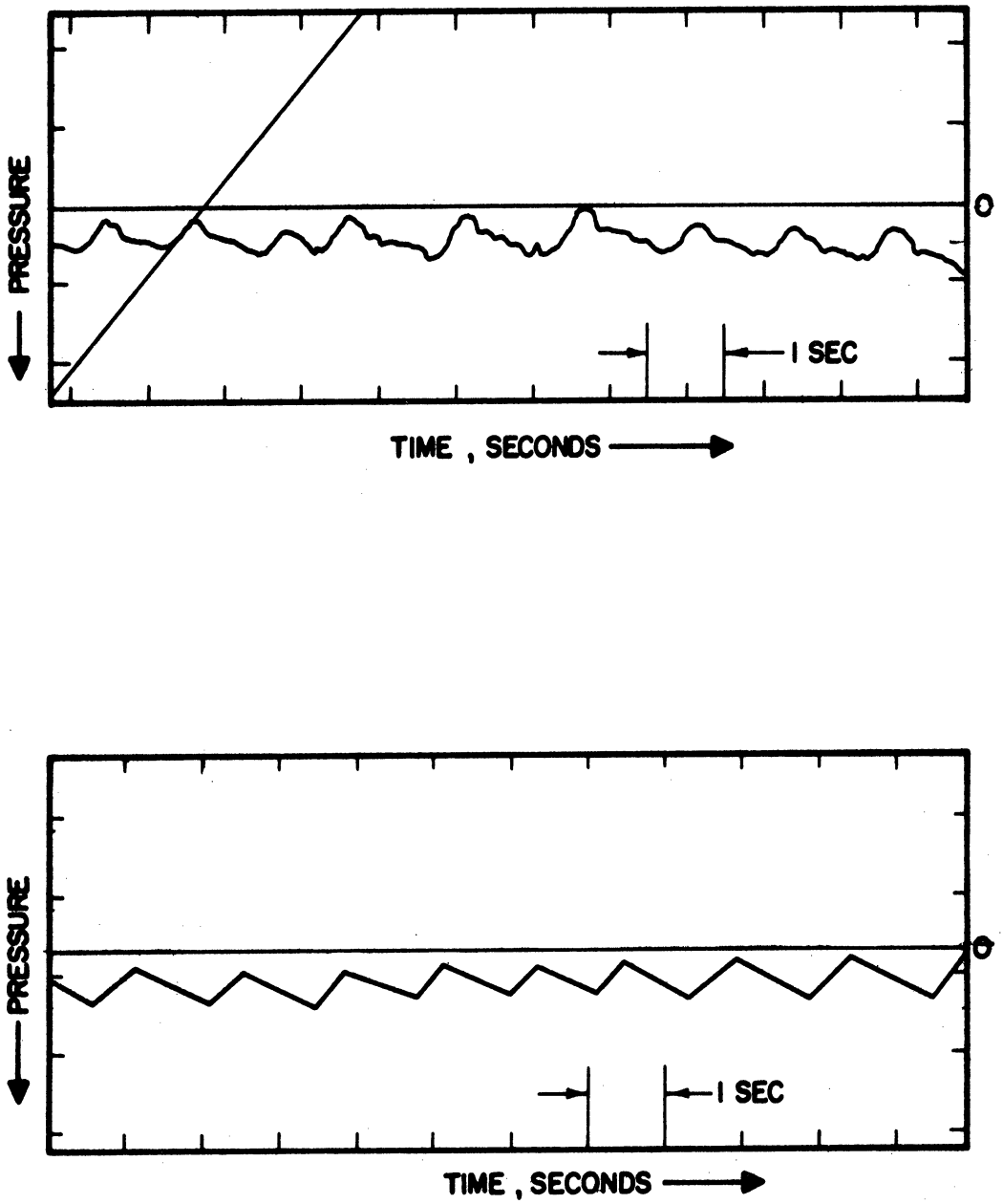

Figure 45. Experimental and Predicted Pressure-Time Curves Between Taps Located at 75.8 and 120 cm above Bed Support. Upper Curve is Experimental, Lower is Predicted. System is 100-150 Mesh Sand in a 2.00" Bed at an Air Velocity of 7.00 cm/sec. The Indicated Slope Should Be $(v_{xs} + \theta)(\frac{\Delta p}{L})$ (See Table XV). Static Bed Height is 74.cm.

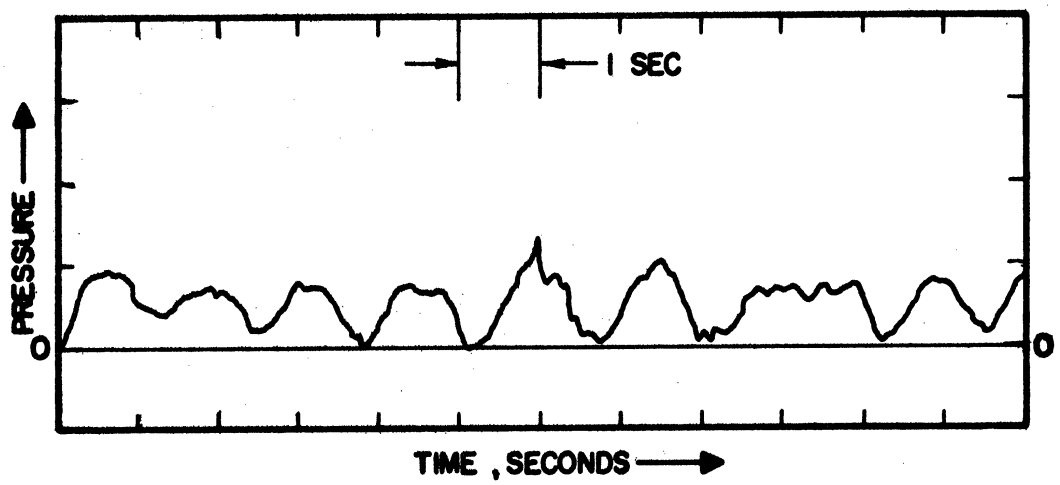

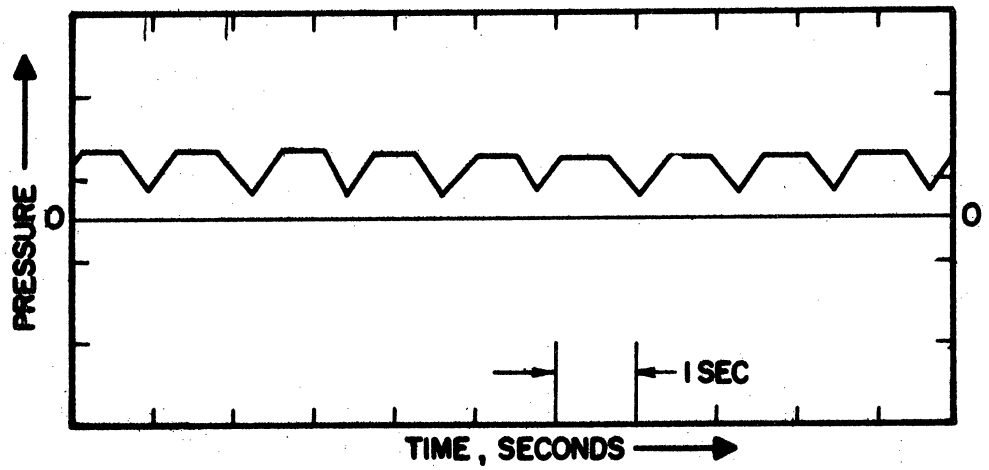

Figure 46. Experimental and Predicted Pressure-Time Curves Between Taps Located at 60.0 and 75.8 cm Above Bed Support. Upper Curve is Experimental; Lower is Predicted. System is 100-150 Mesh Sand in a 2.00" Bed at an Air Velocity of 7.00 cm/sec. Static Bed Height is 74 cm.

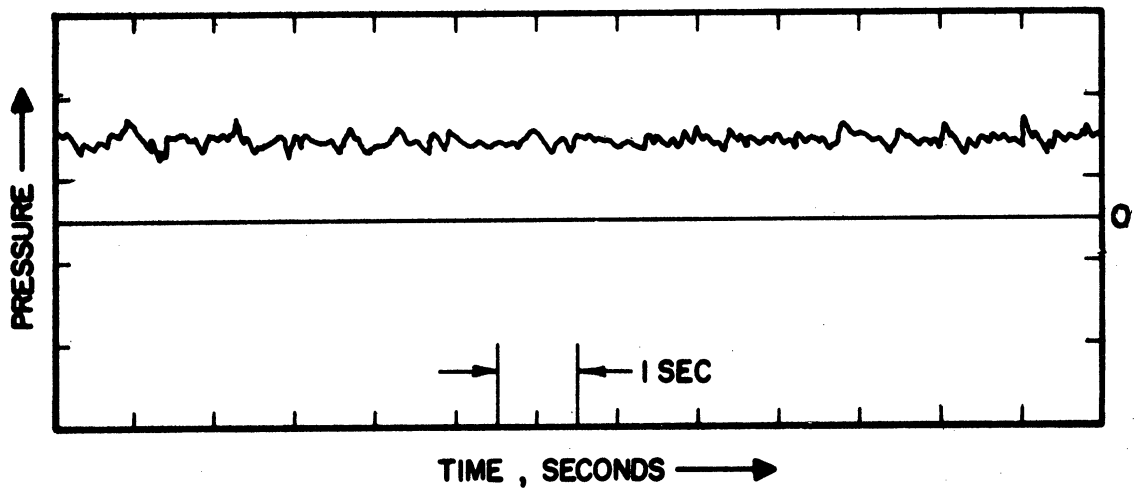

Figure 47. Experimental Pressure-Time Curve Between Taps Located at 15.0 cm Above Bed Support and Just Beneath Bed Support. System is 100-150 Mesh Sand in a 2.00" Bed at an Air Velocity of 7.00 cm/sec. Static Bed Height is 74 cm.

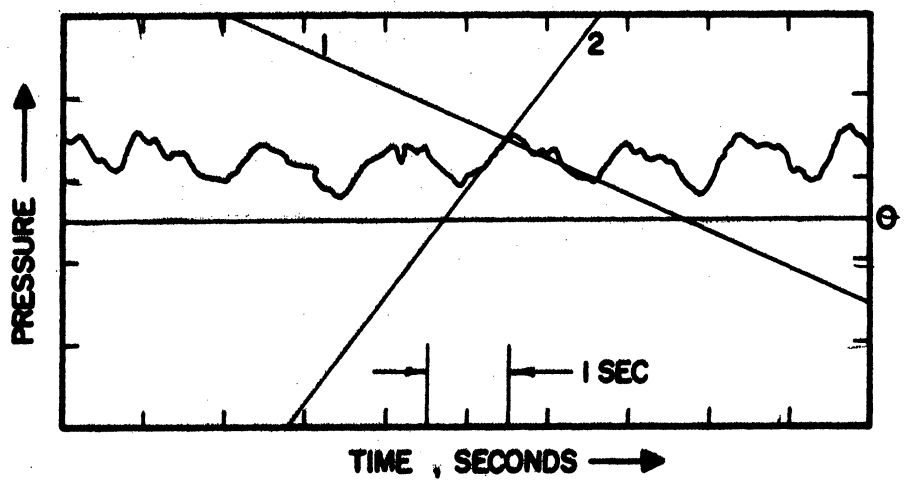

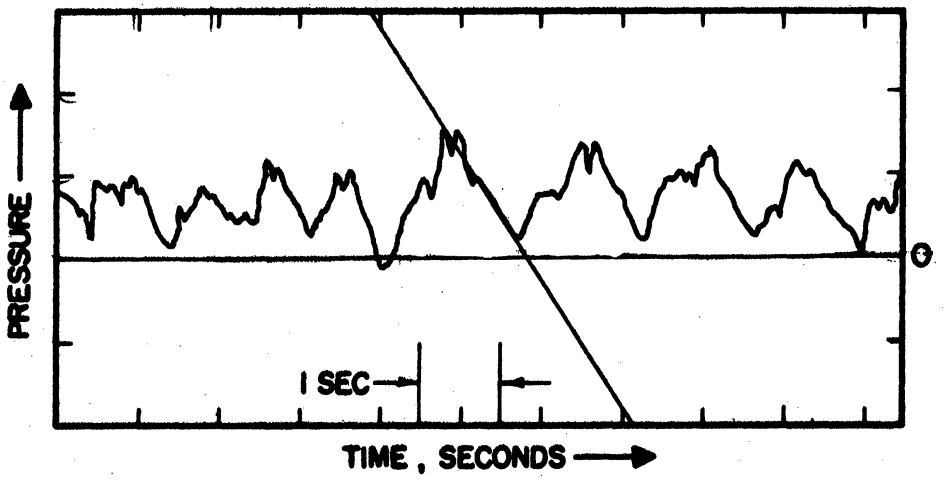

Figure 48. Experimental Pressure-Time Curves Between Taps Located at 75.8 and 120 cm Above Bed Support. System for Upper Curve is 100-150 Mesh Sand in a a 2.00" Bed at an Air Velocity of 10.0 cm/sec. Slope 1 Should be $v_{xs}(\frac{\Delta p}{L})$; Slope 2 Should Be $(v_{xs} + \theta)(\Delta p/L)$. Static Bed Height is 74 cm.

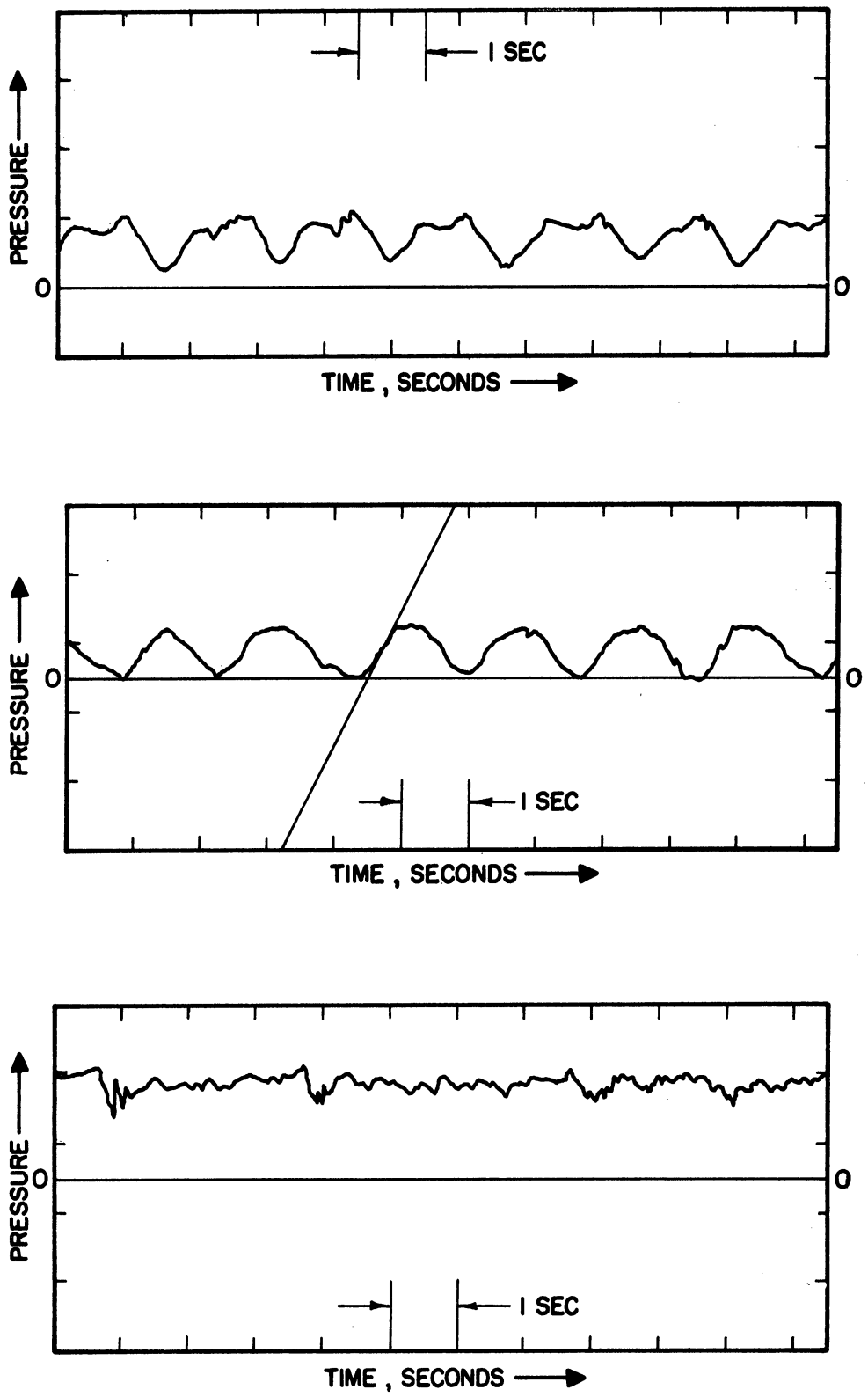

Figure 49. Experimental Pressure-Time Curves for the System of 100-150 Mesh Sand in a 2.00" Bed at a Helium Velocity of 30.2 cm/sec. Upper Curve is Between Taps 60.0 and 75.8 cm Above Bed Support. Middle Curve is Between Taps 45.0 and 60.0 cm Above Bed Support. The Slope Indicated Should Be $(\theta + U_{ks})(\Delta p/L)$. (See Table XV). Lower Curve is Between a Tap Below the Bed Support and a Tap at 15.0 cm Above the Bed Support. Static Bed Height is 72 cm.

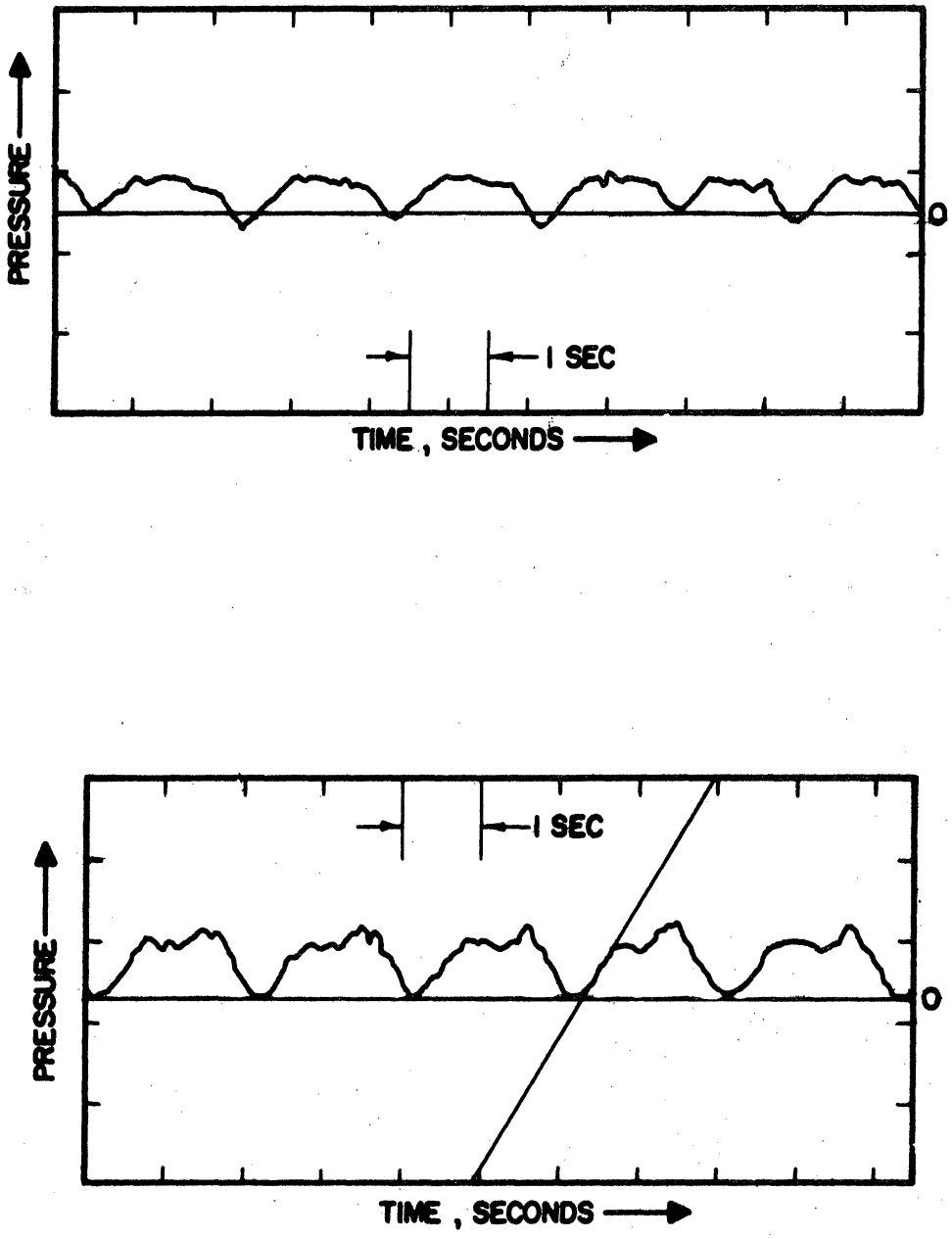

Figure 50. Experimental Pressure-Time Curves for the System of 100-150 Mesh Sand in a 2.00" Bed Between Taps Located 60.0 and 75.8 cm Above Bed Support. The Upper Curve is for a Helium Velocity of 12.7 cm/sec. Slope Should be $(\theta + v_{xs})(\Delta p/L)$. (See Table XV). Static Bed Height is 72 cm.

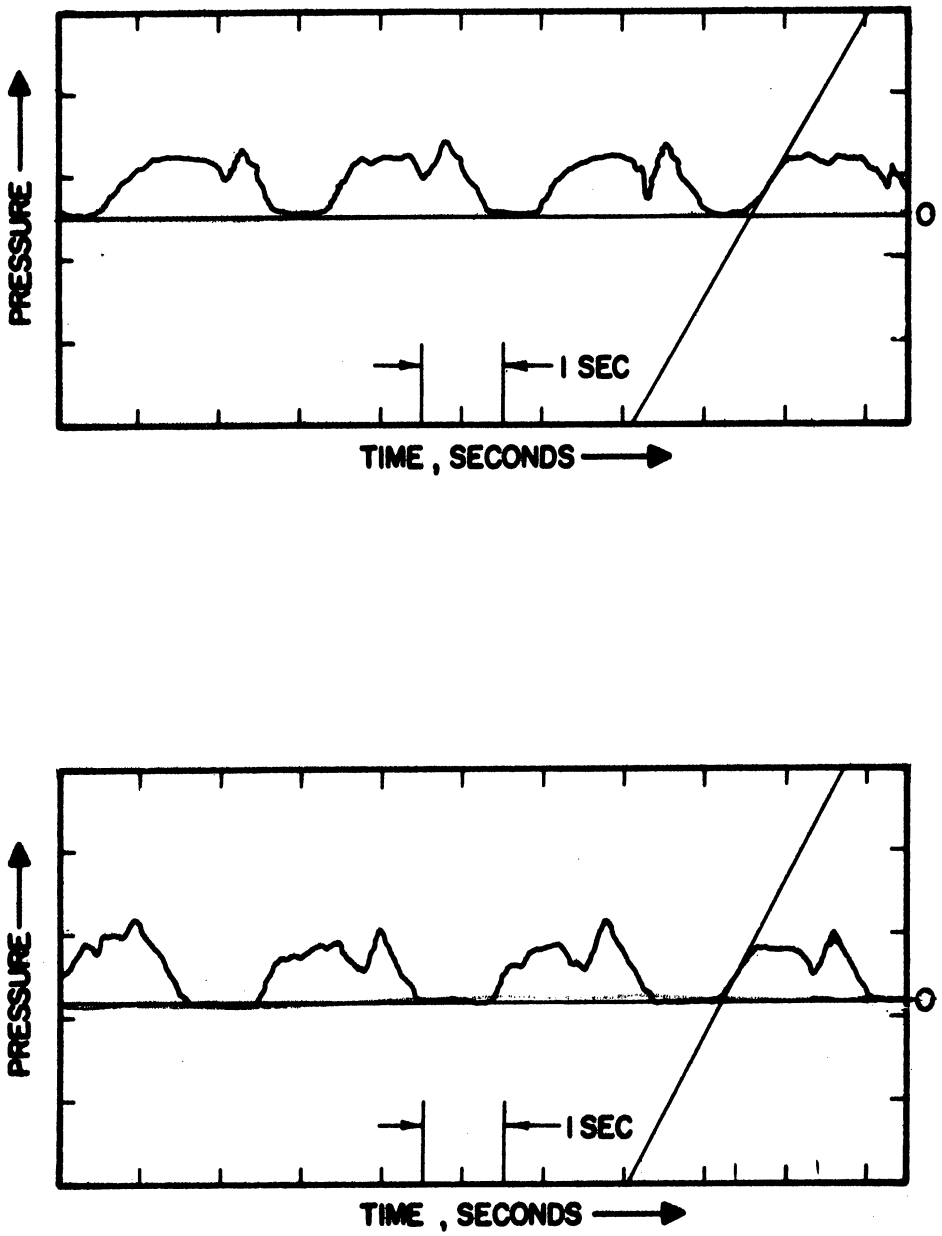

Figure 51. Experimental Pressure-Time Curves for the System of 100-150 Mesh Sand in a 2.00" Bed Between Taps Located 60.0 and 75.8 cm Above Bed Support. The Upper Curve is for a Helium Velocity of 18.3 cm/sec. The Slope Should be $(\theta + v_{xs})(\Delta p/L)$. (See Table XV). Static Bed Height is 72 cm.

Figures 52, 53, and 54 show pressure-time profiles for the system of 100-150 mesh sand in a 1.00" diameter bed fluidized with air at three velocities.

These curves are presented for two reasons. First, they demonstrate the regularity of fluctuations in pressures in these systems and to show how these fluctuations change with elevation in the tube. Second, they demonstrate the raw data from which the model-confirming slopes were taken, and how this data varies with gas velocity for different gases and different tube diameters.

A summary of predicted and observed values of $\Theta + \bar{v}_{xs}$ and $\bar{v}_{xs}$ for all systems studied is given in Table XV. The two values agree quite well for the quantity $\Theta + \bar{v}_{xs}$ for 2.00 inch diameter beds. The few data available for $\bar{v}_{xs}$ do not check as well. This is at least in part due to the large errors likely to exist in the measurements underlying both values of $\bar{v}_{xs}$. Good agreement is also found for data for the 21.2 cm bed in the 1.00 inch tube fluidized with air, and for the 42 cm bed in the 1.00 inch tube fluidized with carbon dioxide.

Data for the remaining systems is out of line. This is due to the frictional effects noticed in the some of these small (1.00 inch) diameter systems. The assumption of no slug friction with the bed wall apparently is not valid for beds with a static L/D_t greater than about 15. This is not the case in the larger diameter (2.00 inch) beds, where an L/D_t of 15 causes no trouble whatsoever.

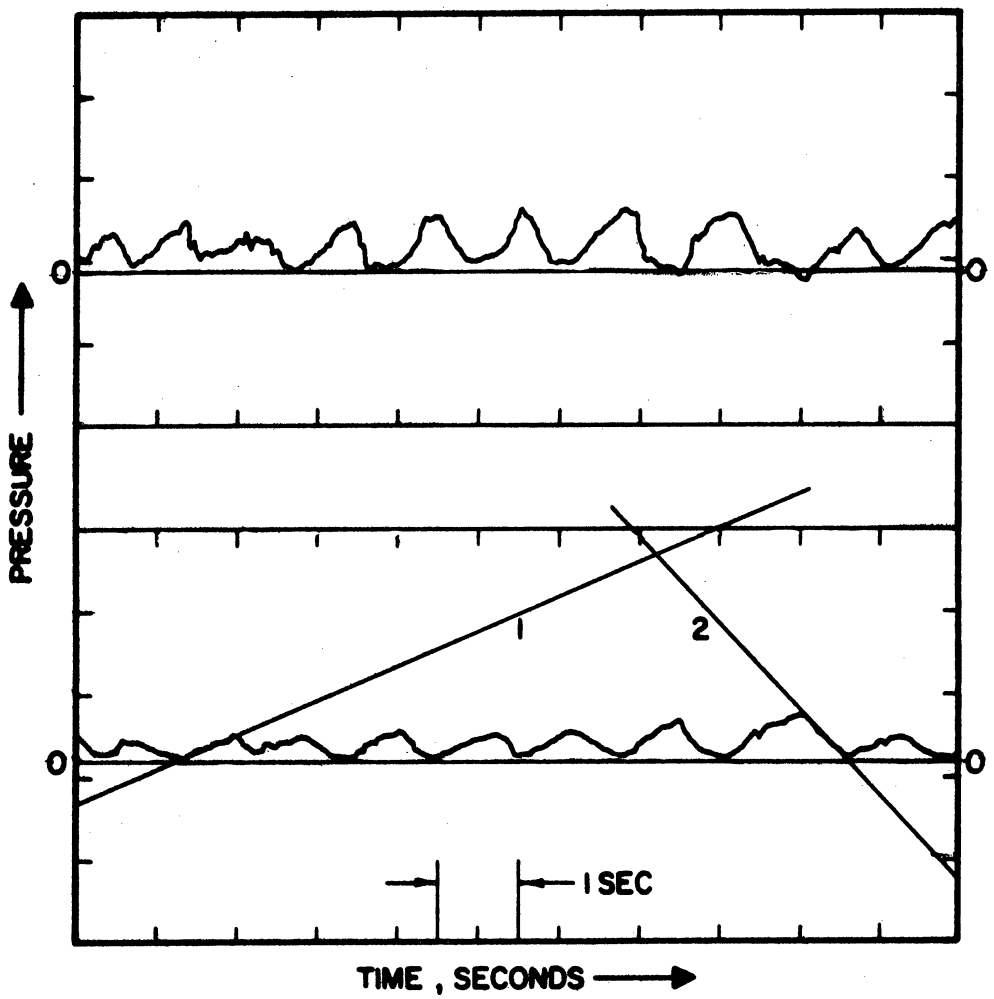

Figure 52. Experimental Pressure-Time Curves for the System of 100-150 Mesh Sand in a 1.00" Bed at an Air Velocity of 8.7 cm/sec. Upper Curve is Between Taps Located 45.0 and 60.0 cm Above Bed Support. Lower Curve is Between Taps Located 60.0 and 75.0 cm Above Bed Support. Slope 1 Should be $v_{xs}(\Delta p/L)$. Slope 2 Should be $(v_{xs})(\Delta p/L)$. (See Table XV). Static Bed Height is 21.2 cm.

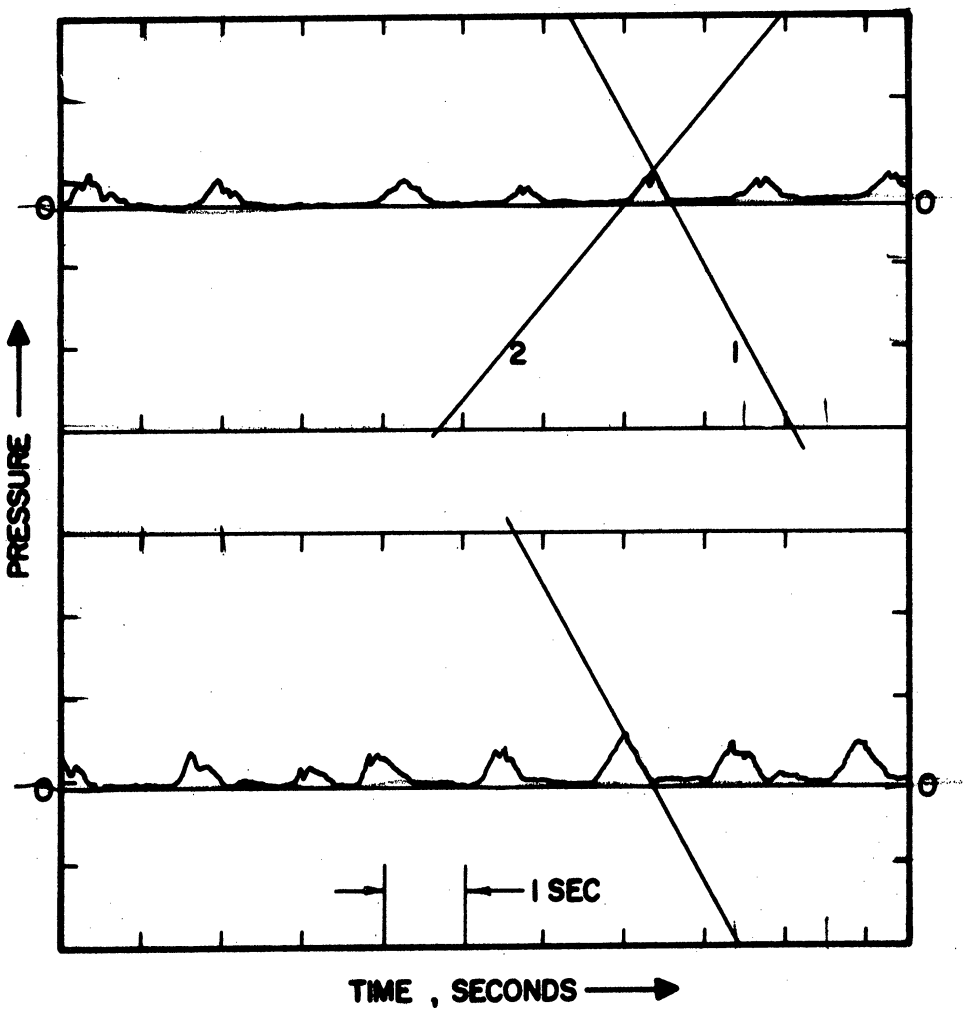

Figure 53. Experimental Pressure-Time Curves for the System of 100-150 Mesh Sand in a 1.00" Bed at an Air Velocity of 24.0 cm/sec. Upper Curve is Between Taps Located 60.0 and 75.0 cm Above Bed Support. Slope 1 Should be $v_{xs}(\Delta p/L)$. Slope 2 Should be $(\theta + v_{xs})(\Delta p/L)$. Lower Curve is Between Taps Located 45.0 and 60.0 cm Above Bed Support. Slope Should be $(\theta + v_{xs})(\Delta p/L)$. (See Table XV). Static Bed Height is 21.2 cm.

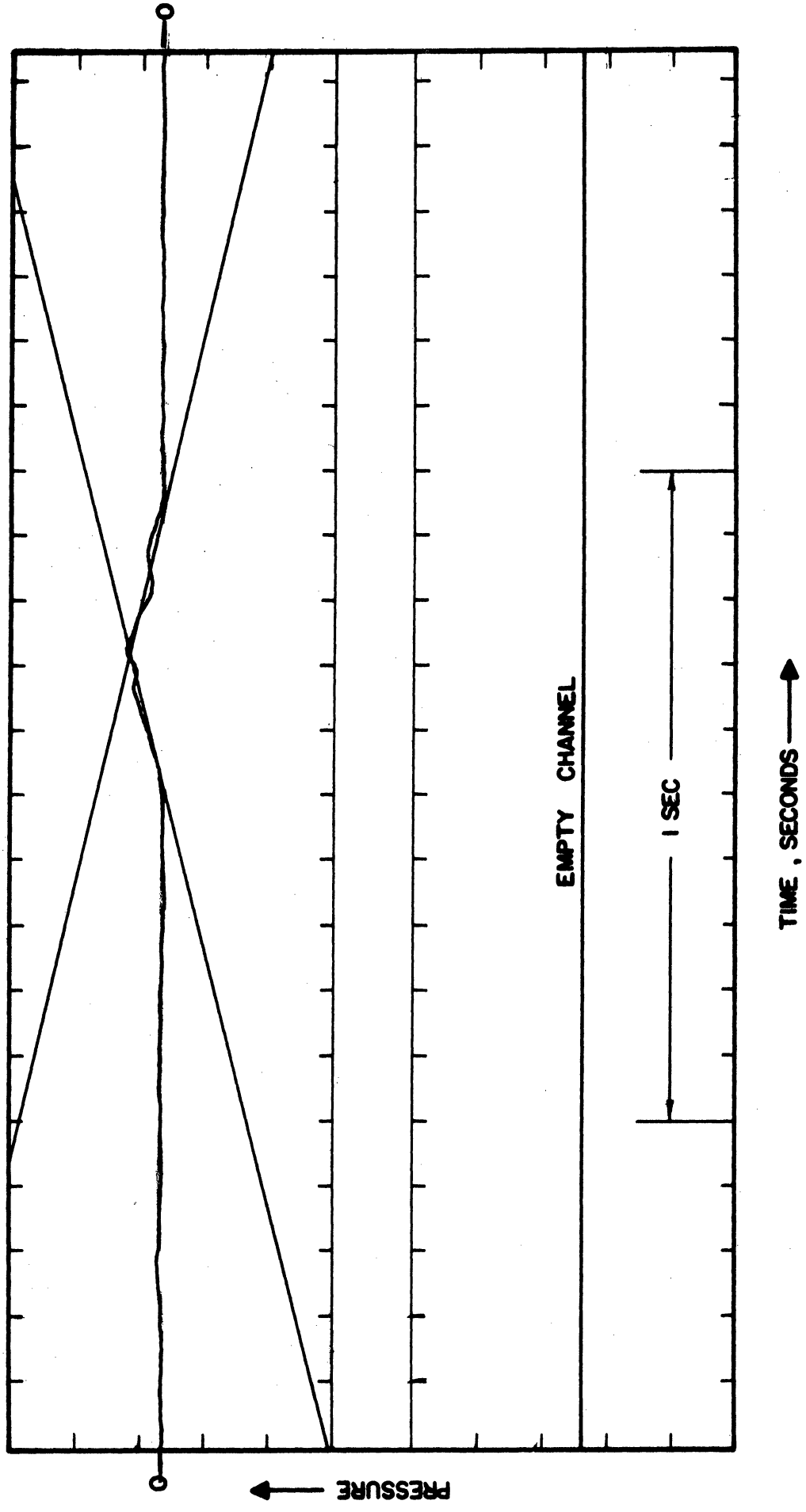

Figure 54. Experimental Pressure-Time Curve for the System of 100-150 Mesh Sand in a 1.00" Bed at an Air Velocity of 36.4 cm/sec. The Curve is Between Taps Located 60.0 and 75.0 cm Above Bed Support. Both Slopes Should be $(\theta + v_{xs})(\Delta p/L)$. (See Table XV). Static Bed Height is 21.2 cm.

TABLE XV

Summary of Results of Pressure Profile Measurements

Bed Dia. cm	Bed Height cm	Gas	Solid	Gas Velocity cm/sec	v_{gmf} cm/sec	v_{xs} cm/sec	θ cm/sec	$\theta + v_{xs}$ Pred. cm/sec	$\theta + v_{xs}$ Obs. cm/sec	v_{xs} Obs. cm/sec
5.08	74.0	Air	Sand A	7.00	3.14	3.9	22.8	26.7	26.6	7.3
5.08	74.0	Air	Sand A	10.00	3.14	6.9	22.8	29.7	28.6	9.6
5.08	74.0	Air	Sand A	13.00	3.14	10.9	22.8	33.7	33.2	—
5.08	72.0	Helium	Sand A	12.7	3.60	9.1	23.7	32.8	31.5	—
5.08	72.0	Helium	Sand A	16.4	3.60	12.8	23.7	36.5	36.7	—
5.08	72.0	Helium	Sand A	18.3	3.60	14.7	23.7	38.4	38.0	—
5.08	72.0	Helium	Sand A	21.4	3.60	17.8	23.7	41.5	42.5	—
5.08	72.0	Helium	Sand A	30.2	3.60	26.6	23.7	50.3	43.3	—
2.54	21.2	Air	Sand A	8.7	1.10	7.6	17.7	24.3	23.0	9.2
2.54	21.2	Air	Sand A	24.0	1.10	22.9	17.7	40.6	39.4	24.0
2.54	21.2	Air	Sand A	36.4	1.10	35.3	17.7	53.0	52.0	—
2.54	58.0	Air	Sand A	11.8	1.82	10.0	17.7	27.7	>100	40.8
2.54	42.0	CO_2	Sand A	7.0	1.52	5.5	13.8	19.3	22.3	—
2.54	42.0	CO_2	Sand A	17.5	1.52	16.0	13.8	29.8	32.4	—
2.54	42.0	Helium	Sand A	26.7	6.60	20.1	16.1	26.2	58.3	9.8
2.54	42.0	Helium	Sand A	43.7	6.60	37.1	16.1	53.2	>300	>100
2.54	33.0	Air	Sand B	25.2	2.95	22.2	17.9	40.1	20	—*

* Results of this run were erratic.

The effect of wall-slug friction is to create pressure buildups in the bed. This pressure buildup becomes very noticeable in attempts to predict pressures, but has no great effect on the period of fluctuations nor the assumption of linear pressure and level changes in the system. Figure 55 demonstrates this linearity in the worst case encountered.

An attempt to include this pressure buildup in the proposed model is certain to encounter great difficulty. The problem created is the one of unsteady compressible fluid flow through a porous medium of varying length and varying motion. An extremely simplified version of this problem is unsteady flow of a compressible fluid through a porous bed of constant size and possessing no motion. The equation for pressure variation in such a solids plug is

$$(84) \quad \frac{\partial^2 P^2}{\partial x^2} = (c'/P)\frac{\partial P^2}{\partial t}$$

where c is a constant, P is pressure, t is time, and x is length. No analytical solution for this simplified problem is available, indicating the hopelessness of engaging with the parent problem.

Conclusions.

The model meets all requirements for the prediction of the shapes and slopes of pressure curves in the bed in the majority of cases.

There is an upper limit of static bed L/D_t, at least for small diameter beds, above which pressure buildup invalidates the use of

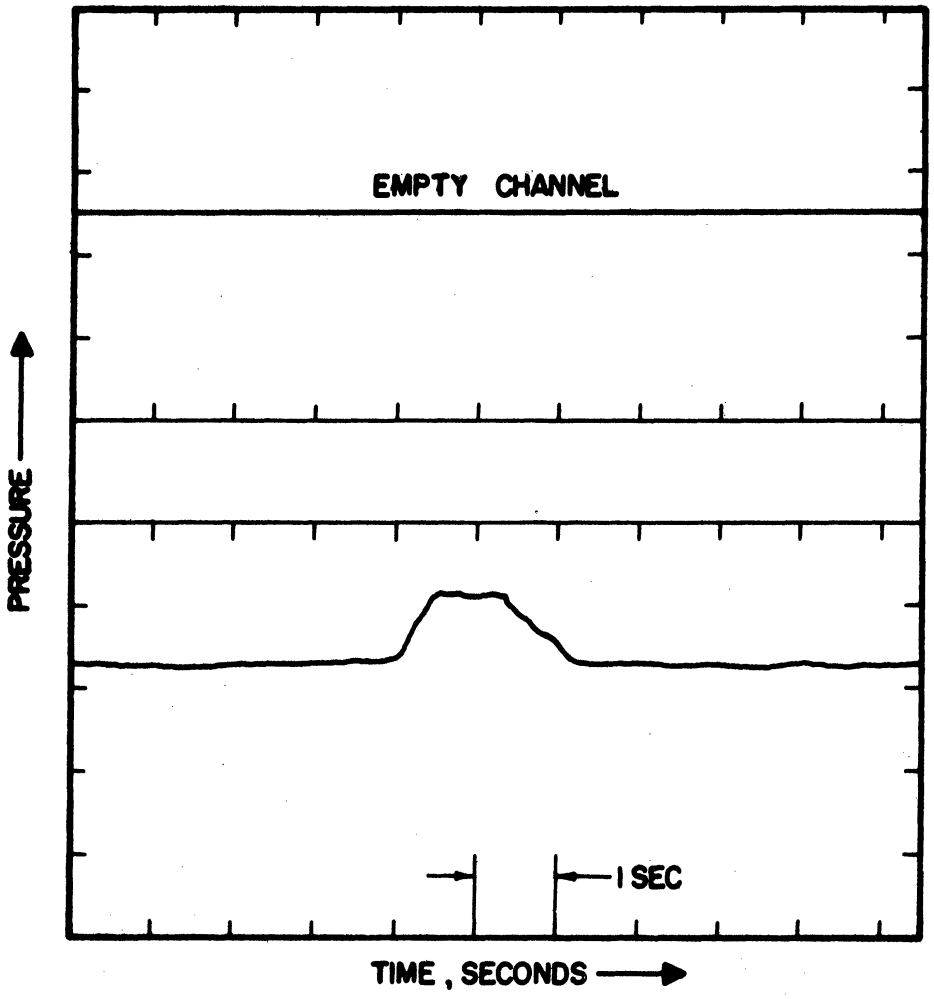

Figure 55. Experimental Pressure-Time Curve For the System of 100-150 Mesh Sand in a 1.00" Bed at a Helium Velocity of 43.7 cm/sec. The Curve is Taken Between Taps Located 90.0 and 105.0 cm Above the Bed Support. Static Bed Height is 42 cm.

the model for predicting pressure variations. This limit does not greatly affect the prediction of bed fluctuation period. The lower limit of L/D_t appears to be merely the limit for the slugging regime of fluid bed operation.

EXTENSION OF THE MODEL TO BUBBLING SYSTEMS.

A pertinent question is: what value has this model in fluidized systems which are not in the slugging regime? A thorough investigation of this question is beyong the scope of this work, but a quick check on the applicability of the model to the bubbling regime will be made here. Baumgarten and Pigford[3] have obtained data on the rate of bubble rise versus bubble diameter in systems which contained much the same solids as the sands used in this study. The fluidizing gas used was air.

Suppose one considers that a bubble is just a slug proceeding up through a column the walls of which are composed of solids. If this is true, then the velocity of the "void space" should be given by the model. There is, however, one important difference between this sort of "slugging" system and the ones studied in this work. It is that the friction between solids and a "column" wall of solids will be very much greater than between solids and a smooth wall. Let us assume that the bubble, or "slug", cannot push solids up the "column" at all. Then the only way that the bubble can proceed upward is by the transfer of solids vertically downward through the bubble. This solids downflow rate has been investigated in this study. The resultant bubble velocity must be:

$$(85) \qquad V_B = \Theta = \frac{W_A}{\rho_S}$$

Since the effect of tube diameter on θ has been established, it is no great task to translate the words "tube diameter" to "bubble" diameter" and thus have a prediction of bubble velocity versus bubble diameter. The information of Figure 23 is applicable. Figure 56 shows the curve predicted from this work together with Baumgarten and Pigford's data. The scatter in their data is large, but the predicted curve goes through the midst of their data.

Thus the scope of this study is not necessarily limited.

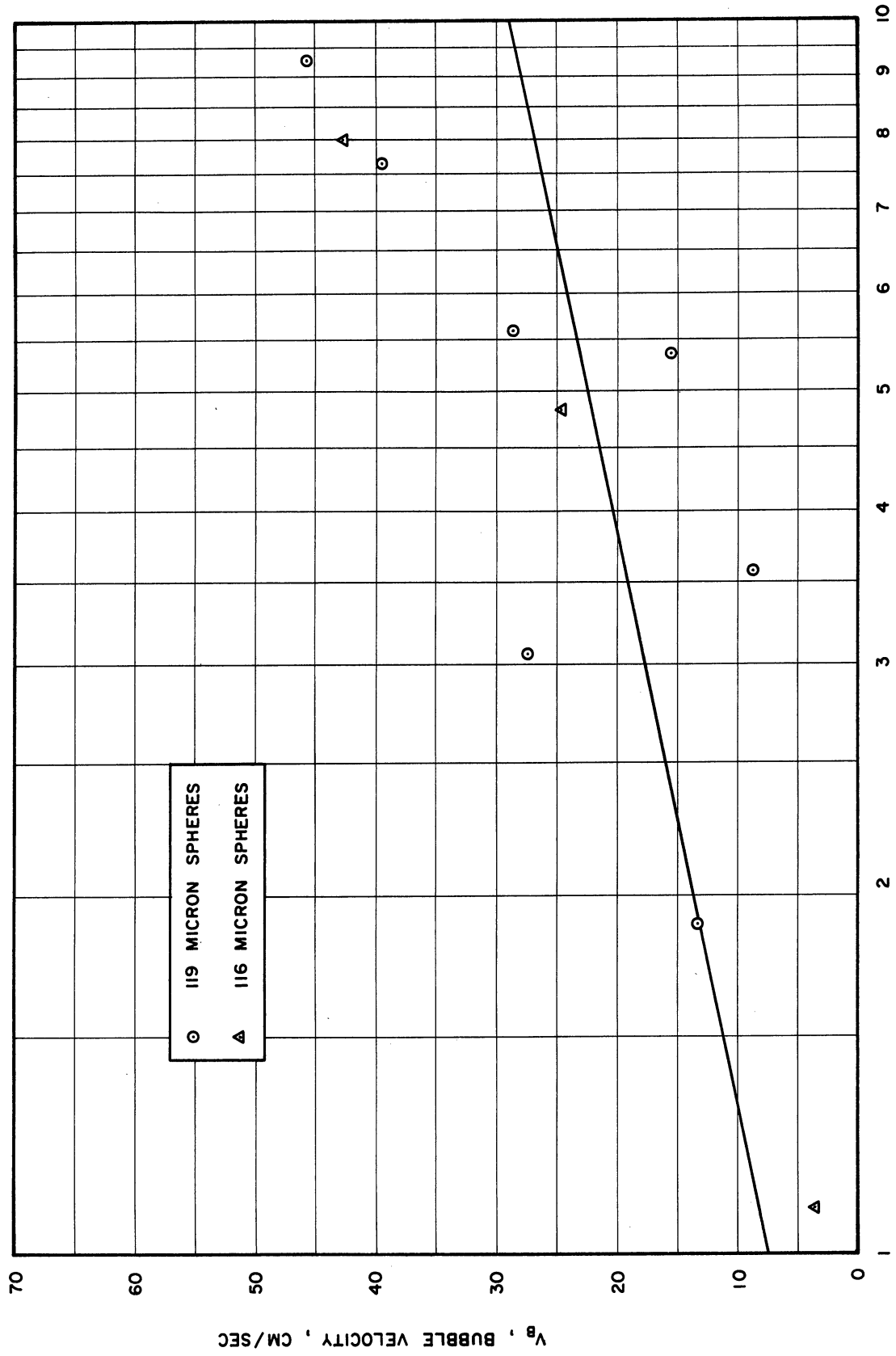

Figure 56. Bubble Velocity Versus Bubble Diameter. Curve is Predicted. Points are the Data of Baumgarten and Pigford.

SUMMARY

Let us now re-examine the results of this study. A microscopic approach was tried and abandoned. The useful result is the acquistion of an equation which should predict collision frequencies in gas-particle systems. An unsteady-state macroscopic approach was tried and abandoned. The useful result is the solution of the mass and momentum balances for slugs of changing size and mass. A steady-state macroscopic slug model was then proposed. The procedure was then to investigate the necessary areas, verifying assumptions in route, and then to verify the results predicted by the model.

The first topic considered was the total bed pressure drop as a function of velocity. The normal "break point" at incipient fluidization was noted in each case. Pressure drops at this point were observed to be the weight of the bed per unit area. The pressure drop per unit length of bed was tabulated for future use.

Solids downflow rates were checked next. Bin-flow techniques yielded a solids downflow rate which varied with gas velocity, exhibiting a maximum at the velocity for incipient fluidization. This maximum was subsequently shown to be a good estimate of the single solids downflow rate existing in the operating system. Pressure measurement techniques showed that a single solids downflow rate exists in each system at all velocities. This rate was found to be linear in solids density and moderately dependent on

bed diameter. Gas properties do not appreciably affect this rate. This work verified the assumptions that (1) there is a unique solids downflow rate for a given system for all velocities, (2) gas flows through a slug at the velocity of minimum fluidization, (3) There is negligible gas pressure drop in void spaces, (4) slugs do not accelerate. Auxiliary measurements verify the assumption that particles fall through void spaces at relatively large velocities. The system-to-system differences point out the validity of the assumption that only one system at a time may be dealt with.

The problem of determining what type of slugs exist at various points in the bed was treated next. The answer was found in three characteristic elevations in the bed which yielded the necessary information. The effect of operating variables on these levels was discussed. This work verified, qualitatively via visual observation, the assumptions of no variation in radial solids concentration and well defined slugs.

The final preliminary, the matter of slug generation, was treated in a manner suggested by the experience of others. The process is a reasonable representation of actual events.

None of this work guaranteed the accuracy of the model. This was tested in three ways. Fluctuation periods were observed to agree well with the predictions for all systems studied. Internal bed pressure changes were predicted well for the majority of cases.

In a few extremes of low diameter and large static bed height, the assumption of no wall friction was observed to be invalid. A third, and very important, verification was found in the fact that bubble velocities could be predicted from bubble diameter within the accuracy of the available data. Thus the proposed model appears reasonable in most respects.

APPENDIX A

Details of the Development of Average Collision Frequency.

The assumed forms of the distribution functions for the random cartesian components of velocity are:

$$(85)\quad P(v_x)dv_x = 1/\sigma_x\sqrt{2\pi}\; e^{-v_x^2/2\sigma_x^2}\, dv_x$$

$$(86)\quad P(v_y)dv_y = 1/\sigma_y\sqrt{2\pi}\; e^{-v_y^2/2\sigma_y^2}\, dv_y$$

$$(87)\quad P(v_z)dv_z = 1/\sigma_z\sqrt{2\pi}\; e^{-(v_z-w)^2/2\sigma_z^2}\, dv_z$$

The distribution function for particle speed c is then obtained as follows:

$$(88)\quad P(v_x,v_y,v_z)dv_x dv_y dv_z = P(v_x)\,P(v_y)\,P(v_z)\,dv_x\,dv_y\,dv_z$$

Introducing spherical coordinates:

$$(89)\quad v_x = c\cos\theta\sin\phi$$

$$(90)\quad v_y = c\sin\theta\sin\phi$$

$$(91)\quad v_z = c\cos\phi$$

$$(92)\quad dv_x dv_y dv_z = c^2\sin\phi\, d\phi\, d\theta\, dc$$

If one also assumes that

$$(93)\quad \sigma_x = \sigma_y = \sigma_z = \sigma$$

then

$$(94)\quad P(c,\theta,\phi) = \frac{c^2 \sin\phi}{\sigma^3 (2\pi)^{3/2}} e^{-\frac{c^2\sin^2\phi + (c\cos\phi - w)^2}{2\sigma^2}}$$

One then integrates over the entire ranges of θ and ϕ to remove angular dependence and obtain speed distribution:

$$(95)\quad P(c,\phi) = \frac{c^2 \sin\phi}{\sigma^3 (2\pi)^{3/2}} e^{-\frac{c^2\sin^2\phi + (c\cos\phi - w)^2}{2\sigma^2}} \int_0^{2\pi} d\theta$$

$$(96)\quad P(c,\phi) = \frac{c^2 \sin\phi}{\sigma^3 (2\pi)^{1/2}} e^{-\frac{c^2\sin^2 + (c\cos\phi - w)^2}{2\sigma^2}}$$

Thus one angular dependence is removed.

$$(97)\quad P(c) = \frac{c^2}{\sigma^3\sqrt{2\pi}} \int_0^{\pi} e^{-\left[\frac{c^2\sin^2\phi + (c\cos\phi - w)^2}{2\sigma^2}\right]} \sin\phi\, d\phi$$

$$(98)\quad P(c) = \frac{2c}{w\sigma\sqrt{2\pi}} e^{-\frac{(c^2+w^2)}{2\sigma^2}} \sinh\left(\frac{cw}{\sigma^2}\right)$$

The remaining angular dependence has been removed and the speed distribution obtained.

Now consider a particle moving with constant speed c through a collection of identical and stationary particles. The particle will execute a series of zig-zag motions, moving in straight lines between encounters. If one imagines this trajectory as the axis of a cylinder of radius equal to the particle diameter, then any particle with its center inside this cylinder will collide with the moving particle. The "collision volume" swept out per unit time will then be equal to $\pi D_p^2 c$. If the number density of particles is N_p, the

collision frequency will be given by:

$$(99) \quad Z_c = \pi D_p c N_p$$

The assumption underlying Equation (99) is that the particles are spheres of identical diameter. A more realistic case may readily be handled; namely, when the particles are spheres with a normal distribution of diameters. One assumes a distribution function of the form:

$$(100) \quad P(D_p) = 1/\sigma_1 \sqrt{2\pi}\, e^{-(D_p - \bar{D}_p)^2/2\sigma_1^2}$$

One can now consider a moving particle of diameter Dp. The "collision volume" swept out will be $\pi(D_p + \bar{D}_p)^2 c$. However, since half the encounters will be, on the average, with particles smaller than $\bar{D}_p$, the collision frequency will be

$$(101) \quad Z_c(D_p) = \frac{1}{2} \pi (D_p + \bar{D}_p)^2 N_p c$$

If this collision frequency is averaged over the entire distribution of particle diameters, one obtains

$$(102) \quad \bar{Z}_c = \int_0^\infty \frac{N_p c \pi}{2} (D_p + \bar{D}_p)^2 e^{-\frac{(D_p - \bar{D}_p)^2}{2\sigma_1^2}} \frac{dD_p}{\sigma_1 \sqrt{2\pi}}$$

or

$$(103) \quad \bar{Z}_c = N_p c \pi \left[\bar{D}_p^2 + \frac{\sigma_1^2}{4} \right]$$

For simplicity, let

$$(104) \quad d_p^2 = \left[\bar{D}_p^2 + \frac{\sigma_1^2}{4} \right]$$

Then (19) may be written

$$(105)\quad \bar{\bar{z}}_c = N_p c \pi d_p^2$$

One must now average this collision frequency over the speeds of particles colliding. First, consider a particle moving with speed c_1. Now, instead of the remaining particles being stationary, let them move with some speed c_2. It can be shown [4] for this case that:

$$(106)\quad \bar{\bar{z}}_c = N_p \pi d_p^2 V_r$$

$$(107)\quad V_r = c_1 + c_2^2/3c_1 \qquad c_1 > c_2$$

$$(108)\quad V_r = c_2 + c_1^2/3c_2 \qquad c_1 < c_2$$

Consequently, if we permit the considered particle to move at c_1 and allow a distribution of speeds c_2 according to Equation (98), the collision frequency will be given by:

$$(109)\quad \bar{\bar{z}}_c = \frac{2 N_p \pi d_p^2}{w \sigma \sqrt{2\pi}} \left\{ \int_0^{c_1} c_2 \left(c_1 + \frac{c_2^2}{3c_1}\right) e^{-\frac{(c_2^2+w^2)}{2\sigma^2}} \sinh\left(\frac{c_2 w}{\sigma^2}\right) dc_2 \right.$$
$$\left. + \int_{c_1}^{\infty} c_2 \left(c_2 + \frac{c_1^2}{3c_2}\right) e^{-\frac{(c_2^2+w^2)}{2\sigma^2}} \sinh\left(\frac{c_2 w}{\sigma^2}\right) dc_2 \right\}$$

This is the expression for the average collision frequency of a particle moving at speed c_1 with particles moving at distributed speeds c_2. The integration in Equation (109) is long and involved. However the result may be obtained analytically, and has the following form:

$$(110)\quad \overline{\overline{\overline{Z}}}_c = \frac{\sqrt{2\pi}\, N_p \sigma d_p^2}{6\varepsilon\gamma}\left\{\left[2(\varepsilon+\gamma)^3+3(\varepsilon+\gamma)\right]\left[\frac{\sqrt{\pi}}{2}\operatorname{erf}(\varepsilon+\gamma)\right]\right.$$
$$-\left[2(\varepsilon-\gamma)^3+3(\varepsilon-\gamma)\right]\left[\frac{\sqrt{\pi}}{2}\operatorname{erf}(\varepsilon-\gamma)\right]$$
$$\left.+\, e^{-(\varepsilon+\gamma)^2}\left[(\varepsilon+\gamma)^2+1\right]-e^{-(\varepsilon-\gamma)^2}\left[(\varepsilon-\gamma)^2+1\right]\right\}$$

where

$$\varepsilon = \frac{c_1}{\sqrt{2}\,\sigma}$$

$$\gamma = \frac{w}{\sqrt{2}\,\sigma}$$

One more step remains before the problem of interest is solved. The speed of the considered particle is not constant but is also distributed according to Equation (98). The desired collision frequency is obtained by averaging the frequency given by Equation (110) over all speeds c_1, or corresponding values of ε.

$$(111)\quad \overline{\overline{\overline{Z}}}_c = \int_0^\infty \overline{\overline{\overline{Z}}}_c\, P(c_1)\, dc_1$$

The procedure is to change variable from c_1 to ε and substitute expression (110) for $\overline{\overline{\overline{Z}}}_c$. The hyperbolic sine in the distribution function is expanded into the sum of two exponential terms. This results in the production of 16 complex integrals (eight terms in $\overline{\overline{\overline{Z}}}_c$ times two terms in $P(c_1)$) which can be evaluated analytically. It would perhaps be of interest to demonstrate one such integration:

$$(112)\quad I_4 = \int_0^\infty e^{-2(\varepsilon+\gamma)^2}\, d\varepsilon$$

change variable to $\alpha = \varepsilon + \gamma$

$$(113) \qquad I_4 = \int_{\gamma}^{\infty} e^{-2\alpha^2} d\alpha$$

change variable to $\beta = \sqrt{2}\,\alpha$

$$(114) \qquad I_4 = \frac{1}{\sqrt{2}} \int_{\sqrt{2}\gamma}^{\infty} e^{-\beta^2} d\beta = \left[\frac{1}{\sqrt{2}} \frac{\sqrt{\pi}}{2} \operatorname{erf}\beta\right]_{\sqrt{2}\gamma}^{\infty}$$

$$(115) \qquad I_4 = \frac{\sqrt{2}}{2} \frac{\sqrt{\pi}}{2} (1 - \operatorname{erf}\sqrt{2}\gamma)$$

This is the simplest of the integrations.

The result for average collision frequency is of the form:

$$(116) \qquad \equiv\!\equiv\!\equiv_c = 4\sqrt{\pi} N_p \sigma d_p^2 \left[\frac{1}{6}\left(\frac{e^{-2\gamma^2} - 1}{\gamma^2}\right) + \frac{\sqrt{2}}{6}\left(4\gamma + \frac{3}{\gamma}\right)\frac{\sqrt{\pi}}{2} \operatorname{erf}\sqrt{2}\gamma + \frac{2}{6} e^{-2\gamma^2}\right]$$

A check on the accuracy of this result is provided by the fact that the limit of $\equiv\!\equiv\!\equiv_c$ as γ vanishes, or in other words, as the non-random component of vertical velocity approaches zero, is precisely the result demonstrated for pure random motion by the kinetic theory of gases(4).

APPENDIX B.

Solution of the mass and momentum balances for a slug.

Case 1. No solids inflow or outflow.

The solution of the mass balance is trivial:

(117) $\dot{y} = 0$

(118) $y(0) = y_0$

(119) $y = y_0$

The solution of the momentum balance is also quite easy.

(120) $\ddot{x} = C$ $\qquad V_s \leqq V_g - V_{gmf}$

(121) $\dot{x}(0) = \dot{x}_0$

(122) $x(0) = x_0$

where $C = \frac{K}{\rho_s} - g$

In this case the solution is trivial:

(123) $x = x_0 + \dot{x}_0 t + \frac{C}{2} t^2$ $\qquad V_s \leqq V_g - V_{gmf}$

The second form of the momentum balance is

(124) $\ddot{x} + A\dot{x} = AV_g - g$ $\qquad V_s > V_g - V_{gmf}$

(125) $\dot{x}(0) = \dot{x}_0$

(126) $x(0) = x_0$

where $A = \frac{K}{\rho_s V_{gmf}}$ Laplace transforms are used.

The transformed equation is:

$$(127)\quad s^2X(s) - \dot{X}_o - sX_o + A[sX(s) - X_o] = \frac{1}{s}(Av_g - g)$$

Solving for x(s):

$$(128)\quad X(s) = \frac{\dot{X}_o + sX_o + \frac{1}{s}(Av_g - g) + AX_o}{s(s+A)}$$

Taking the inverse transform,

$$(129)\quad X = X_o e^{-At} + \frac{(\dot{X}_o + AX_o)}{A}(1 - e^{-At}) + \frac{(Av_g - g)}{A^2}[e^{-At} + At - 1]$$

$$v_s > v_g - v_{gmf}$$

Equations (119), (123), and (129) are the solutions to the mass and momentum balances for a Case 1 slug.

Case 2. Solids outflow only.

The solution of the mass balance is obvious:

$$(130)\quad \dot{y} = -\theta$$

$$(131)\quad y(0) = y_o$$

$$(132)\quad y = y_o - \theta t$$

The momentum balance in the first instance is:

$$(133)\quad \ddot{X} = C + \frac{1}{2}\frac{\theta^2}{y} \qquad v_s \leqq v_g - v_{gmf}$$

$$(134)\quad \dot{X}(0) = \dot{X}_o$$

$$(135)\quad X(0) = X_o$$

Substituting y from mass balance:

$$(136)\quad \ddot{X} = C + \frac{1}{2}\frac{\theta^2}{(y_o - \theta t)}$$

Using direct integration once:

$$(137)\quad \dot{X} - \dot{X}_o = Ct - \frac{\Theta}{2} \ln \frac{Y}{Y_o}$$

Integrating again:

$$(138)\quad X = X_o + \dot{X}_o t + \frac{C}{2} t^2 + \frac{\Theta}{2} t + \frac{Y}{2} \ln \frac{Y}{Y_o}$$

$$V_s \leqq V_g - V_{gmf}$$

which is the desired result.

The momentum balance in the second instance is:

$$(139)\quad \ddot{X} + A\dot{X} = AV_g - g + \frac{1}{2} \frac{\Theta^2}{Y} \qquad V_s > V_g - V_{gmf}$$

$$(140)\quad \dot{X}(o) = \dot{X}_o$$

$$(141)\quad X(0) = X_o$$

The solution can proceed as follows. Define

$$(142)\quad P = \dot{X}$$

Then the equation is reduced to

$$(143)\quad \dot{P} + AP = AV_g - g + \frac{1}{2} \frac{\Theta^2}{Y}$$

$$(144)\quad P(0) = P_o = \dot{X}_o$$

The solution of this first order linear equation is:

$$(145)\quad P e^{At} = \int \left[AV_g - g + \tfrac{1}{2} \frac{\Theta^2}{Y} \right] e^{At} dt + C'$$

or

$$(146)\quad P e^{At} = \left(\frac{AV_g - g}{A} \right) e^{At} + \frac{1}{2} \Theta^2 \int \frac{e^{At} dt}{Y_o - \Theta t} + C'$$

Which upon evaluating the integral becomes:

$$(147)\quad P e^{At} = \left(\frac{AV_g - g}{A}\right) e^{At} + 0.5\theta^2\left[-\frac{1}{\theta} e^{\frac{Ay_0}{\theta}}\left(\ln\frac{y}{y_0} + \sum_{n=1}^{\infty}\frac{(-1)^n\left(\frac{A}{\theta}\right)^n\left(y^n - y_0^n\right)}{n \cdot n!}\right)\right] + C'$$

Using the boundary condition (144) to evaluate C', one obtains:

$$(148)\quad P = P_0 e^{-At} + \left[\frac{AV_g - g}{A}\right]\left[1 - e^{-At}\right] - \frac{1}{2}\theta e^{\frac{Ay}{\theta}}\left[\ln\frac{y}{y_0} + \sum_{n=1}^{\infty}\frac{(-1)^n\left(\frac{A}{\theta}\right)^n\left(y^n - y_0^n\right)}{n \cdot n!}\right]$$

Now one may solve for x by noting

$$(149)\quad X - X_0 = \int_0^t P\,dt$$

Performing this integration, one obtains:

$$(150)\quad X = X_0 - \frac{\dot{X}_0}{A}\left(e^{-At} - 1\right) + \left[\frac{AV_g - g}{A}\right]t + \frac{1}{A}\left[\frac{AV_g - g}{A}\right]\left[e^{-At} - 1\right] + \frac{1}{2}\int_{y_0}^{y} e^{\frac{Ay}{\theta}}\left[\ln\frac{y}{y_0} + \sum_{n=1}^{\infty}\frac{(-1)^n(A/\theta)^n\left(y^n - y_0^n\right)}{n \cdot n!}\right]dy$$

Which upon integration of the last integral yields

$$(151)\quad X = X_0 + \left[\frac{AV_g - g}{A}\right]t + \left[\frac{g - A(V_g - \dot{X}_0)}{A^2}\right]\left[1 - e^{-At}\right] + \frac{1}{2}\frac{\theta}{A}\ln\frac{y}{y_0}\left[1 - e^{\frac{Ay}{\theta}}\right] + \frac{1}{2}\frac{\theta}{A}e^{\frac{Ay}{\theta}}\sum_{n=1}^{\infty}\frac{(-1)^n\left(\frac{A}{\theta}\right)^n\left(y^n - y_0^n\right)}{n \cdot n!}$$

$V_s > V_g - V_{gmf}$

Euqations (132), (138) and (151) are the solutions to the mass and momentum balances for a case 2 slug.

Case 3. Solids inflow only.

The solution of the mass balance is elementary:

$$(152)\quad \dot{y} = \theta$$

(153) $y(0) = y_0$

(154) $y = y_0 + \theta t$

The momentum balance in the first instance is:

(155) $\ddot{x} = c + \frac{\theta u_1}{y} + \frac{1}{2}\frac{\theta^2}{y} - \frac{\theta \dot{x}}{y}$ $\qquad V_s \leq V_g - V_{gmf}$

(156) $\dot{x}(0) = \dot{x}_0$

(157) $x(0) = x_0$

The solution proceeds as follows. Define

(158) $p = \dot{x}$

Substituting, the momentum balance becomes:

(159) $\dot{p} + \frac{\theta}{y} p = c + \frac{\theta u_1 + 0.5\theta^2}{y}$

(160) $p(0) = p_0 = \dot{x}_0$

Solving the first order linear differential equation, one obtains:

(161) $yp = \frac{cy^2}{2\theta} + \theta(u_1 + 0.5\theta)t + c'$

Evaluating c' from boundary condition (44) and substituting:

(162) $p = \frac{p_0 y_0}{y} + \frac{c}{2\theta}\left[y - \frac{y_0^2}{y}\right] + \frac{\theta(u_1 + 0.5\theta)t}{y}$

Noting that

(163) $x = x_0 + \int_0^t p\,dt$

one obtains

(164) $x = x_0 + \left[\frac{\dot{x}_0 y_0}{\theta} - \frac{c y_0^2}{2\theta^2} - \frac{y_0(u_1 + 0.5\theta)}{\theta}\right] \ln \frac{y}{y_0}$

$+ \frac{(u_1 + 0.5\theta)}{\theta}(y - y_0) + \frac{c}{4\theta^2}(y^2 - y_0^2)$

$V_s \leq V_g - V_{gmf}$

which is the desired result.

The momentum balance in the second instance is:

$$\ddot{X} + \left(A + \frac{\theta}{Y}\right)\dot{X} = A(V_g + \theta) - g + \frac{\theta u_1}{Y} + \frac{1}{2}\frac{\theta^2}{Y} \tag{165}$$

$V_s > V_g - V_{gmf}$

$$\dot{X}(0) = \dot{X}_0 \tag{166}$$

$$X(0) = X_0 \tag{167}$$

Again, define

$$p = \dot{X} \tag{168}$$

Whereupon the momentum balance is reduced to

$$\dot{p} + \left(A + \frac{\theta}{Y}\right)p = A(V_g + \theta) - g + \frac{\theta}{Y}\left(u_1 + \frac{1}{2}\theta\right) \tag{169}$$

$$p(0) = p_0 = \dot{X}_0 \tag{170}$$

To solve this first order linear differential equation, make a change of variable from to to y:

$$y = y_0 + \theta t \tag{171}$$

$$dy = \theta dt \tag{172}$$

$$p = \dot{x} = \theta x' = \theta \bar{p} \tag{173}$$

$$\dot{p} = \ddot{X} = \theta^2 x'' = \theta^2 \bar{p}' \tag{174}$$

Then Equation (169) becomes:

$$\theta^2 \bar{p}' + \theta\left(A + \frac{\theta}{Y}\right)\bar{p} = D + \frac{E\theta}{Y} \tag{175}$$

where $\bar{p} = \dfrac{dx}{dy}$

and

$$D = A(V_g + \theta) - g$$

and

$$E = u_1 + 0.5\theta$$

Solving (175) one obtains:

$$(176)\quad \bar{P} y e^{\frac{Ay}{\theta}} = \frac{D}{\theta^2} e^{\frac{Ay}{\theta}}\left[\frac{\theta y}{A} - \frac{\theta^2}{A^2}\right] + \frac{E}{A} e^{\frac{Ay}{\theta}} + C'$$

Using boundary condition (170), with variable changed:

$$(177)\quad \bar{P}(y_o) = \frac{\dot{X}_o}{\theta} = X_o'$$

One obtains C' and substituting into (176) the result is

$$(178)\quad \bar{P} = X' = \frac{dx}{dy} = \left[X_o' y_o - \frac{D}{\theta^2}\left(\frac{\theta y_o}{A} - \frac{\theta^2}{A^2}\right) - \frac{E}{A}\right]\frac{e^{\frac{A(y-y_o)}{\theta}}}{y} + \frac{D}{\theta A} + \left(\frac{E}{A} - \frac{D}{A^2}\right)\frac{1}{y}$$

One final integration yields x:

$$(179)\quad x = \int_{y_o}^{y} \bar{P}\, dy$$

The result is:

$$(180)\quad X = X_o + e^{\frac{Ay_o}{\theta}}\left[\frac{\dot{X}_o y_o}{\theta} - \frac{D y_o}{\theta A} + \frac{D}{A^2} - \frac{E}{A}\right]\left[\ln\frac{y}{y_o} + \sum_{n=1}^{\infty}\frac{(-1)^n\left(\frac{A}{\theta}\right)^n (y^n - y_o^n)}{n \cdot n!}\right] + \frac{D}{\theta A}(y - y_o) + \left[\frac{E}{A} - \frac{D}{A^2}\right]\ln\frac{y}{y_o}$$

$$V_s > V_g - V_{gmf}$$

Case 4. Solids inflow and solids outflow.

The mass balance may be solved by inspection:

$$(181)\quad \dot{y} = 0$$

$$(182)\quad y(0) = y_o$$

(183) $$Y = Y_o$$

The momentum balance in the first instance is, after substituting the solution for the mass balance:

(184) $$Y_o \ddot{X} + \theta \dot{X} = C Y_o + \theta(u_1 + \theta) \qquad V_S \leqq V_g - V_{gmf}$$

(185) $$\dot{X}(0) = \dot{X}_o$$

(186) $$X(0) = X_o$$

Rearranging and taking the Laplace transform:

(187) $$\ddot{X} + \frac{\theta}{Y_o} \dot{X} = C + \frac{\theta}{Y_o}(u_1 + \theta) = \alpha$$

(188) $$S^2 X(S) - \dot{X}_o - S X_o + \frac{\theta}{Y_o}[S X(S) - X_o] = \frac{\alpha}{S}$$

Solving for x(s):

(189) $$X(S) = \frac{\dot{X}_o + \frac{\alpha}{S}}{S(S + \frac{\theta}{Y_o})} + \frac{X_o}{S}$$

Taking the inverse transform:

(190) $$X = X_o + \frac{\alpha Y_o}{\theta} t + \left[\frac{\dot{X}_o Y_o}{\theta} - \frac{\alpha Y_o^2}{\theta^2}\right]\left[1 - e^{-\frac{\theta t}{Y_o}}\right]$$

$$V_S \leqq V_g - V_{gmf}$$

where

$$\alpha = C + \frac{\theta}{Y_o}(u_1 + \theta)$$

Thus the first instance is solved.

The momentum balance for the second alternative, after substitution of the mass balance, is:

(191) $$\ddot{X} + (A + \frac{\theta}{Y_o})\dot{X} = A(V_g + \theta) - g + \frac{\theta u_1}{Y_o} + \frac{\theta^2}{Y_o} = \beta$$

$$V_S > V_g - V_{gmf}$$

(192) $\dot{x}(0) = \dot{x}_0$

(193) $x(0) = x_0$

This equation, (191), is seen to be precisely similar to Equation (187). Therefore, if one substitutes for $\frac{\theta}{\gamma_0}$ in Equation (190) the quantity $(A+\frac{\theta}{\gamma_0})$, and β for α, the result will be the desired solution:

(194) $$x = x_0 + \frac{\beta t}{(A+\frac{\theta}{\gamma_0})} + \left[\frac{\dot{x}_0}{(A+\theta/\gamma_0)} - \frac{\beta}{(A+\theta/\gamma_0)^2}\right]\left[1 - e^{-(A+\frac{\theta}{\gamma_0})t}\right]$$

where

$$\beta = A(V_g+\theta) - g + \frac{\theta u_1'}{\gamma_0} + \frac{\theta^2}{\gamma_0} \qquad V_s > V_g - V_{gmf}$$

Equations (183), (190), and (194) represent the solutions of the mass and momentum balances for Case 4.

In all four cases, the solutions of all equations have been checked by differentiation.

APPENDIX C

I. Calibration of Pressure Gage C2-174.

Figure 57 shows the calibration curve. This pressure gage was used to measure gas rotameter pressure.

II. Pressure Pickup Calibration.

Six pressure pickups were used to measure pressures in the fluid bed. Figures 58 through 63 show their calibration. These calibrations all involved a simultaneous calibration of pickup and oscillographic recorder.

III. Rotameter Calibrations.

The Manostat company publishes a set of curves and data which are supposed to yield an accurate a priori calibration of their instruments, "Predictability" flowmeters. It was deemed wise to check their data with one water displacement calibration. Figure 64 shows their predicted calibration and my data. It was judged from these results that the prediction could be trusted.

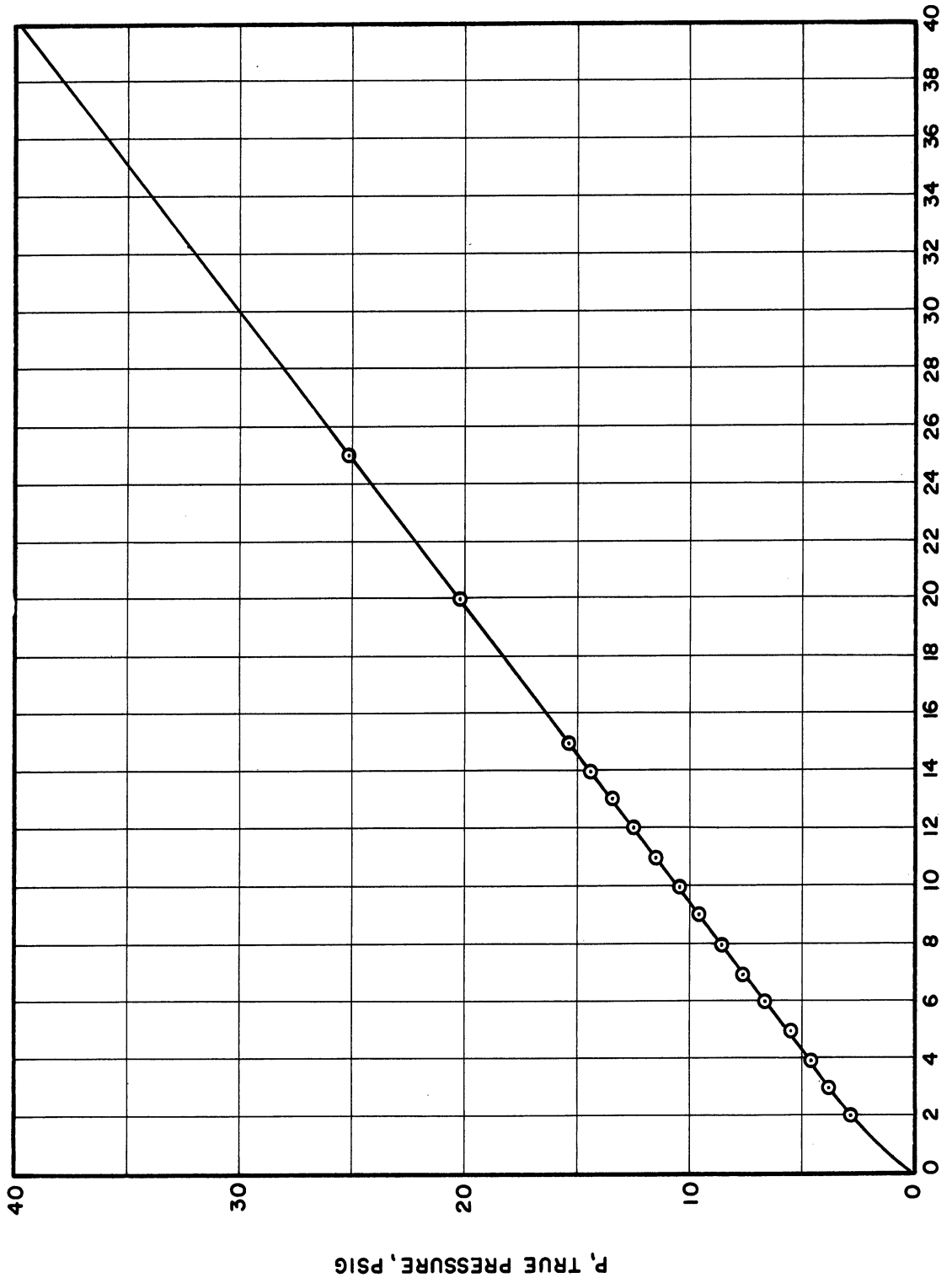

Figure 57. Calibration for Pressure Gage C2-174.

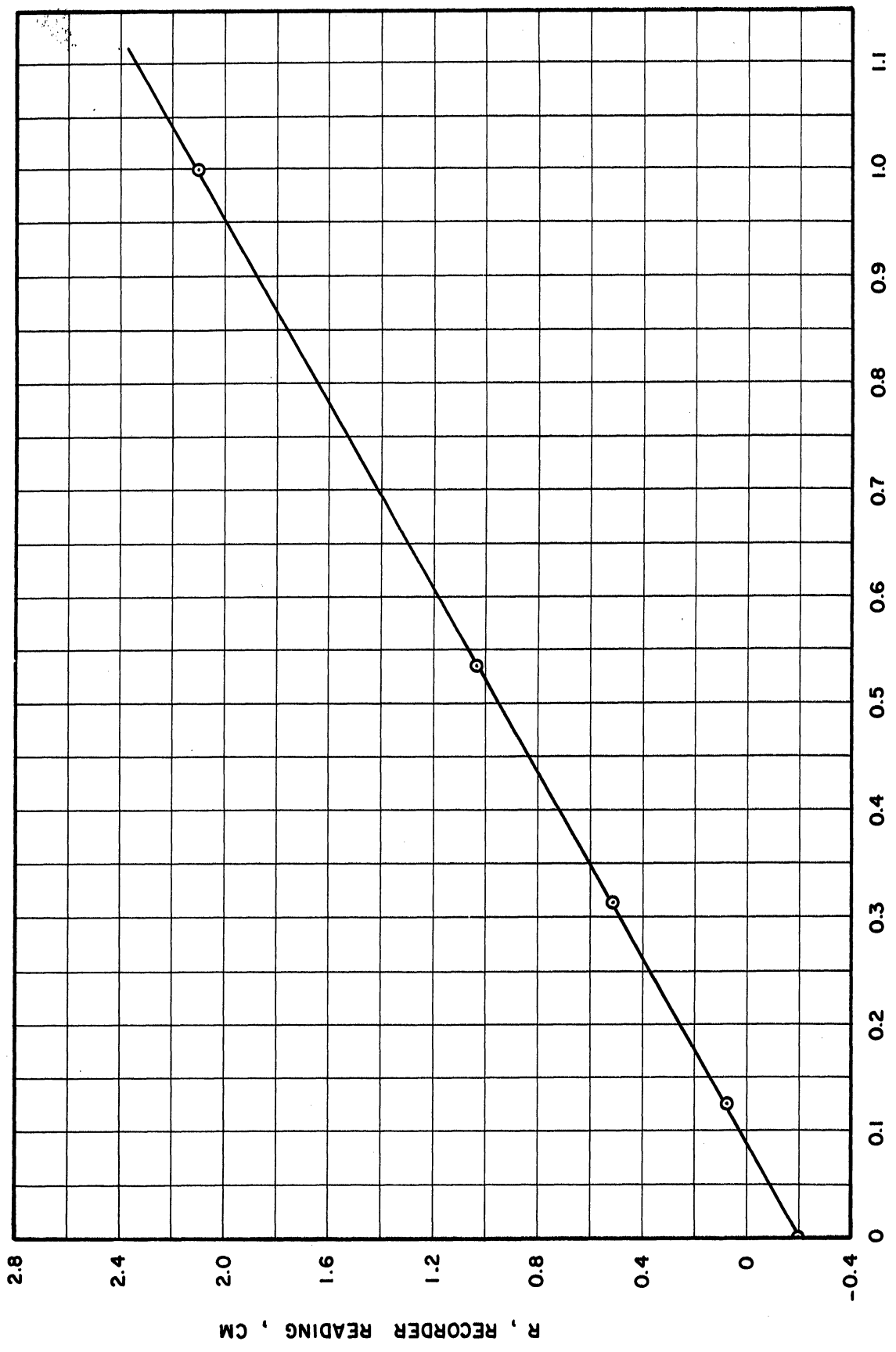

Figure 58. Calibration of Recorder and Pickup 2172.

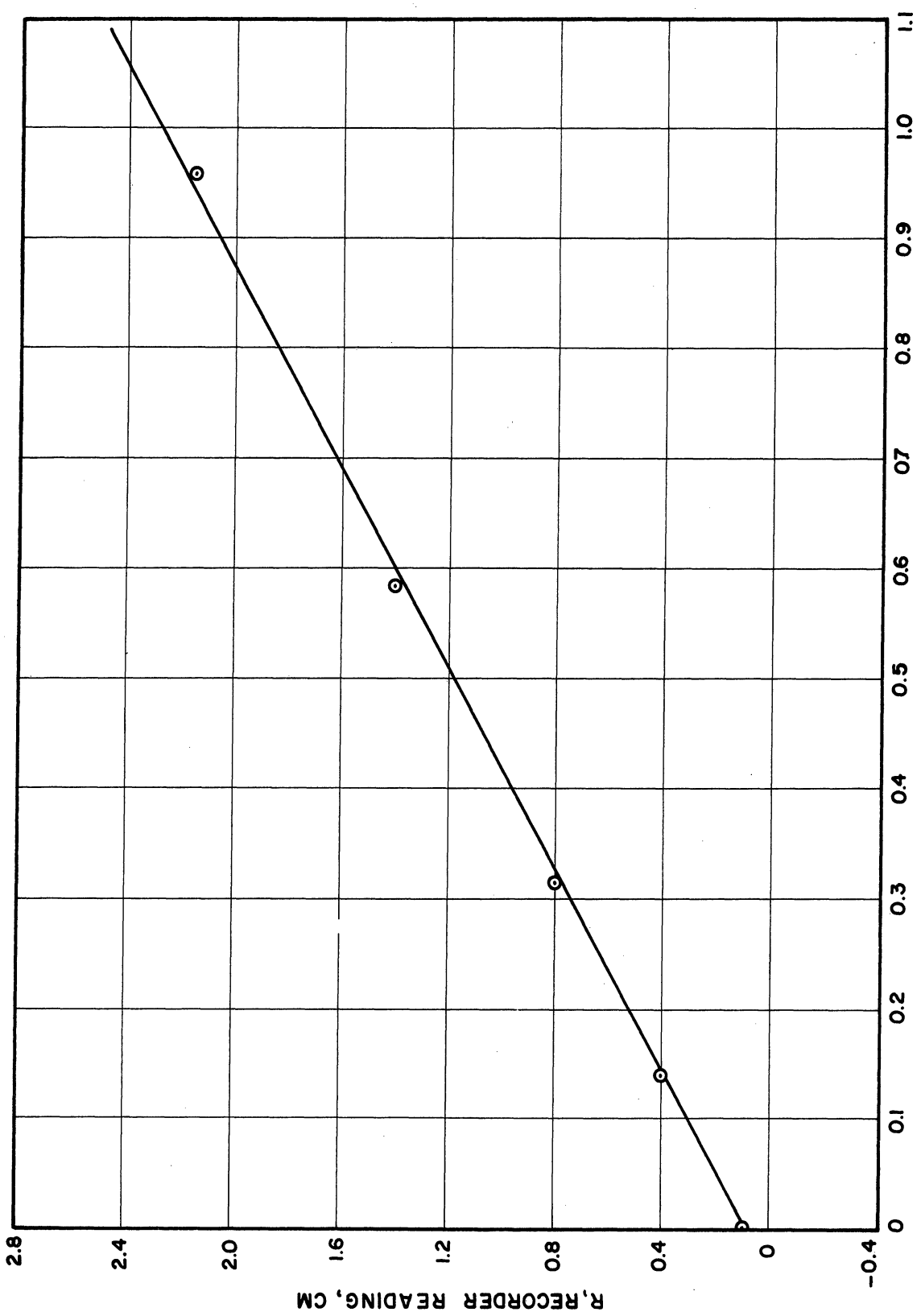

Figure 59. Calibration of Recorder and Pickup 2171.

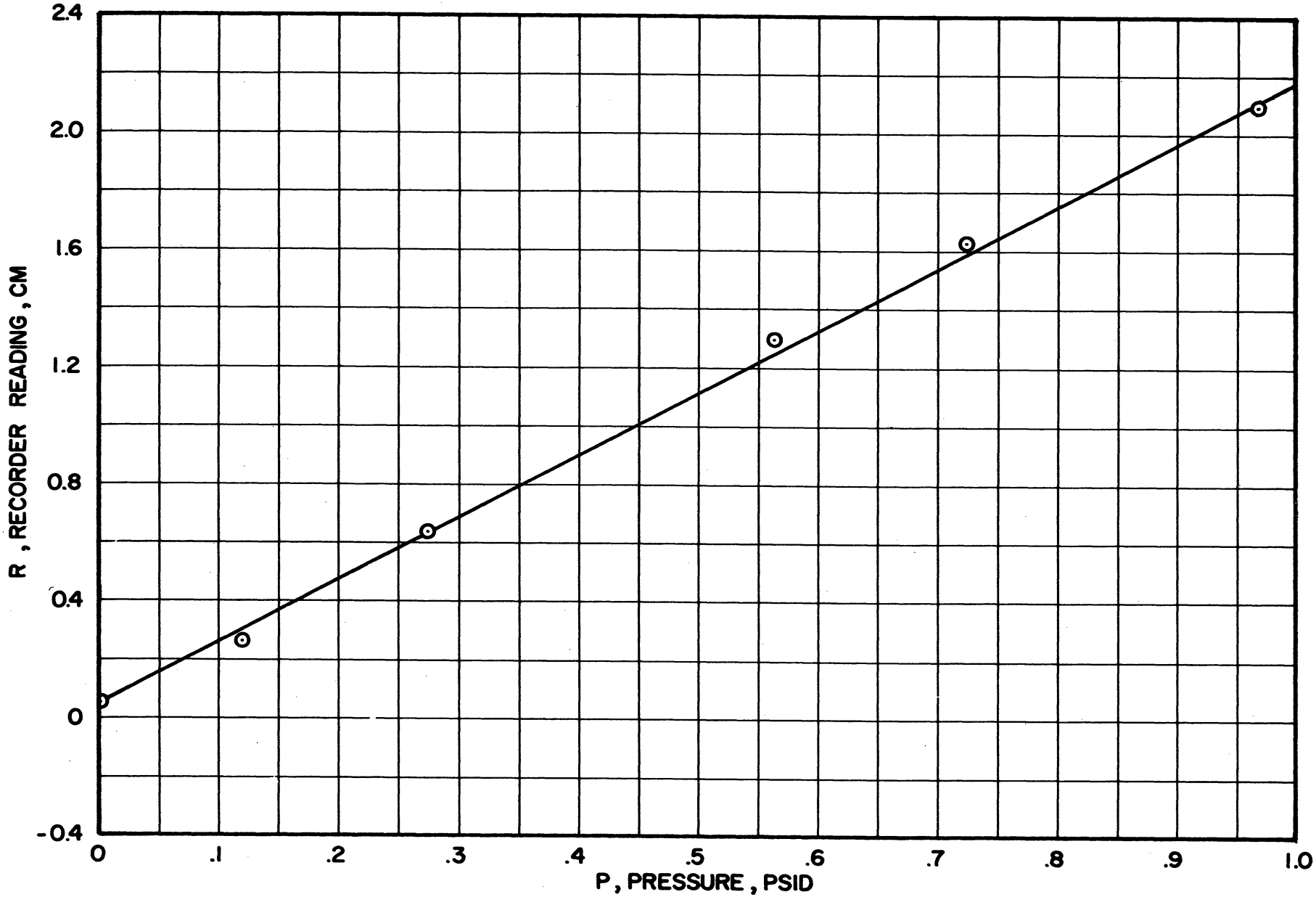

Figure 60. Calibration of Recorder and Pickup 2150.

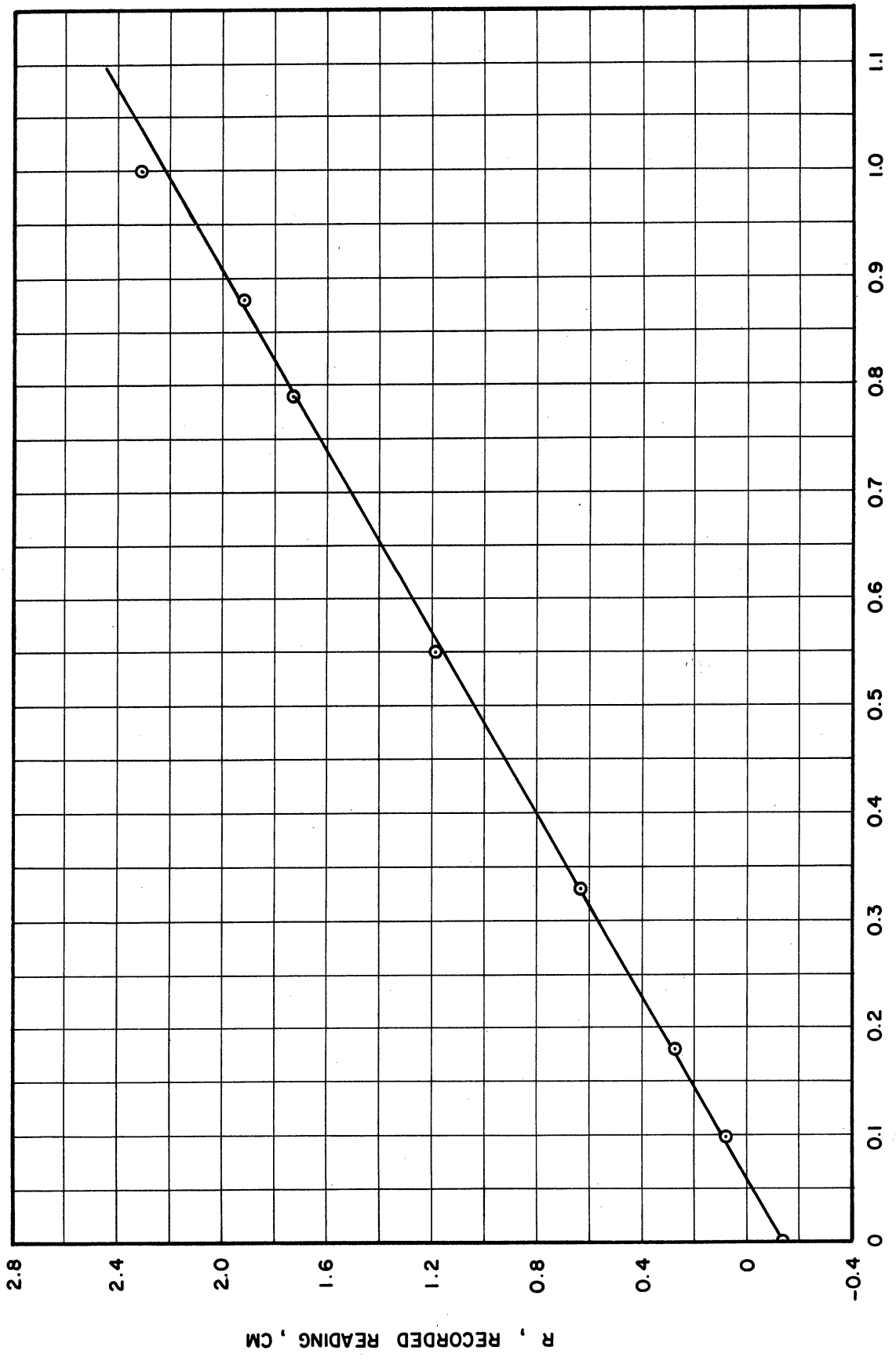

Figure 61. Calibration of Recorder and Pickup 2144.

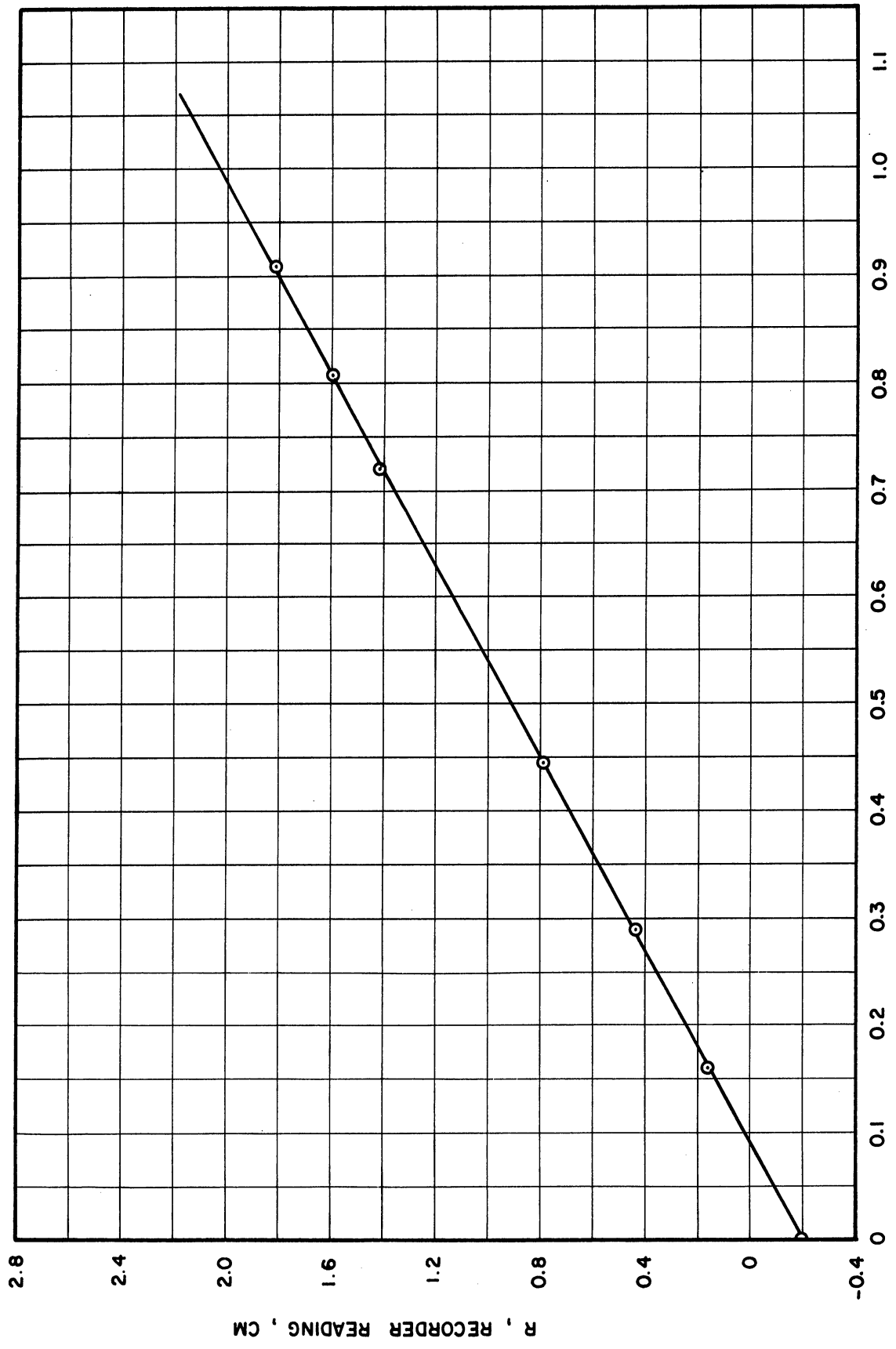

Figure 62. Calibration of Recorder and Pickup 2133.

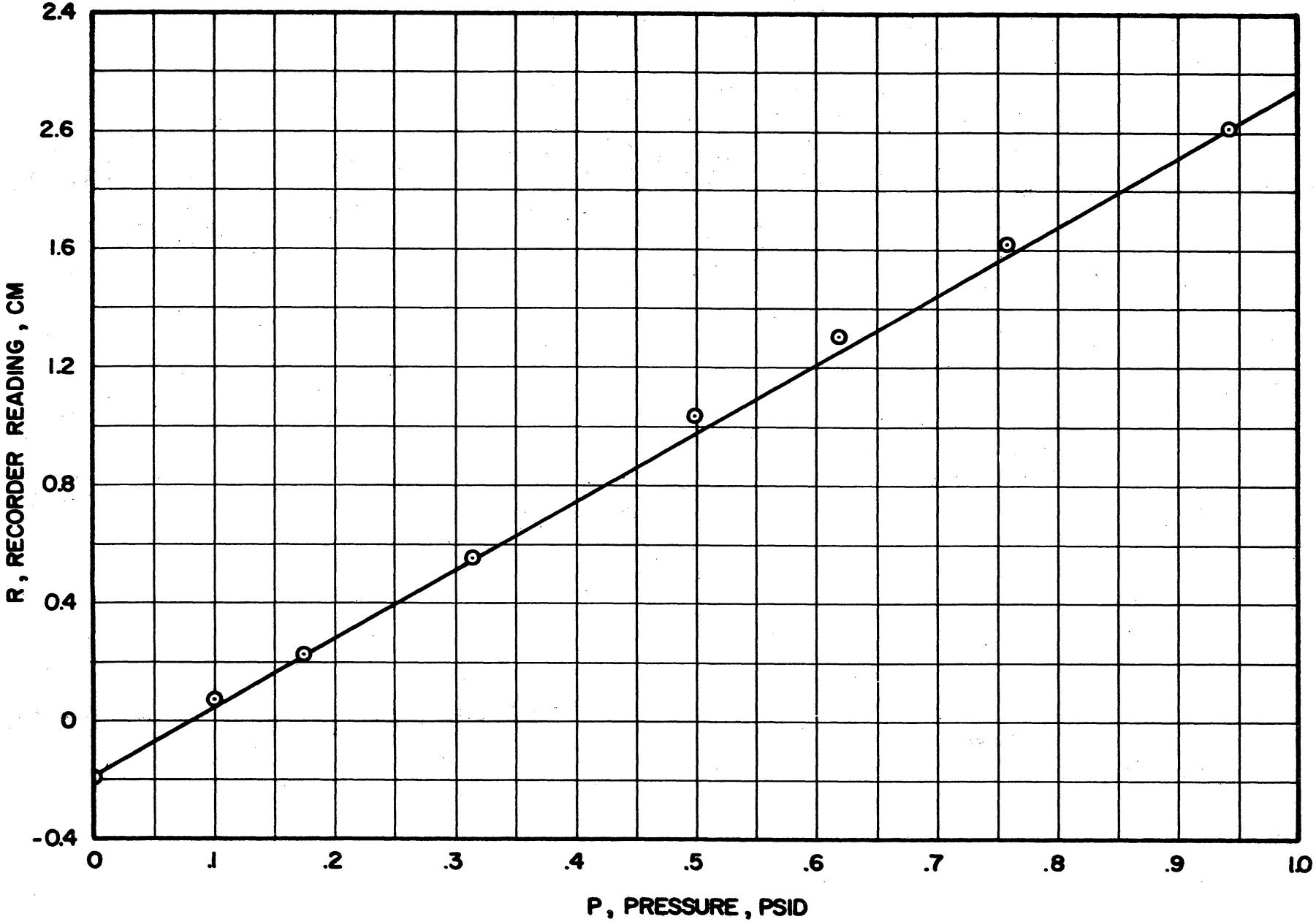

Figure 63. Calibration of Recorder and Pickup.2100.

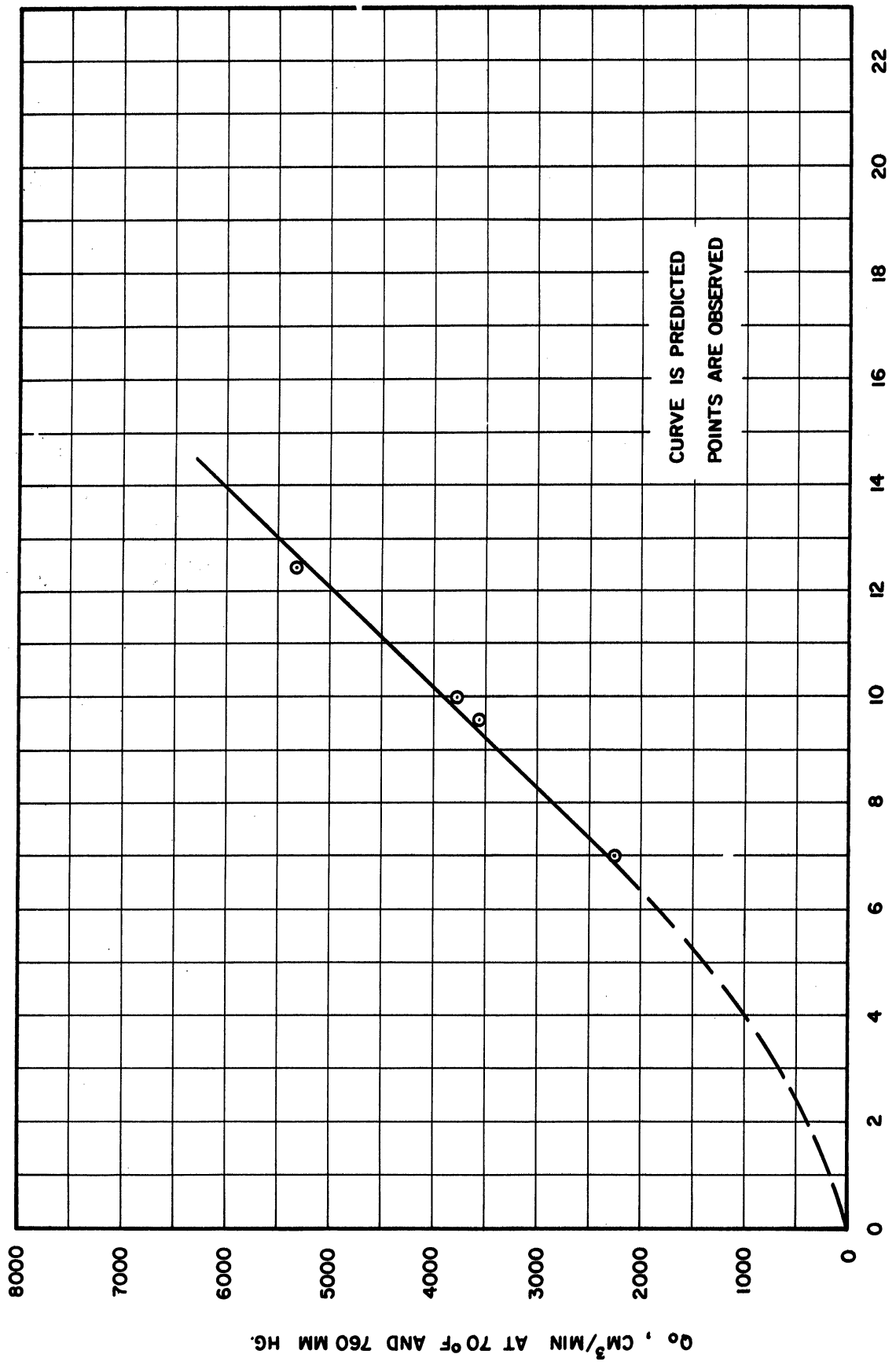

Figure 64. Calibration of Rotation 9145B With Glass Float for Air Flowing at Standard Conditions 70°F, 760 MMHg.

APPENDIX D.

Response of pressure measuring system.

The times involved in the pressure variations measured were small enough to cause worry about the dynamic response of the measuring system. Therefore several checks were made on the response of the pressure measuring system.

I. Response of measuring system to step pressure inputs.

Equipment.

The apparatus used for applying a step input to the measuring system is shown in Figure 65. An air line was led through a valve into a 28-liter tank. The tank pressure was read from a manometer. An outlet line led from the tank to a two-way solenoid valve. One outlet of this solenoid valve was vented through a valve to the atmosphere. The other outlet was tied directly to the measuring system used for pressure determination. The solenoid valve was actuated by a switch which, when closed, also caused a mark to be made on the margin of the oscillographic record.

Procedure.

In order to put a step impulse into the system, the tank was pressurized to the desired level. The vent of the solenoid was closed for this purpose. The solenoid was switched on and a record of the pressure change was made.

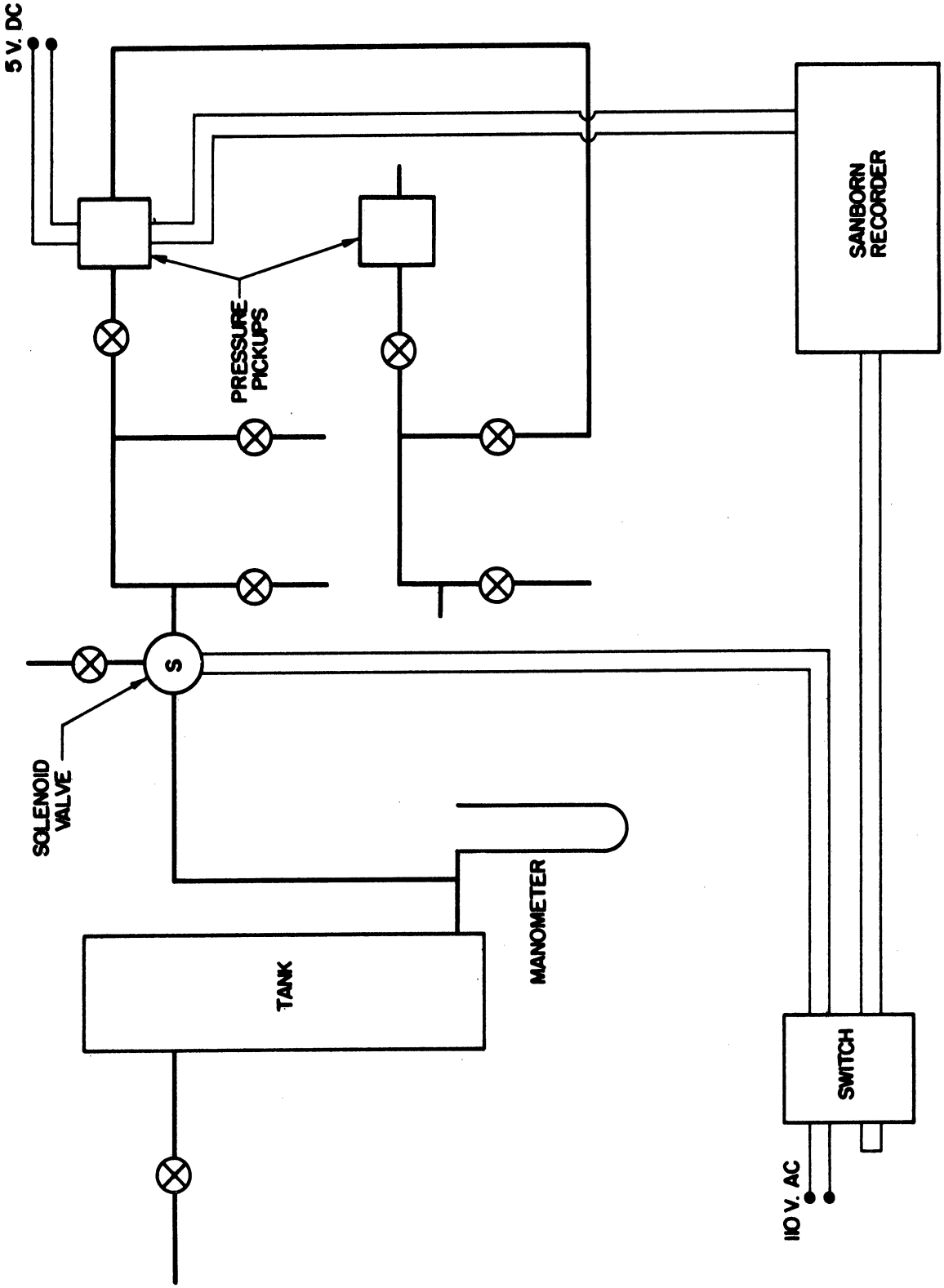

Figure 65. Apparatus for Applying Step Input to Measuring System.

Results.

Figure 66 shows a typical response curve. The usual exponential curve is observed. The lag observed is about 0.05 seconds.

Conclusions.

The system responds satisfactorily to step pressure impulses.

II. Response of measuring system to ramp pressure inputs.

Equipment.

The apparatus of Figure 65 was used.

Procedure.

The vent of the solenoid was opened and a reasonable air flow rate established through the tank and solenoid. The solenoid was then switched to direct this flow into the measuring system by closing the vent and opening to the measuring system. A record of the response was made.

Results.

Figure 67 shows a typical response curve. A lag of about 0.03 seconds is found in the response.

Conclusions.

The system responds satisfactorily to ramp pressure input changes.

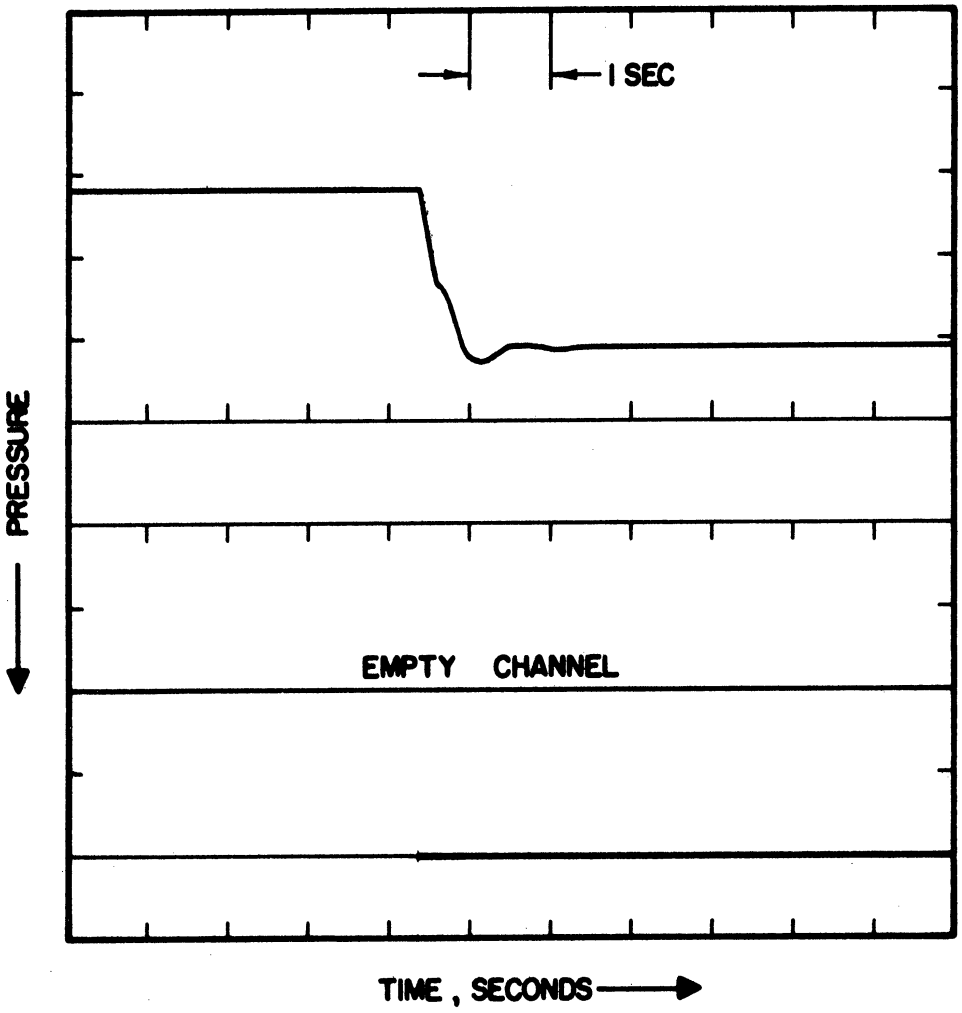

Figure 66. Response of Recording System to a Step Pressure Increase.

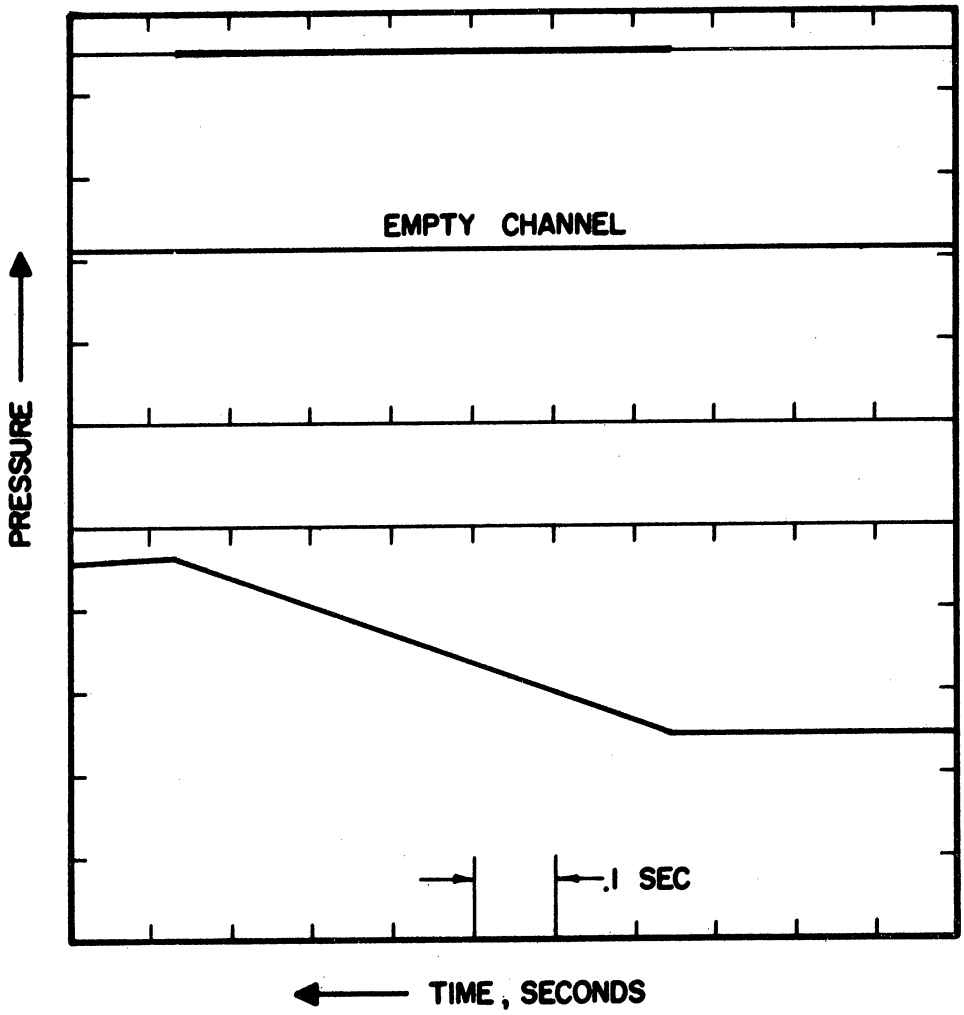

Figure 67. Response of the Measuring System to a Ramp Pressure Input.

III. Response of measuring system to sinusoidal pressure inputs.

Equipment.

A large diameter flexible tube was filled with mercury and one end attached to the measuring system. The other end was attached to an eccentric shaft on an electric motor. When the eccentric was at the high position, it tripped a switch which marked the margin of the record. The resulting pressure input was very nearly sinusoidal. The apparatus is shown in Figure 68.

Procedure.

The motor was turned on and the variations in pressure recorded.

Figure 69 shows an example of the results of these measurements. The mark at input maximum corresponds well to the output maximum. A lag of less than 0.02 seconds is observed.

Conclusions.

The system responds satisfactorily to sinusoidal pressure inputs.

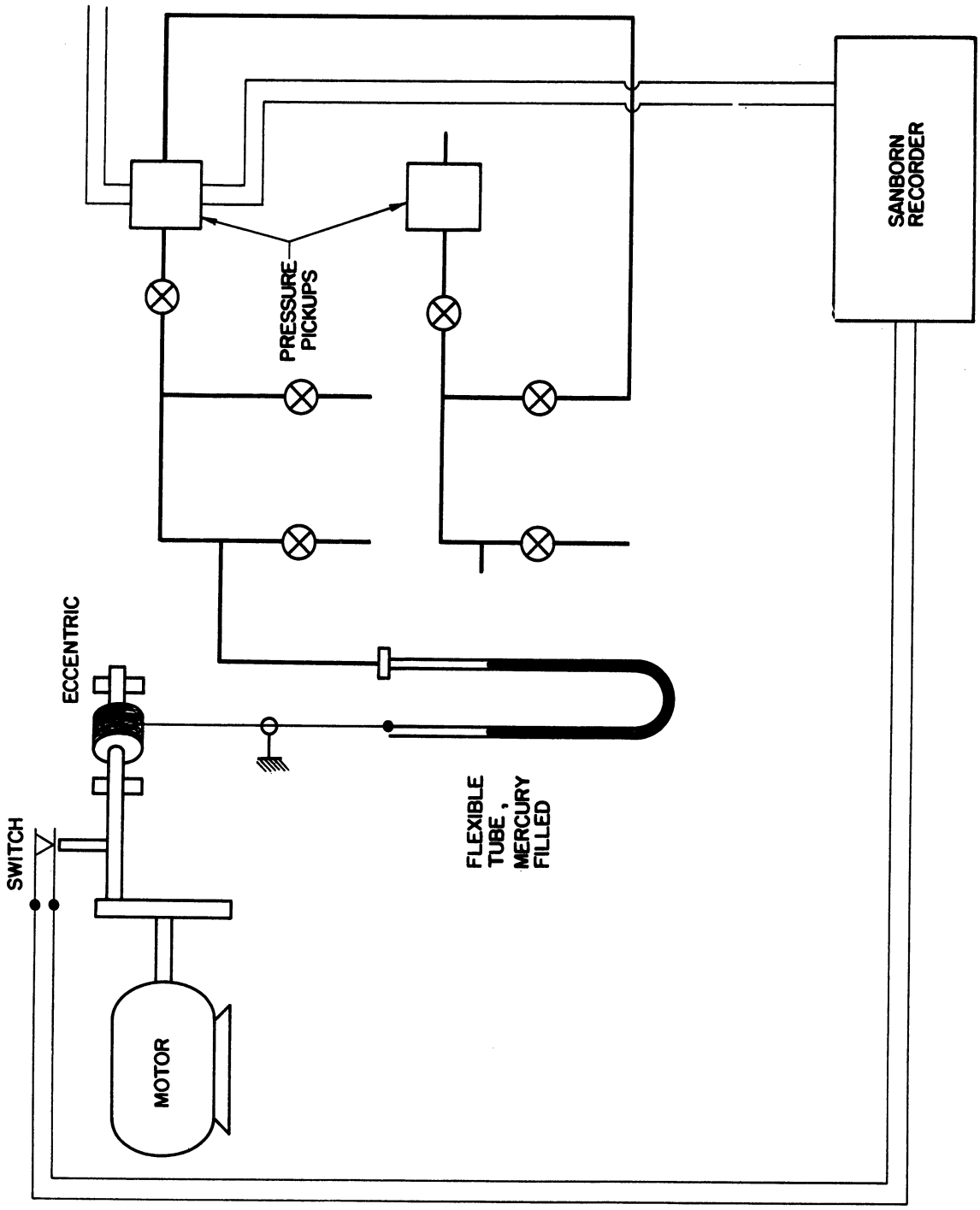

Figure 68. Apparatus for Applying Sinusoidal Pressure Input to the Measuring System.

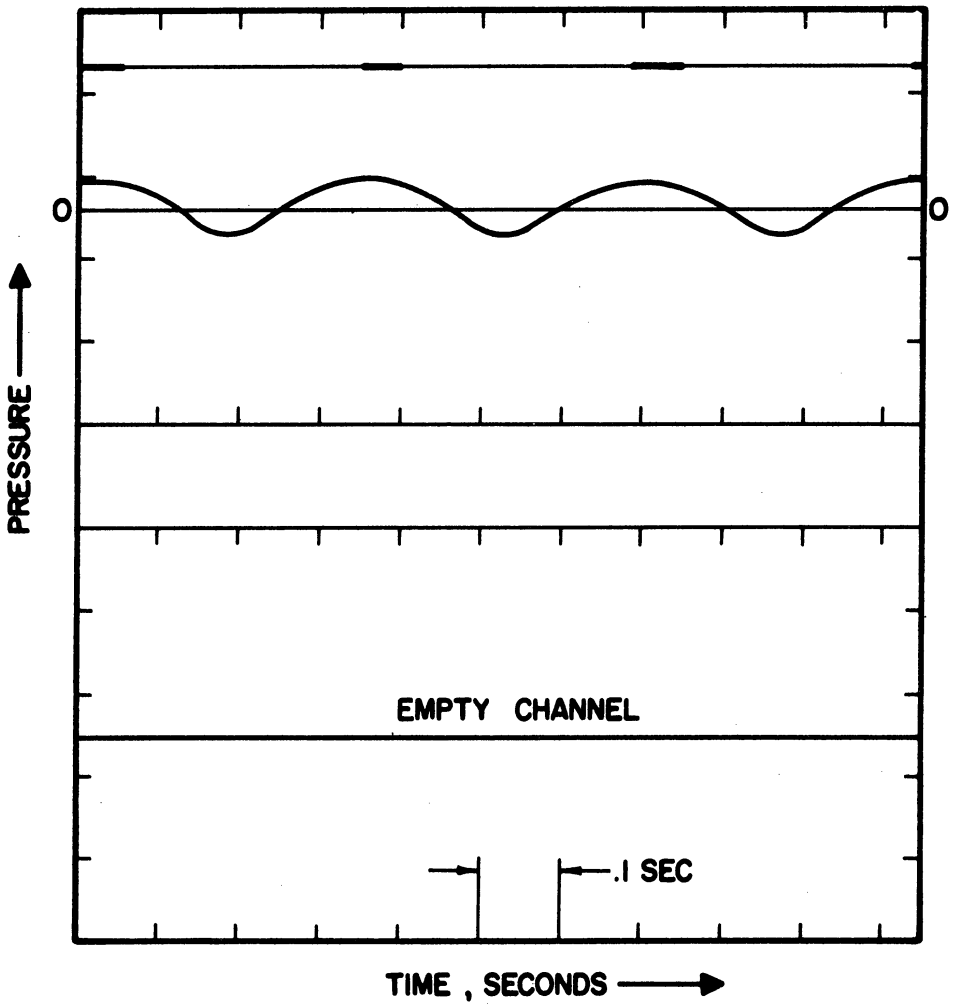

Figure 69. Response of the Measuring Syststem to a Simusoidal Input.

Calibration Certificate

FOR PRESSURE PICKUP

TYPE 4-315 SERIAL NUMBER 2172

PRESSURE RANGE ±1 PSID DATE 11-18-60

EXCITATION 5.0 VOLTS D-C OR A-C RMS

TEST TEMPERATURE	°F	°F	°F
	-65	+80	+165
SENSITIVITY: MILLIVOLTS FULL RANGE	±10.725	±10.650	±10.500
LINEARITY: % FULL RANGE	± .29	± .17	± .24
HYSTERESIS: % FULL RANGE	.23	.29	.30

ZERO SHIFT WITH TEMPERATURE ±.003 % FULL RANGE/°F

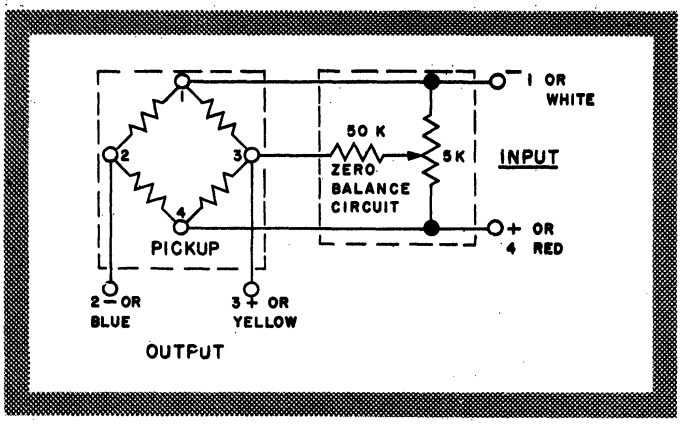

INPUT IMPEDANCE 345 OHMS

OUTPUT IMPEDANCE 345 OHMS

STABILITY OK C.E.C.

SIGNED D.J. Nickelsen
QUALITY CONTROL ENGINEER

Consolidated Electrodynamics
CORPORATION
Transducer Division
MONROVIA, CALIFORNIA

2083

BIBLIOGRAPHY

1. Bailie, R. E., Liang-Tseng Fan and J. J. Stewart, Industrial and Engineering Chemistry, 53, 567-69 (1961).

2. Baron, Thomas, and R. A. Mugele, "Quality of Fluidization," Shell Development Company, Emeryville, California.

3. Baumgarten, P. K., and R. L. Pigford, AIChE Journal 6, 115 (1960).

4. Benson, S. W., "The Foundations of Chemical Kinetics," McGraw-Hill, New York, 1960.

5. Dotson, J. M., AIChE Journal 5, 169-74 (1959).

6. Duncan, A. J., "Quality Control and Industrial Statistics," Richard D. Irwin, Inc., Homewood, Ill. 1955.

7. Gregory, S. A., Journal of Applied Chemistry 2, suppl. issue 1, si (1952).

8. Kelley, A. E., Petroleum Engineer, 16, 136 (1945).

9. Leva, Max, "Fluidization," McGraw-Hill, New York, 1959.

10. Morse, R. E. and C. O. Ballou, Chem. Engr. Progr., 55, 49 (1959).

11. Shuster, N. W. and P. Kisliak, Chem. Engr. Progr., 48, 455-8 (1952).

12. Zenz, F. A. and D. F. Othmer, "Fluidization and Fluid Particle Systems," Reinhold, New York, 1960.